A Chewing Robot Based on Parallel Mechanism – Analysis and Design

A thesis presented in partial fulfilment of the
requirements for the degree of

Master of Engineering

in

Mechatronics

at

Massey University,
Palmerston North, New Zealand

József-Sebastian Pap
Dipl.-Ing. (FH)

2006

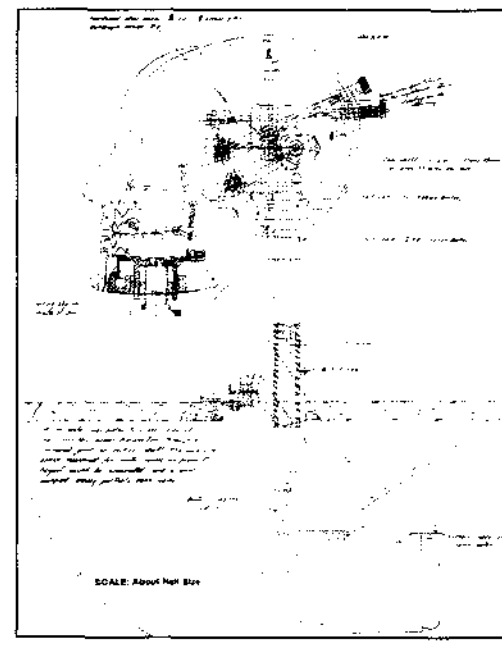

A copy of an original drawing of the "Dental Prosthetic Demonstrator" invented by the dentist George Burtenshaw and manufactured by the engineer Mel Harris from Taumarunui, New Zealand, dated in January 1938 (Cooke 1982).

ABSTRACT

Masticatory efficiency, dependent on number and condition of the teeth, length of time spent in chewing a bolus and the force exerted when chewing, influences an individual with the selection of food and therefore nutritionally diet. A characterisation of the masticatory efficiency could be possible with a chewing robot that simulates human chewing behaviours in a mechanically controllable way (Pap *et al.* 2005; Xu *et al.* 2005).

This thesis describes such a chewing robot, developed from a biological basis in terms of jaw structure and muscles of mastication according to published articles. A six degrees of freedom parallel mechanism is proposed with the mandible as a moving platform, the skull as a fixed platform, and six actuators representing the main masticatory muscle groups, temporalis, masseter, and lateral pterygoid on the left and right side. Extensive simulations of inverse kinematics (i.e., generating muscular actuations with implementing recorded human trajectories) were conducted in SolidWorks and COSMOS/Motion to validate two mathematical models of the robot and to analyse kinematic properties.

The research showed that selection of appropriate actuation systems, to achieve mandible movement space, velocity, acceleration, and chewing force, was the key challenge in successfully developing a chewing robot. Two custom designed actuation systems, for the six actuators, were developed and built.

In the first approach, the muscle groups were presented as linear actuators, positioned so as to reproduce the resultant lines of action of the human muscles. However, with this design concept the spatial requirements specified from the human masticatory system made the physical building of the model impossible.

The second approach used a crank mechanism based actuator. This concept did not allow a perfectly linear actuator movement that copied the muscle line of action. However, it was possible to fulfil the spatial requirements set by the human system and to allow reproduction of human chewing behaviours in relation to kinematic requirements and chewing force.

The design, manufacture and testing of the entire chewing robot with crank actuators was then carried out. This included the implementation of realistic denture morphology, a mechanical jaw and the framework design for the whole system.

In conclusion, this thesis research has developed successfully a mathematical and a physical robotic model. Future work on the control and sensing of the robot and design of a food retention system are required in order to fully functionalise the device.

ACKNOWLEDGEMENTS

Getting this thesis written was like getting a tooth pulled. Although writing this thesis was hard work, there have been many people who have helped me along this way.

Firstly, I like to thank my supervisors Assoc Prof Peter Xu and Dr John Bronlund for providing me with something I could really sink my teeth into. Soon I realised that I bit of more than I could chew. However, I am really grateful for the invitation to do my Master of Engineering. Both gave me the great feeling of being an essential part of a big research group. I am especially thankful for providing me with the opportunities in attending conferences and visiting research groups all over New Zealand during my study as well as support for my thesis work. I am also thankful for the financial support to attend the biggest robotic conference in Europe after completing my master study.

Thanks also to the staff of the mechanical workshop of the ITE, Massey University, Palmerston North. Although there were a few teething problems with building this robot, I am really thankful for all advice provided and for successfully building the physical models.

I also would like to thank Assoc Prof Andrew Pullan and Dr Oliver Röhrle at the Bioengineering Institute at the University of Auckland, Auckland, New Zealand, Prof Jules Kieser and Ionut Ichim at the School of Dentistry at the University of Otago, Dunedin, New Zealand, and Dr Kylie Foster and Christine Lawrence at the Institute of Food, Nutrition and Human Health at Massey University, Auckland, New Zealand. I really enjoyed working together with you guys. Thanks a lot for showing me all these interesting things in your research fields and for chewing over ideas. All these

opportunities broadened my knowledge considerably.

Furthermore, I would like to thank Dr Rory Flemmer, Creig McLeay, Matthew van der Werff, Darren Lewis and Jonathan Torrance for their advice and help during my study.

I also like to thank Joan Brookes who helped me a lot and makes postgraduates a valuable part of ITE.

Thank goes also to Barbara Gawith and Claire Hastings for proofreading my thesis.

I like to thank Katrin Wiegand for her support before and during my master study.

I am very grateful to the Foundation of Research, Science and Technology, New Zealand (contract number UOAX0406), for providing the scholarship and paying the tuition fees.

Cheers to Fly My Pretties for their Live at Bats.

Finally, I want to thank my parents. Since they do not speak any English, I would like to write some words in German.

Ich bin euch für all eure Unterstützung während meiner Schul- und Studienzeit unendlich dankbar. Ihr glaubt gar nicht wieviel mir dies bedeutet. Herzlichen dank.

For those about to read this thesis, I hope you can grind your way through and digest all the relevant ideas.

Palmerston North, 21st of March 2006.

CONTENTS

LIST OF FIGURES

LIST OF TABLES

GLOSSARY

All definitions of anatomic orientation terms are obtained from MedicineNet (2005).

Anterior – The front, as opposed to the posterior.

Anteroposterior – From front to back.

Horizontal – Parallel to the floor, a plane passing through the standing body parallel to the floor.

Inferior – Below, as opposed to superior.

Lateral – Toward the left or the right side of a body, as opposed to medial.

Mandible – lower jaw.

Mastication – chewing or grinding or crushing.

Maxilla – upper jaw.

Medial – In the middle or inside, as opposed to lateral.

Posterior – The back or behind, as opposed to anterior.

Sagittal – A vertical plane passing through the standing body from front to back.
Superior – Above, as opposed to inferior.

Superoinferior – From above to below.

Vertical – Upright, as opposed to horizontal.

ABBREVIATIONS AND ACRONYMS

DOF – Degrees of freedom.

FEM – Finite Element Method.

PCS – Physiological cross-sectional area.

TMJ – Temporomandibular joint.

a	Distance	$[m]$
a	Linear acceleration	$[m/s^2]$
A	Cross-sectional area	$[mm^2]$
b	Distance	$[m]$
B	Resolution	[-]
c	Distance	$[m]$
c	Permissible load	$[N]$
d	Diameter	$[mm]$
d	Distance	$[m]$
e	Distance	$[m]$
E	Young's modulus	$[N/mm^2]$
f	Distance	$[m]$
f	Factor	[-]
f	Accuracy	$[mm]$
F	Force	$[N]$
g	Gravitational constant	$[m/s^2]$
i	Gear reduction	[-]
I	Geometrical Moment of Inertia	$[mm^4]$
l	Length	$[mm]$
L	Vector length	$[m]$
m	Mass	$[kg]$

m	Module	[-]
n	Rotational speed	$[min^{-1}]$
r	Radius	$[mm]$
R	Lead	$[m]$
s	Displacement	$[m]$
s	Stroke	$[mm]$
t	Number of teeth	[-]
T	Torque	$[Nm]$
v	Velocity	$[m/s]$
x	Factor	$[mm/s]$
α	Angular acceleration	$[s^{-2}]$
α	Angle	[°]
β	Angle	[°]
γ	Angle	[°]
γ	Density	$[kg/mm^2]$
$\hat{o}$	Angle	[°]
δ	Tensile-compressive stress	$[N/mm^2]$
Δ	Difference	[-]
λ	Mounting coefficient	[-]
ζ	Angle	[°]
ϕ	Angle	[°]
μ	Efficiency	[-]
ω	Angular velocity	$[s^{-1}]$

Indices

0	Point of origin
0a	Static
1	First factor
2	Second factor
3	Third factor
a	Actual factor
acc	Under acceleration
axial	Axial
b	Buckling
BC	Ball centre
c	Cylinder
c	Constant
cs	Crank shaft
cs	Critical speed
dec	Under deceleration

DN	DN value
driven	Driven gear
driving	Driving gear
e	Entire
e	Extended
f	Folded
F	Force
GB	Gearbox
k	Minimum Thread
L	Load
M	Motor
Mass	Masseter muscle group
M.Ptery	Medial pterygoid muscle group
max	Maximum value
Occ	Occlusion
Ptery	Lateral pterygoid muscle group
Spindle	Spindle
tc	Tensile-compressive
Temp	Temporalis muscle group
u	Unsupported
x	Direction
y	Direction
z	Direction
α	Throughout acceleration

1 INTRODUCTION

Masticatory efficiency is among other things, dependent on the number and the condition of the teeth presented in the mouth, the length of time spent in chewing a bolus and the force exerted when biting. It is believed that optimal masticatory efficiency allows an individual to select a wider variety of food, which leads to the potential for a more nutritionally balanced diet (Martin 1999). An analytical characterisation of the masticatory efficiency is possible with continuous measuring over the mastication cycles. Such measurements include: frequency, length of chewing, tracking of jaw movement, force distribution, application of compression and shear forces on the food and particle size distribution and structure of the bolus just prior to swallowing. The high variation of these factors in subjects (e.g., different jaw geometries, teeth shape) and food texture (e.g., elasticity, hardness, etc.) means, there is a real need for the development of quantitative methods for evaluating the capability of a person to effectively chew food. One method to achieve this could be the development of a robotic jaw that simulates the chewing behaviour. With the robotic jaw, dental researchers could study the response of dental implants to the chewing of different foods and evaluate the impact of bad or missing teeth on chewing efficiency. Furthermore, the robot would allow studying the dynamics of texture changes in foods during chewing.

The aim of this thesis research was to design and build such a chewing robot based on the principle of a parallel platform robot, as proposed by Pap *et al.* (2005) and Xu *et al.* (2005). This work was carried out within the following scope:

- *Biological fundamentals*. The robot needs similar proportions to the human system to allow comparisons between the human system and the chewing

robot. In particular, the jaw structure and properties of the muscle of mastication would have to be considered.

- *Degrees of freedom.* To reproduce human chewing behaviours, the robot requires the same degrees of freedom (DOF) as in the human system. This would enable the robot jaw to reach the same positions and orientations as the human mandible.
- *Kinematic simulations.* To ensure that the chewing robot is able to reproduce human chewing behaviour, kinematic simulations could be used for the verification.
- *Chewing force.* The robot should be able to produce the forces observed during human chewing.
- *Controlling.* The robot needs to be designed in such a way that controlling with a Galil Motion Control System is possible. This system includes two amplifiers AMP-19540 and one Galil motion control card DMC-1860.

2 LITERATURE REVIEW

2.1 Introduction

Before starting to design a chewing robot, the design and the function of the human masticatory system have to be understood. Therefore, the roles of the human masticatory system in the digestion process, jaw border movement, chewing cycles, and chewing forces must be described. Furthermore, the functional, rather the anatomical consequences of the masticatory apparatus must be reviewed with a focus on bones, joints, muscles of mastication, and dentition. This forms the first part of this chapter.

In the second part, a brief overview of different chewing projects, classified into mathematical and physical models, is given to understand their advantages and disadvantages.

2.2 Human masticatory system

The following review of design and function of the human masticatory system helps to define the specifications that are required in designing a chewing robot.

2.2.1 The chewing process

The human mastication process is the first stage in the digestion of food. It is a complex process whereby the food taken to the mouth is processed under use of saliva into a form (bolus) suitable for swallowing. The bolus is also brought to approximately body temperature before transfer to the stomach, where digestion, absorption and utilisation begin (Bourne 2002). Health and Prinz (1999) described the masticatory

sequence in three phases:

1) Ingestion (which is the transfer of food to between the teeth by the tongue),
2) Main sequence (in which the food gets formed to a bolus through rhythmic chewing), and
3) Clearance and swallowing.

The most relevant phase to this project is the main sequence, where the food gets broken down. Jaw movement trajectories while chewing, rhythms and chewing forces are factors which influence this sequence.

Jaw border movement

Ulf Posselt (1957) described an envelope of mandibular movement. This is a three dimensional figure that represents an infinite number of maximum extensions, which is commonly recorded by tracing the lower incisor teeth as the jaw is guided through the border paths. To analyse mandibular movement and its mechanical relationship to the teeth, the movement can be separated into three planes of space (sagittal, frontal, and horizontal) as seen in Figure 2-1.

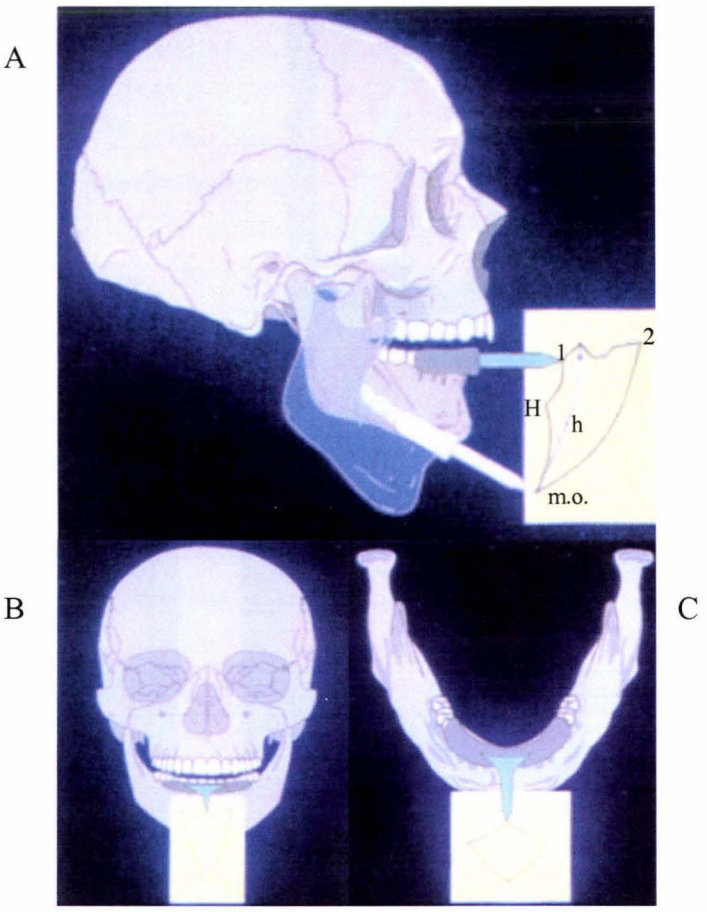

Figure 2-1. Posselt envelope in (A) the sagittal plane, (B) the frontal plane, and (C) the horizontal plane (Douglass and DeVreugd 1997).

The movement space has a characteristic shape in most individuals, although it differs somewhat from one person to another. Several important positions, such as the occlusal position, the rest position, retruded position and the maximum opening position (m.o.) have been analysed and classified. The most commonly used plane is the sagittal plane, which shall be used to describe the maximum mandibular movement space in the following discussion.

The maximum mandibular movement space can be subdivided into three movement paths: the extreme posterior opening, the extreme anterior closing and the maximum upper glide. The *extreme posterior opening*, which is indicated by the line 1-m.o. is divided into two parts (see Figure 2-1). The first part describes the so-called hinge movement (1-H), which is a rotation of about 10 degrees around the hinge axis. Further jaw-opening requires the hinge movement to be overlaid with a forward movement, which is indicated by the second part of the curved line (H-m.o.). The *anterior extreme opening*, indicated by the line 2-m.o., is also an overlaid hinge movement. The biological reasons for those movements are outlined in chapter 2.2.2. The *forward and backward glide* between the points 1 and 2 is irregular because of incisal and other tooth guidances.

It is noted that a specific masticatory movement should be within the maximum movement space described by Posselt. This leads to the conclusion that the desired robotic movement space can be validated using the Posselt figure. Klineberg (2005) determined the approximate range of jaw movement in adults in the sagittal plane as follows: 2-m.o. with 40-70 *mm*, 1-H with 15-20 *mm*, and 2-5 with 5-10 *mm* (see Figure 2-1). However, this is not enough to represent the whole envelope, which makes it impossible with this technique to validate the robot. Therefore, another approach has to be chosen.

Chewing cycle

Masticatory movements can be described as rhythmically repeated, coordinated and smooth movements, which vary greatly among individuals. To better understand the differences between the movement area while chewing and the maximum movement area, a chewing cycle has to be reviewed.

Trajectories have been recorded by various techniques. For example, Figure 2-2 illustrates a representative path of an incisor, which has been recorded from a healthy subject by using an Optotrak® camera (Anderson *et al.* 2002).

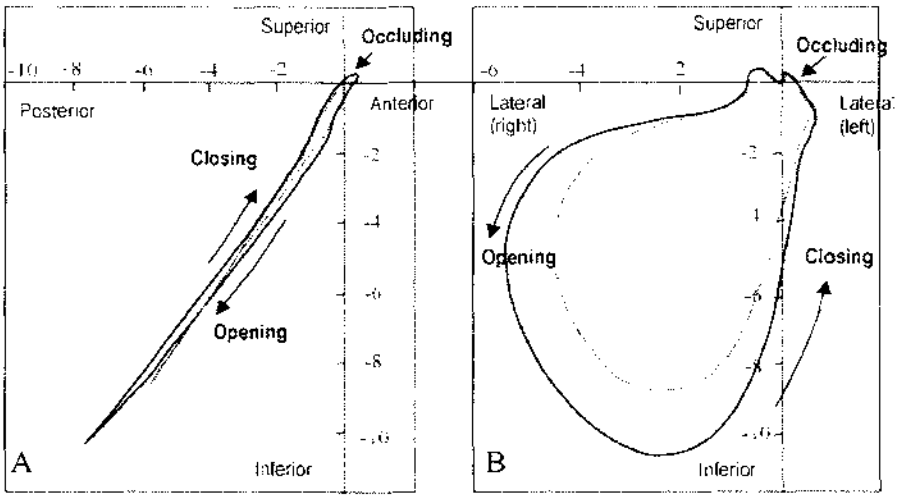

Figure 2-2. Trajectories of the incisor point in (A) the sagittal plane and (B) the frontal plane. The dotted line represents soft food and the solid hard food. The figure has been adapted from Anderson *et al.* (2002).

Basically the chewing cycle can be divided into three phases, the opening, the closing, and the occlusal phase. Ogawa *et al.* (2001) concluded that the occlusal area ends 0.5 *mm* from the maximum intercuspation (MI). The opening phase starts at this point and ends at the most inferior point of the chewing circle. The closing phase starts from the most inferior point and ends at a point 0.5 *mm* before the MI.

Other important characteristics are the amplitude of vertical opening (distance between the MI and the most inferior point), the lateral displacement of the opening path and the lateral displacement of the closing path (distance between the most lateral point and the balancing plane).

In several publications it is noted that chewing circle trajectories of the incisor in terms of three dimensional coordinates have been recorded (Anderson *et al.* 2002; Foster *et al.* 2005; Ogawa *et al.* 2001; Peyron *et al.* 1996; Röhrle *et al.* 2005). The implementation of such trajectories in a mathematical model will give information about the chewing kinematics and chewing movement space.

Chewing trajectories

Human chewing trajectories measured for different positions on the mandible, such as incisor teeth and molar teeth position, are a necessary tool for various purposes (i. e., the determination of illnesses related to the mandibular movement and the assessment of chewing efficiency). The Institut National de la Recherche Agronmique (INRA), Clermont-Ferrand, France, measured trajectories with a Carstens 2D Articulograph in two-dimensions (Peyron *et al.* 1996). One set of data was made

available, where the only available data were the time history of the lateral and superoinferior movements of the incisor point as plotted in Figure 2-3.

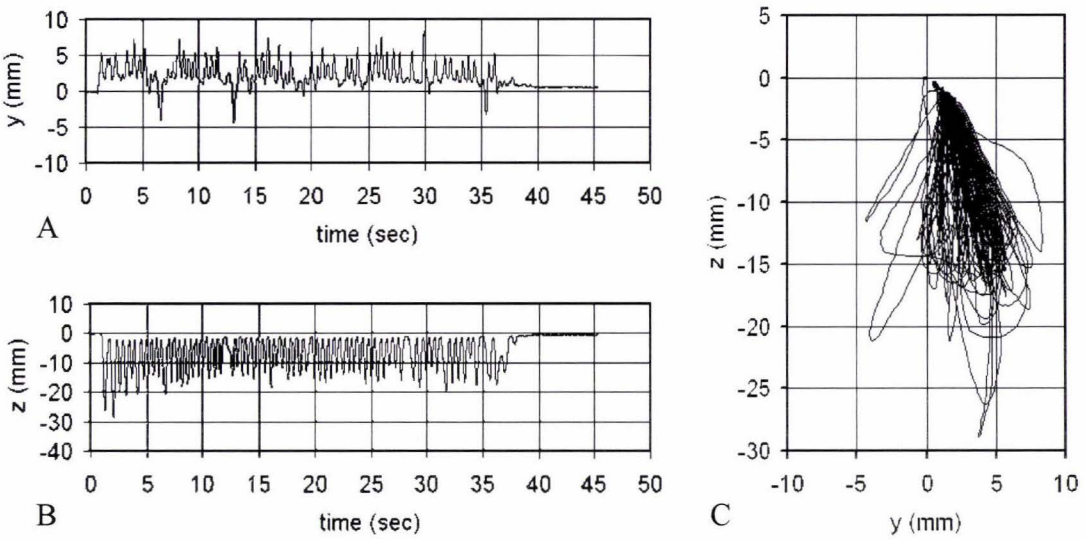

Figure 2-3. Recorded chewing trajectory of the incisor point plotted as (A) lateral movement, (B) superoinferior movement, and in (C) frontal plane.

The above data show the displacement changes for the incisor point around its initial state in a timeframe of 45.32 seconds, which were given in time steps of 0.01 seconds. The test food had hard elastic properties (Peyron *et al.* 2002). It can be seen that the subject chewed on the left side except for three peaks of the lateral excursion movement which were performed to the right side. This can be traced back to the work of the tongue, which influences the chewing cycle with collecting or replacing food to an accurate position. Furthermore, it can be seen in the superoinferior movement that the chewing amplitudes vary between 30 *mm* and 20 *mm* for the beginning and the end of the chewing cycle, respectively. This chewing trajectory in the following text is called trajectory one.

Another approach to measure human chewing trajectories was used by the Bioengineering Institute at the University of Auckland, Auckland, New Zealand. With a custom made brace (Figure 2-4) and a motion capturing system VICON MX, chewing data with six DOF were obtained (Röhrle *et al.* 2005).

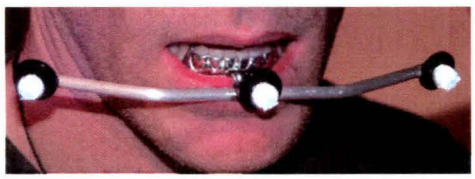

Figure 2-4. Enlarged view of the custom-made brace.

However, since they were not interested in reporting on clinical-type study involving different food types, no details on the food samples could be made available.

Three chewing trajectories were provided, which are described in this thesis as trajectories two to four (Röhrle 2005). All three trajectories described the incisor movement in its three dimensional coordinates x, y, and z, and the angular movement of the mandible about its x, y and z axes. In appendix A the incisor trajectories for chewing samples two to four can be seen.

Table 2-1 lists the maximum values for the incisor displacements and the angular movements of the mandible, as well as the chewing times for all four chewing trajectories.

Table 2-1. Maximum incisor displacements and angular movements of the mandible and chewing times for all four chewing trajectories.

	Chewing trajectory			
	One	Two	Three	Four
Incisor displacement				
x (*mm*)	-	+5; -15	+3; -18	+3; -27
y (*mm*)	−7; -5	+5; -5	+11; -8	+10; -14
z (*mm*)	0; -30	−2; -23	−3; -30	−5; -38
Angular movement (mandible)				
about x (°)	-	+2; -2	−0.5; -0.7	+1; -4
about y (°)	-	−7; -13	+5; -13	−5; -18
about z (°)	-	+0.2; -0.1	−3; -4	+6; -8
Chewing time (*s*)	45.32	32.86	68.86	62.24

First of all, it should be noted that all trajectories have different time-frames, which, however, do not influence the results of simulations, but the needed calculating time for the computer. Furthermore, big differences for the incisor displacement can be seen, where chewing trajectory two has the smallest lateral and superoinferior movement and trajectory four the biggest. However, it is curious that positive vertical displacement changes occur. The maximum angular movements of the mandible about the y and z axis are also obtained for the chewing trajectories two to four. Positive values for the angular movements about the y-axis especially for chewing trajectory three and four occur. A participant while recording these chewing trajectories explained a few concerns as to the suitability of the custom made brace for recording "natural" chewing behaviour (Foster 2005). The subject was not able to close his mouth probably, which caused the participant to salivate more than normal. Due to the fact that increased saliva production alters the breakdown of food in the mouth and

therefore changes the bolus properties, the jaw movement gets influenced.

The positive values of either the vertical displacement or the angular movement and the not predictable influence of the metal brace, in terms of chewing velocity and acceleration, leads to the conclusion to use trajectory two to four only to verify the incisor movement space.

However, the implementation of chewing trajectory one in a mathematical model is an appropriate tool to verify the model and to determine needed system requirements for designing the chewing robot.

Chewing forces

Beside masticatory movement space, another important factor for designing a chewing robot is the forces applied while chewing. They occur between the teeth in horizontal, vertical and anteroposterior direction. Furthermore, the difference between maximum biting forces and maximum chewing forces needs to be distinguished.

Helkimo and Ingervall (1978) measured the biting and chewing forces of a representative group of people. They showed that the average bite force at the incisor was 40% of the force at the molars, whereas the chewing force at the incisors was about 47% of that at the molars. Furthermore, they determined that the average chewing force was 52% of the average bite force at the molars and 60% at the incisors. These measurements were confirmed by various researchers, for example, maximum biting forces between the upper and the lower molars are usually in the range 500 - 700*N*, whereas the maximum mouth opening forces generally do not exceed 150*N* (Sharkey *et al.* 1984; Wood and Williams 1981). Anderson (1956) measured that forces applied to a single tooth during chewing of foods such as biscuits, carrots, and cooked meat were in the range 70-150*N*. Forces of total bite across all contacting teeth for dentate individuals were reported in between 190-260*N* by Gibbs *et al.* (1981).

Furthermore, it can be said that forces increase as the chewed foods become hard and the chewing forces are always less than the maximum biting force. This leads to the specification that for designing a chewing robot a chewing force across all contacting teeth of 260 *N* is required.

2.2.2 Mastication apparatus

The human masticatory apparatus consists of a mandible which is able to move in relation to the skull and is guided by two temporomandibular joints through

contractions of the masticatory muscles. This section gives an insight into the morphology of the mastication apparatus with the bones of interest, temporomandibular joints, muscle of mastication, and human dentition. The tongue, the cheeks and the sensory system as well as the use of saliva play important roles in the human masticatory process. However, they are not an integral part of the given task and, therefore, not considered in this work.

The main focus is on mechanical consequences of joints and muscular system rather their anatomy. More comprehensive descriptions and illustrations of the human masticatory apparatus may be found in Gray's anatomy (Gray 1918).

Bones of skull and jaw

Figure 2-5 shows the most project relevant bones of the skull and the jaw. All medical terms have been taken from Gray's anatomy (Gray 1918).

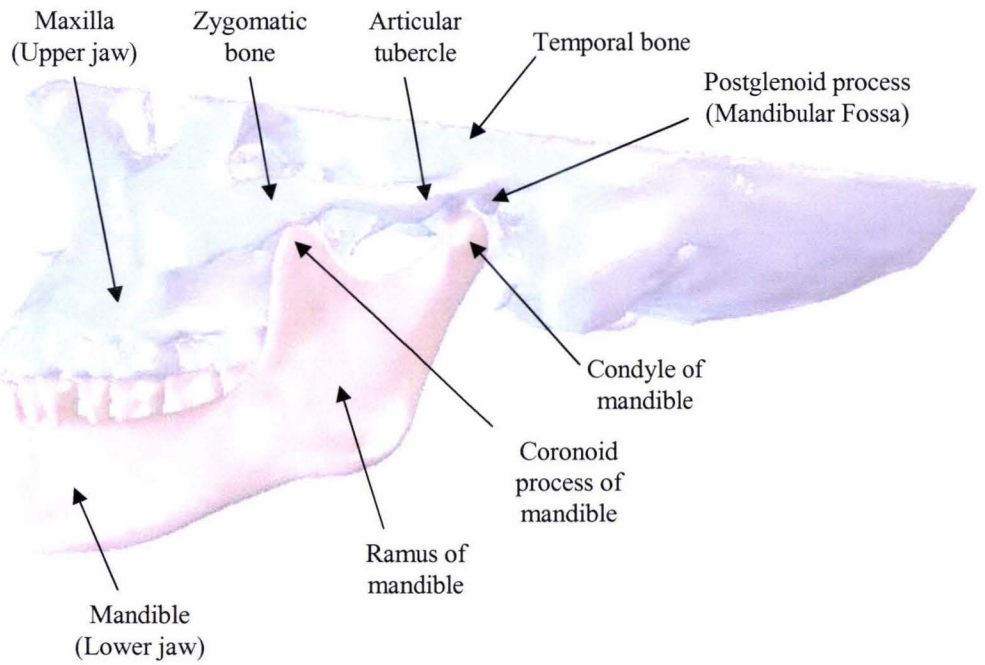

Figure 2-5. Bones of skull and mandible in lateral view.

Temporomandibular joint (TMJ)

The TMJ is literally the joint between the temporal bone of the skull and the condyle of the mandible. However, the TMJ differs completely from other joints in the human body. Classical joints, like the hip or knee joint in terms of their ball and socket construction, rotate around more or less fixed joint axes, which limit the body parts'

movement space (their DOF). The mandible instead is guided by two articular surfaces (discs), which reside on the temporal bone of the skull, involving a articular tubercle and a mandibular fossa, and on the roughly shaped condyle of the mandible (Koolstra 2002) (Figure 2-6).

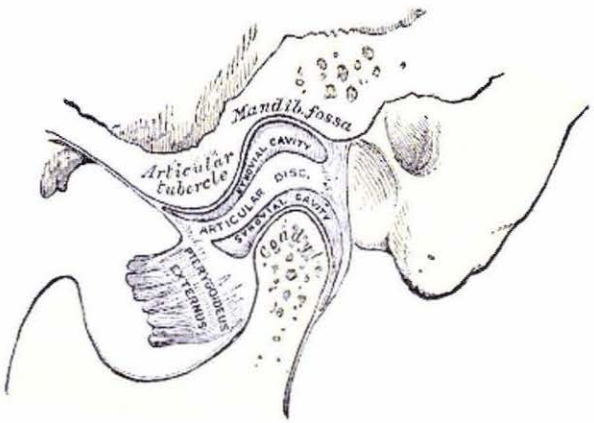

Figure 2-6. Sagittal section of the temporomandibular joint (Gray 1918).

It can be seen that the articular disc separates the condyle and the temporal bone. Furthermore, the discs enable the jaw to move along the mandibular fossa and the articular tubercle and absorb shocks to the TMJ from chewing and other movements.

As a consequence the movement in the joints is not restricted to rotations around fixed joint axes and the mandible may be able to move with six DOF. Theoretically, a rotation around an axis through any point on the mandible is possible, which makes the system kinematically redundant (Koolstra 2002). Furthermore, the incisor point may move from one point to another point along a straight path or along a detour; therefore, the number of possible paths is infinite.

Muscles of mastication

The human masticatory system consists of a big bundle of contracting muscle groups which can be divided from a classical anatomical point of view into groups of mouth-opening and mouth-closing muscles. Mouth opening muscle groups, such as the geniohyoid, the mylohyoid, and the digastric, are muscle groups with relatively small physiological cross-sectional areas (PCS). Supported by the gravity force, they are able to move the mandible away from the maxilla with high velocity, but under appliance of small forces. Mouth-closing muscle groups, such as the temporalis, the masseter and the medial pterygoid have, in comparison to the mouth-opening muscle groups, large PCS that allow movement of the mandible against the maxilla with high forces. The lateral pterygoid muscle group completes the muscular system, but can not be regarded

exclusively as a mouth-opening or closing muscle group because of its anatomy and function.

The most important muscle groups for this project are temporalis, masseter, medial and lateral pterygoid muscle groups (Figure 2-7).

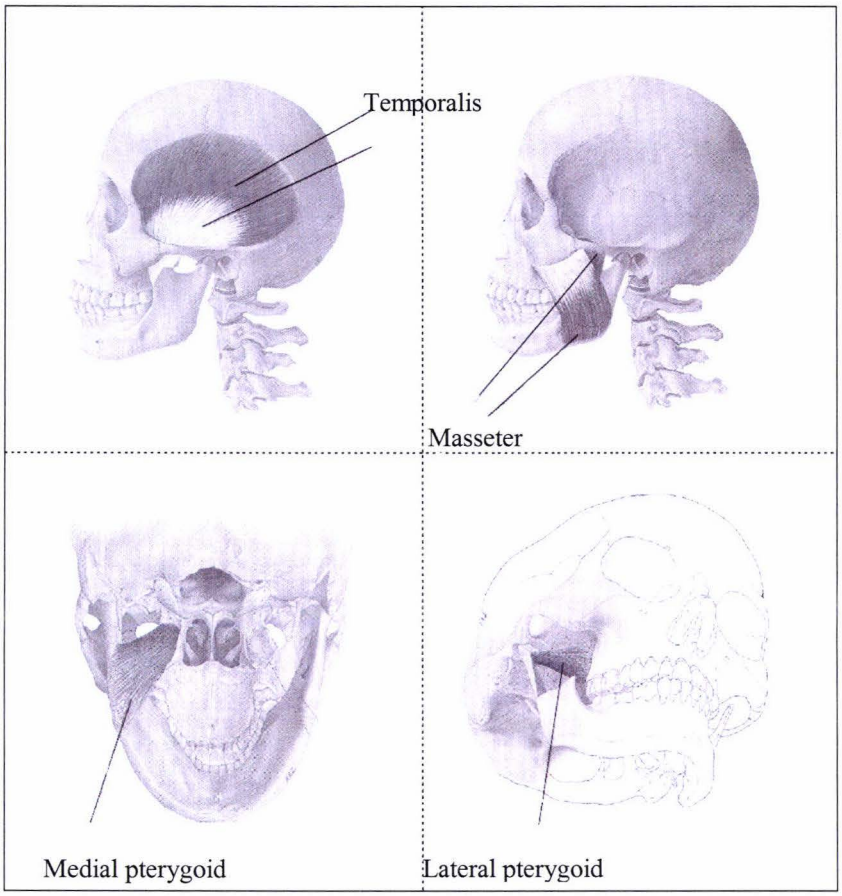

Figure 2-7. Muscles of mastication: temporalis, masseter, medial and lateral pterygoid (Hannam 1997).

Every muscle group has its own properties consistent with its location and role, but human muscle groups in general work as an ensemble, which includes muscle groups on both sides of the facial middle plane. The central nervous system controls the complex patterns. Due to spatial requirements related to the adjacent airway and alimentary tract, the masticatory system contains more muscle groups than apparently necessary to accomplish its tasks. Due to the need of constant adaptation to the texture of food between the teeth, the muscle ensemble needs to perform many tasks in various ways. This property makes the system mechanically redundant, which means that an infinite number of muscle contraction patterns can cause the same movement (Koolstra 2002).

Each muscle group is acting in a so-called muscle line of action, which is the generated resultingt muscle force vector of all submuscle groups together. However, the combination of a relatively large attachment area and the induced movement of the mandible by other muscle groups may cause the direction of the line of action of such a muscle to vary as well (Hannam 1997; Koolstra 2002).

Dentition

The dentition has an important role in human life, not just for mastication, also for speech, deglutition, and aesthetics. Two sets of teeth make their appearance at different periods of life. The first set is called milk teeth and appears during infancy whereas the second set, called permanent, also appears at an early age and may continue until old age. Basically the dentition consists of incisors, canine teeth (eyeteeth), premolars, and molars, whereas every tooth group has different tasks. The incisors work as scissors to cut or bite the food. As atrophied carnassial teeth, the canine teeth are the strongest teeth with the longest roots and coronas and have more or less sharp edges for cutting food. Premolars and molars work together, where the premolars hold the food in place and cut them roughly and the molar grind the food (Zahntechnik Braunwarth 2005).

Every tooth has a specific position in the dentition to ensure two teeth to one tooth contact, which is necessary to cut and grind the food. The alignment of the teeth in the curve of Wilson (lateral view) and the curve of Spee (posterior view) supports the grinding process in means that no abnormal forces in the mouth occur (Figure 2-8).

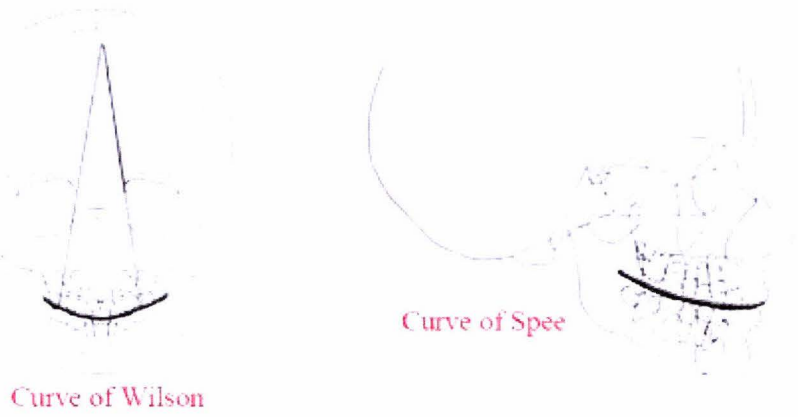

Figure 2-8. Curve of Wilson and curve of Spee (Palmer 2005).

2.3 Modelling of human chewing

Modelling the human mastication process is important due to the difficulty of conceptualising the physical processes occurring in it. Models are helpful to understand different scenarios, explore different ideas, develop novel hypotheses, and gain insight into the consequences of system variations (Hannam *et al.* 1997). Modelling of the functioning human jaw ideally requires three-dimensional representation; therefore, several research groups have been simulating mathematically and physically the human jaw movements for different purposes from biological fundamentals. This section gives a brief overview of the variety of approaches as an introduction to the challenge in developing a chewing robot.

2.3.1 Human biomechanical models

The easiest way to simulate jaw movements is to assume that biological components are rigid. In a stationary system the static equilibrium theory can be applied to calculate translations and rotations induced by input forces. This mathematical description of the human masticatory system is kinematically focused. Another way to describe the human mastication system is to use numerical solutions, such as the finite element method (FEM). In this case the mandible gets treated as a mesh of different nodes to calculate the stresses within the component systems.

The Department of Functional Anatomy at the Academic Centre for Dentistry, Amsterdam, The Netherlands, developed a six DOF dynamic biomechanical model of the human masticatory system (Koolstra and van Eijden 1995; 1996; 1997) (Figure 2-9).

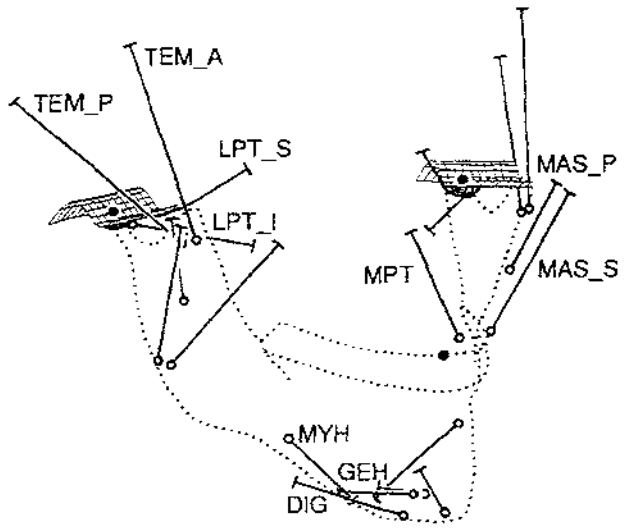

Figure 2-9. Overview of the model used by Koolstra and van Eijden (2001). Ventro-lateral view. Continuous lines: muscle lines of action. Cross-bar: muscle origin. Circle: muscle insertion. MAS S: superficial masseter, MAS P: deep masseter, MPT: medial pterygoid, TEM A: anterior temporalis, TEM P: posterior temporalis, LPT S: superior lateral pterygoid, LPT I: inferior lateral pterygoid, DIG: digastric, GEH: geniohyoid, MYH: mylohyoid. Dots: position of centre of right and left condyle and incisor point.

The model consists of a lower jaw, which is accelerated by forces and accompanying torques with respect to its centre of gravity applied by muscles, joint surfaces, bite points and ligaments (Koolstra and van Eijden 2001). The biological properties of the muscle groups, such as fibre length, sacromere lengths and PCS were obtained from van Eijden, Koolstra *et al.* (1995; 1996) and van Eijden *et al.* (1997). Their aim was to develop a suitable method for generating appropriate muscle activation patterns to simulate goal-directed jaw movements and to explore their spatial limits; however, this model cannot be used to calculate stresses within bones.

Numerical solution models use the FEM to solve the stresses and strains created by loading conditions. Most of these models are focused on the movements and stresses on the TMJ disc and articular surface during jaw opening and clenching. The Bioengineering Institute at the University of Auckland developed a new anatomically realistic generic computational model of the entire human skull and jaw that uses the FEM to calculate stresses and displacements of the masticatory system components (van Essen *et al.* 2005). The full geometry of the skull bone, and the muscles involved in the mastication have been created to allow a higher flexibility of application than any other previously created model (Figure 2-10).

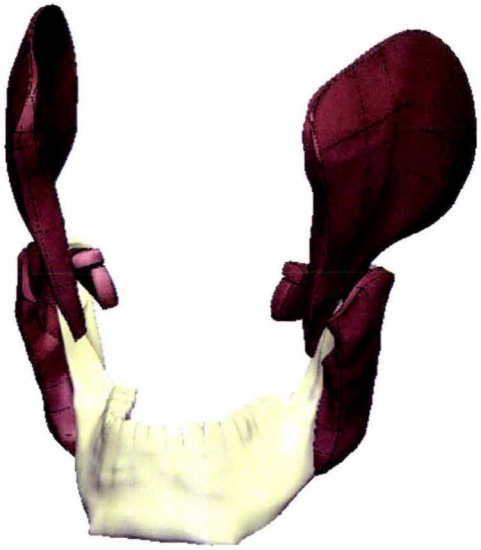

Figure 2-10. Anatomically based mathematical masticatory system with masseter, temporalis, medial and lateral pterygoid developed at the Bioengineering Institute at the University of Auckland, New Zealand (Röhrle 2005).

The School of Dentistry at the University of Otago, Dunedin, used numerical predictions to evaluate the effect of mandibular design on biomechanical masticatory effectiveness (Ichim *et al.* 2005). They used, additionally to a simple mandibular model, an anatomically detailed scan of a human mandible by computer tomography.

2.3.2 Physical models

Mathematical models can be used to simulate the masticatory system or to calculate the stresses and forces on the teeth. If one is interested in the assessment of masticatory efficiency with numerous variations in food properties, dentition, and physiological structure of jaws, or quantitative measurement of the dynamics of food texture, these models are rather inappropriate and a physical model has to be built.

To simulate human mastication, the Niigata University, Japan (Hayashi *et al.* 1999; Hayashi *et al.* 2000), and the Waseda University, Japan (Takanobu *et al.* 1993; 1998; Takanobu *et al.* 1997) have built the JSN/2A and the WJ-series (Figure 2-11), respectively. These models use, among other things a human skull model, a duralumin mandible, wire-tendon DC motors, pressure sensors and strain gauges. However, with just four DOF, these robots are not able to reproduce complete human chewing patterns in terms of both jaw motion and biting forces in three dimensional space.

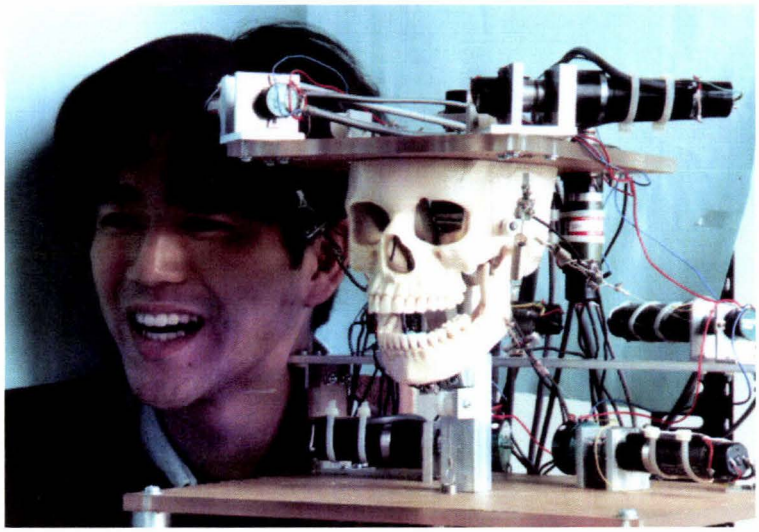

Figure 2-11. Mastication robot WJ-3 developed at the Waseda University, Japan (Takanobu *et al.* 1993).

A second issue is the restricted movement of the TMJ modelled as a fixed joint constrains the condyle to movement along a fixed trajectory, which violates the biological findings with the condylar motion envelope (Scapino 1997). Furthermore, due to nine replaced muscle groups, the system is mechanically redundant and hard to control as long as the movement path is not restricted.

Another approach uses the University of British Columbia, Canada with their speech robot (Lin 2005) (see Figure 2-12). The main aim of this project was to study the role jaw movements play in perceiving and understanding face-to-face conversation.

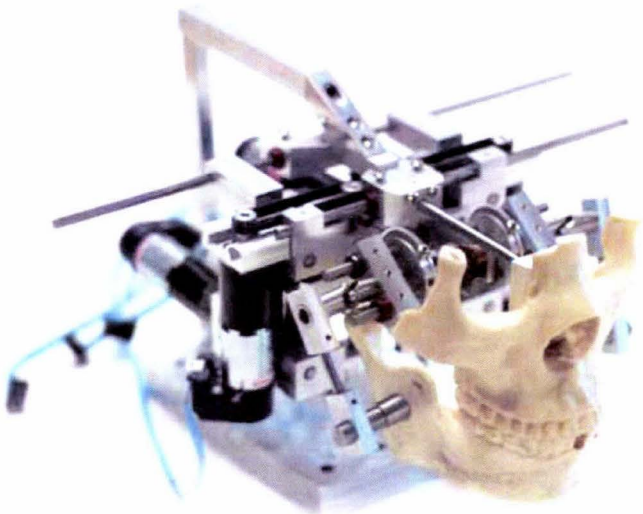

Figure 2-12. 6-DOF speech robot invented by the University of British Columbia (Lin 2005).

It is the first built robotic jaw with six DOF that uses a three DOF parallel

manipulator for each TMJ. Both parallel manipulators together allow a movement of six DOF (Flores and Fels 2005) and, therewith, the possibility of reproducing human jaw movements. However, with the attachment points of the three DOF manipulators located at the back of the jaw, it is likely that the design of this robot will not allow application of human-like chewing forces while moving.

2.4 Closure

The human masticatory apparatus in terms of design and function has been reviewed. The following conclusions were drawn:

1. The lack of published dimensions for the jaw border movement makes it impossible to use it for validating the robot movement space.
2. The use of recorded chewing trajectories in a mathematical model will give information about chewing kinematics and chewing movement space. The most useful jaw trajectory data set were developed by the Institut National de la Recherche Agronmique (INRA), Clermont-Ferrand, France (Peyron *et al.* 2002).
3. A chewing force of 260N over all contacting teeth is required.
4. The mandible can move with six DOF because of the discs in the TMJ. Therefore, the robot needs six DOF to be able to reproduce every three-dimensional jaw movement.
5. The human muscle groups can be seen as contracting actuators that are working in their line of action. Van Eijden's paper "Architecture of human jaw-closing and jaw-opening muscles" (1997) described the muscle locations and line of actions and should be used in actuator location design.
6. The human mastication system is mechanically redundant in terms of the existence of more muscle groups than necessary to describe a mandible movement. A defined robot mechanism without redundancy is desirable to make controlling of the robot possible.
7. Spatial requirements in terms of airway and alimentary tract do not have to be considered in the robot design.
8. The human dentition is so complex and important to masticatory efficiency that a replica in form of an artificial dentition is necessary.

The second part of the literature review has focused on modelling the human chewing process. Mathematical and physical models were described and the following conclusions were drawn:

1. Mathematical models of the human chewing process give information about kinematics as well as stress and strains in bones. However, the assessment of masticatory efficiency with numerous variations in food properties, dentition, and physiological structure of jaws, or quantitative measurements of dynamics of food texture is not possible. Therefore, a physical robotic model is needed.
2. An anatomically detailed model of a mandible should be used in mathematical models to implement human-like proportions.
3. A mechanism should be used, which allows a movement of six DOF, and the reproduction of the full range of motion and force application used during human chewing. To date no such chewing robot has been developed.

3 ROBOTIC JAW MODEL WITH LINEAR ACTUATION SYSTEMS

3.1 Introduction

The review of current literature identified that a complete biologically based chewing robot must be able to move with six DOF following recorded jaw trajectories. To achieve this six actuators are required. Because the human masticatory system is mechanically redundant and the muscles themselves are complicated in structure, appropriate selection of key muscle groups, identification of their attachment points and lines of action are required for the robotic design.

This chapter outlines the development of a kinematically focused mathematical model of the robotic jaw system. The model allows validation that the proposed design could achieve the required jaw trajectories, and the identification of required actuator properties (i.e., displacement change, velocity and acceleration). The required actuator forces, for reproducing human-like chewing forces, are estimated for a reasonable amount of force.

3.2 Model history

To specify design requirements for a physical robotic model, a mathematical model has to be first modelled and analysed through kinematic simulations.

Daumas *et al.* (2005) proposed a parallel mechanism concept where six linear double acting actuators attached via spherical joints to mandible and skull (ground) replace the main human muscle groups (masseter, temporalis and lateral pterygoid) (Figure 3-1). The absence of the medial Pterygoid muscle groups (see chapter 2.2.2), helps in avoiding any redundancy of the actuations, which may be introduced due to

the use of actuators in place of the muscle group. This consequently eliminates any overconstraints that prevent the mandible of the robotic model from being movable. The parallel mechanism enables a movement of six DOF according to the Kutzbach criterion (Shigley and Uicker 1980) with the mandible as a movable platform and the skull as a fixed platform. Position and orientation of the attachment points and the mandible were approximated in their size and shape according to biological properties.

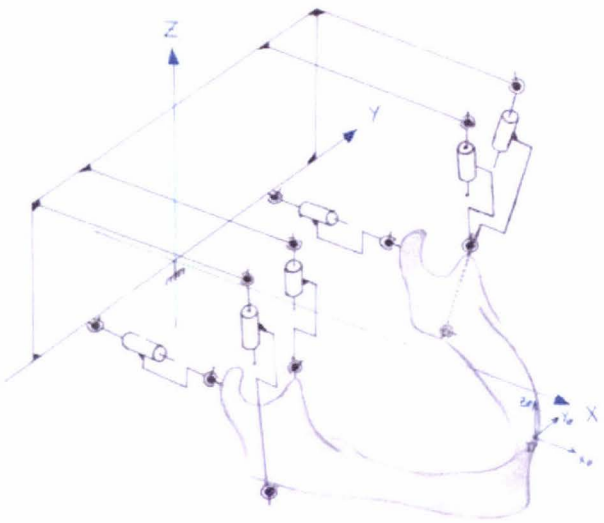

Figure 3-1. 3D kinematic sketch of a parallel mechanism for the robotic jaw (Daumas *et al.* 2005).

Extensive open-loop and closed-loop simulations for motion and control using the Matlab SimMechanics toolbox were conducted. The inputs were three time-functions of the mandible position in the X-, Y- and Z-axis, respectively and three time-functions of the mandible orientation, defined as the angles around the X-, Y- and Z-axis, respectively. The outputs of open-loop simulations showed that the jaw mechanism was modelled properly and enabled jaw movements to be reproduced. The closed-loop simulations, with each actuator controlled by a PID controller independently, showed that the jaw movements are highly coupled dynamically and their tracking is very difficult using a set of simple independent controllers.

Pap *et al.* (2005) and Xu *et al.* (2005) introduced a parallel mechanism based kinematic model of the robotic jaw in SolidWorks (Figure 3-2). In this model mandible and actuators were treated as rigid bodies with properties in their centre of gravity so that no deformation can be applied. The mandible, with its irregular shape, and the skull were approximated from a replica model. The six double acting actuators were regarded as cylindrical joints with the possibility of translation along and rotation

about their longitudinal axis and were fixed via spherical joints to the mandible and skull. This enabled the actuator to always act in the muscle line of action. The actuator attachment points and orientation were approximated from the replica model and from the Daumas's model, respectively. Various reference points on the mandible (i.e., incisor point and molar points) were used to describe chewing behaviours.

To determine the range of the reference points and to verify the mathematical model, forwards kinematics with harmonic time-functions for each actuator were implemented. Each harmonic time-function described the actuator displacement around its initial position. The results showed that the lateral, superoinferior and anteroposterior ranges of the incisor were 8, 25 and 20mm, respectively, which are within the Posselt envelope (see chapter 2.2.1).

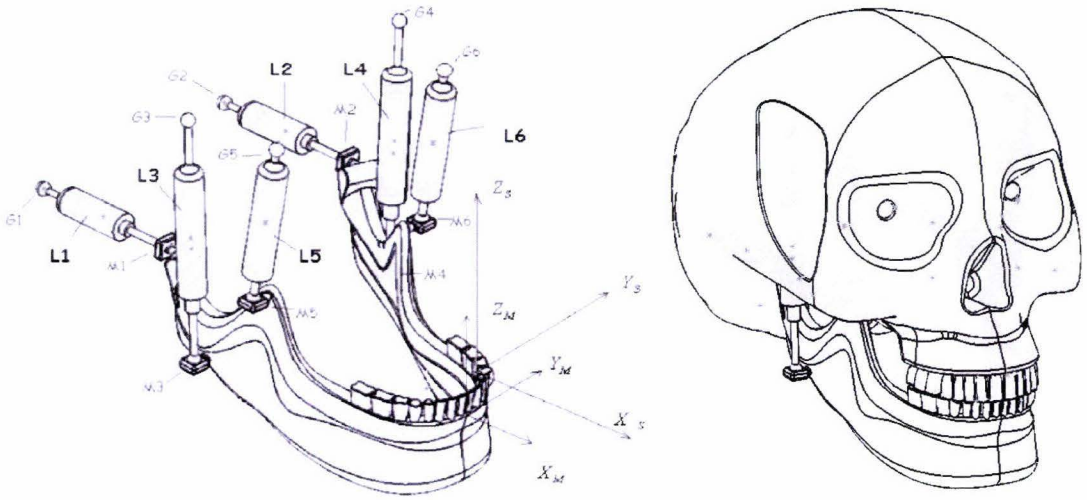

Figure 3-2. Kinematic model of the robotic jaw in SolidWorks (Pap *et al.* 2005). Ventro-lateral view (A) nomenclature and coordinate systems and (B) the robot covered by the skull. $OXYZ_S$: skull coordinate system, $OXYZ_M$: mandible coordinate system. L_x (x = 1, 2, ..., 6): actuator type. G_x (x = 1, 2, ..., 6): muscles' origin. M_x (x = 1, 2, ..., 6): muscles' insertion. *1*: right pterygoid, *2*: left pterygoid, *3*: right temporalis, *4*: left temporalis, *5*: right masseter, *6*: left masseter.

To conduct an inverse kinematics simulation, recorded chewing data in the form of displacement versus time for the incisor point of the mandible was included. The implemented data were the history of y and z coordinates, which made it necessary to constrain the mandible further. This influenced the simulation in such a way that the chewing behaviour could just be estimated. However, this performance enabled determination of actuator properties, such as maximum stroke, velocity and acceleration. These actuator properties will be useful for designing actuation systems at a later stage. Therefore, the same approach was used in the following model.

Since the robot needs similar proportions to the human system to allow

comparisons between the human system and the chewing robot, changes of the jaw structure and properties of the muscle of mastication needed to be undertaken.

3.3 Mathematical model

Based on the previous proposed model by Pap *et al.* (2005) and Xu *et al.* (2005), a mathematical model has been developed. Several changes have been made to bring the model in terms of size and spatial requirements as closely as possible to the human system.

The previously used mandible was replaced with an accurate replica of a human jaw from the School of Dentistry at the University of Otago, New Zealand that was obtained from a human cadaver by computer tomography (Ichim 2005). This ensures that human-like proportions were used. A bone density of 900 kg/m^3 was used for the mandible mass.

Furthermore, the position, orientation and length of the actuators were actualised. Several research teams have focused on the architecture of masticatory muscle groups to provide a set of data that can be used in biomechanical modelling of the masticatory system (Koolstra and van Eijden 1997; Osborn and Baragar 1985). Van Eijden *et al.* (1997) registered in eight cadavers, the three-dimensional coordinates of the muscle attachment sites to determine the spatial position of the line of action of various masticatory muscle groups. They differentiated *inter alia* in superficial and deep masseter, anterior and posterior temporalis, and inferior and superior lateral pterygoid. Table 3-1 shows the right side attachment coordinates and the total muscle length of the main masticatory muscle groups.

Since, in the proposed robotic model, there was just one actuator representing one muscle group, the following simplifications to enable the use of van Eijdens coordinates were carried out:

- An actuator length in the closed-mouth position was specified for each muscle group.
- A resultant muscle line of action was calculated from the sub muscle group lines of action for each muscle group using force-vector-analysis.
- The insertion coordinates were specified according to shape of the mandible.
- New origin coordinates were determined by using the calculated resultant muscle line of action, muscle length and the new specified insertion

coordinates.

All simplifications are explained in the following sections.

Table 3-1. Attachment coordinates[1] (*mm*) and total muscle length[2] of the main masticatory muscle groups. Source: Adapted from van Eijden *et al.* (1997).

	Origin			*Insertion*[3]			*Total muscle length (mm)*
	x	*y*	*z*	*x*	*y*	*z*	
Masseter							
Superficial part	37.9	-52.3	-9.1	6.2	-44.9	-40.7	45.6
Deep part	30.7	-43.4	-7	16.7	-44.6	-26	25.3
Temporalis							
Anterior part	27.7	-48	34.4	26.4	-42.6	-14.8	49.7
Posterior part	-6.2	-59.3	32.3	22.4	-45.8	-8.8	52.2
Lateral pterygoid							
Inferior part	19.4	-24.3	-14.9	-0.9	-46.1	-3.1	32.6
Superior part	23	-24.2	6.4	0.2	-44.1	0.5	31.3

Actuator length in the closed-mouth position

To ensure a maximum movement range of the mandible, the total muscle length of the biggest submuscle group was used as reference actuator length in the closed mouth position. This meant that the actuator length for masseter, temporalis and lateral pterygoid were 45.6mm, 52.2mm and 32.6mm, respectively.

Muscle lines of action

The direction of each action line can be defined by three angles: the frontal angle (FA) is the sharp angle between the action line and the vertical axis in the frontal plane, the sagittal angle (SA) is the sharp angle between the action line and the vertical axis in the sagittal plane, and the horizontal angle (HA) is the sharp angle between the action line and the vertical axis in the horizontal plane. The projection of the action lines in the frontal and sagittal plane are shown in Figure 3-3 and the angles of each action line are listed in Table 3-2.

[1] Positive x, y, and z axes are pointing, respectively, forward, left, and upward.

[2] Actuator length for closed mouth position.

[3] Insertion: mandibular attachment.

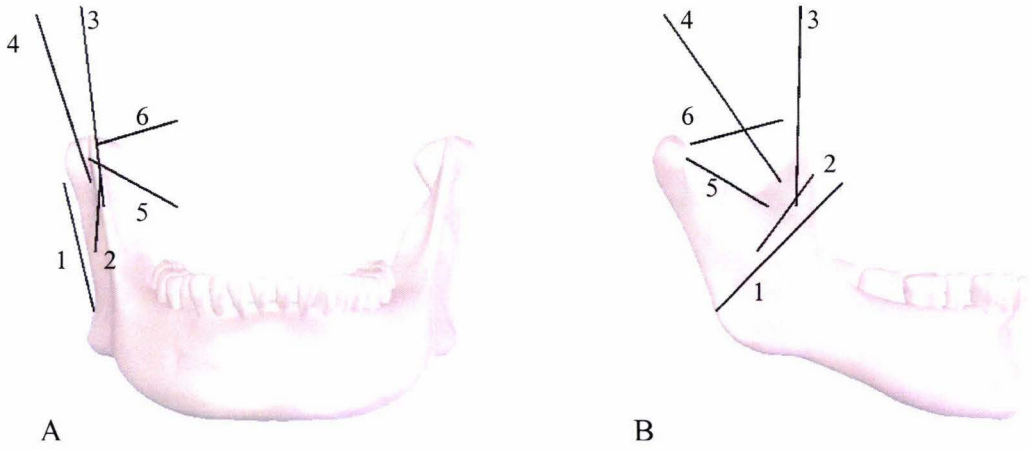

Figure 3-3. Spatial orientation of the sub-muscle action lines. The action lines are projected on the frontal (A) and sagittal (B) planes. 1: superficial masseter; 2: deep masseter; 3: anterior temporalis; 4: posterior temporalis; 5: inferior lateral pterygoid; 6: superior lateral pterygoid.

Table 3-2. Measured frontal, sagittal and horizontal angles of masseter, temporalis and lateral pterygoid sub-muscle groups for the closed mouth position.

	Frontal angle (°)	Sagittal angle (°)	Horizontal angle (°)
Masseter			
Superficial part	13.2	45.1	13.1
Deep part	3.6	36.4	4.9
Temporalis			
Anterior part	6.3	1.5	76.5
Posterior part	18.2	34.8	25.3
Lateral Pterygoid			
Inferior part	61.6	59.8	47
Superior part	73.5	75.5	41.1

To calculate the resulting line of action, the force that each sub-muscle group can produce must be known. According to the magnitude of the muscle force, the representing vector length in the force-vector-diagram will be calculated. Thus, if a muscle can produce a maximal force of 100 *N*, the representing vector length is 100 *mm*. Van Eijden *et al.* (1997) used an index expressing the muscle's so-called absolute muscle force. It can be determined by multiplying relative force by a factor proportional to the PCS. In general, the maximum force that can be produced by 1 cm^2 PCS is about 30 *N* (van Eijden 2005). Thus, if a muscle has a PCS of for example 10 cm^2, the maximal force it can produce is 10 x 30 *N* = 300 *N*. Table 3-3 lists the PCS and the calculated maximal muscle forces for each sub-muscle group.

Table 3-3. Physiological cross-sectional areas as outlined in van Eijden *et al.* (1997) and calculated maximal forces of masseter, temporalis and lateral pterygoid sub-muscle groups.

	Physiological cross-sectional area (cm^2)	*Maximal force (N)*
Masseter		
Superficial part	6.82	204.6
Deep part	3.49	104.7
Temporalis		
Anterior part	7.7	231
Posterior part	5.55	166.5
Lateral Pterygoid		
Inferior part	2.82	84.6
Superior part	0.95	28.5

Because the proposed model combines the sub-muscle groups together as one actuator, the data calculated from van Eijdens measurements must be combined.

To calculate a resultant line of action out of two sub-muscle lines of action in one plane, a diagram such as Figure 3-4 was used.

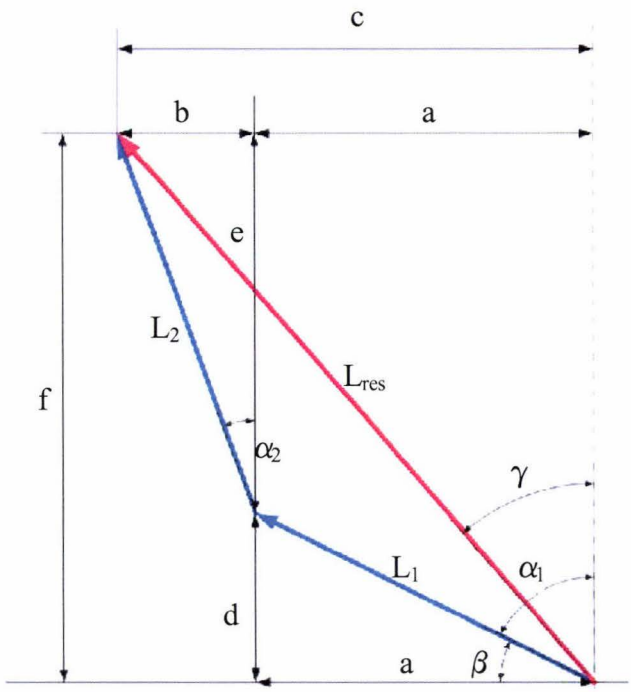

Figure 3-4. Force-vector-diagram to determine the orientation of the resulting muscle lines of action.

L_1 and L_2 represent the vector lengths and α_1 and α_2 the angles in the plane (frontal or sagittal) as outlined in Table 3-2 and Table 3-3, respectively. Both vector lengths L_1 and L_2 are drawn with their orientation α_1 and α_2 to determine the resultant vector orientation γ. The resultant vector orientation γ represents the new actuator orientation in the respective plane. To calculate the corresponding factors *a* to *f*, the Pythagorean

Theorem was used. The resultant muscle orientation was obtained in the frontal and the sagittal plane to determine the actuator orientation in x, y, and z coordinates (see Table 3-4).

Table 3-4. Determined frontal and sagittal angle of the masseter, temporalis and lateral pterygoid muscle group.

	Frontal angle (°)	Sagittal angle (°)
Masseter	9.95	42.02
Temporalis	11.28	13.61
Lateral Pterygoid	72.47	70.84

Muscle insertion coordinates

The insertion coordinates of each muscle group were estimated according to the shape of the scanned mandible and the attachment location of each muscle group found in Hannam (1997). The insertion coordinates are presented in Table 3-5 in the mandible coordinate system.

Muscle origin coordinates

To determine the origin coordinates of each muscle group, the calculated resultant muscle line of action (Table 3-4) and the muscle insertion coordinates were used. Table 3-5 lists the determined attachment coordinates and the total length for all three muscle groups. Figure 3-5 shows the updated model in SolidWorks (see Figure 3-2 as comparison).

Table 3-5. Determined attachment coordinates[4] (*mm*) and total actuator length[5].

	Origin			*Insertion*			*Total actuator length (mm)*
	x	*y*	*z*	*X*	*y*	*z*	
Masseter							
right side	48.2	-52.5	-14.7	18	-44.7	-47.7	45.6
left side	48.2	52.5	-14.7	18	44.7	-47.7	45.6
Temporalis							
right side	13.3	-53.2	51.8	25.6	-43	2	52.2
left side	13.3	53.2	51.8	25.6	43	2	52.2
Lateral Pterygoid							
right side	21.5	-17.5	-12.4	-0.9	-41.1	-3.1	32.6
left side	21.5	17.5	-12.4	-0.9	41.1	-3.1	32.6

[4] Attachment coordinates are presented in the skull coordinate system ($OXYZ_S$).

[5] Actuator length for closed mouth position.

The SolidWorks simulation model can be found in appendix B on the enclosed DVD.

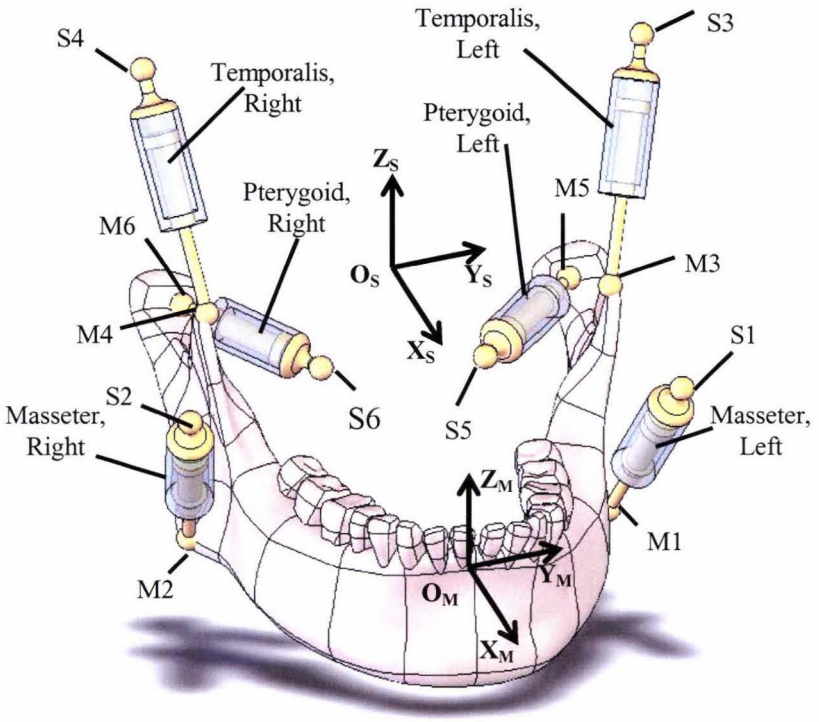

Figure 3-5. Mathematical model of the robotic jaw. S_i and M_i ($i=1,2,..,6$) denote the muscles' origin and insertion location on the skull and the mandible, respectively. The two main coordinate systems are: the skull system or, $OXYZ_S$, and the mandible system or, $OXYZ_M$.

This model has two main coordinate systems, the skull system or, $OXYZ_S$, which is fixed to the skull, and the mandible system or, $OXYZ_M$, which is fixed to the mandible and differs from the skull system by $[x\ y\ z]^T = [78.85\ 0\ -41.87]^T$.

3.4 Kinematic simulations

The developed kinematic model allows two types of simulations: forward kinematics for generating the masticatory patterns by specified actuations of the actuators and inverse kinematics for finding the actuation patterns required for a desired masticatory pattern. To simulate the kinematic model, COSMOS/Motion incorporated in SolidWorks was used. Due to the fact that the mathematical model was kinematically focused, friction was not included.

3.4.1 Initial state of the mandible

The initial state of the mandible was the starting position for every simulation. To describe the initial position in $OXYZ_S$ coordinates, the three reference points IP, LCP, and RCP were used. Their coordinates are given in Table 3-6.

Table 3-6. Reference points for describing the initial position in the skull system (unit: *mm*).

Reference points	*Initials*	x_S	y_S	z_S
Incisor point	IP	78.85	0	-41.87
Left condylar point	LCP	-0.9	41.1	-3.1
Right condylar point	RCP	-0.9	-41.1	-3.1

3.4.2 Reference points

To fully characterise the chewing patterns and the mandibular movement, at least three reference points on the mandible have to be defined. Therefore, the following reference points were chosen: incisor point (IP), left molar point (LMP), right molar point (RMP), left condylar point (LCP), and right condylar point (RCP). The points are shown in Figure 3-6 and their coordinates in the mandibular coordinate system $OXYZ_M$ are given in Table 3-7.

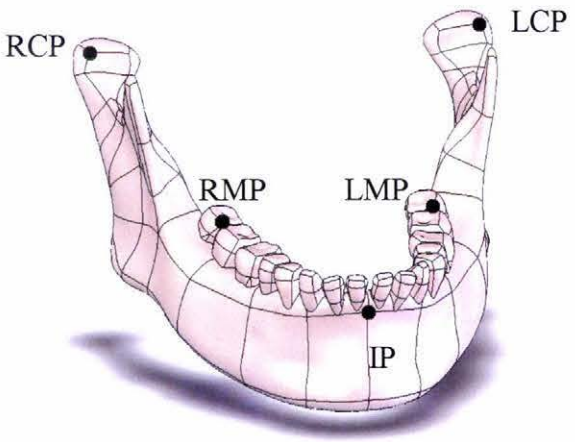

Figure 3-6. Mandible reference points in SolidWorks.

Table 3-7. Reference points' coordinates in the mandible system (unit: *mm*).

Reference points	*Initials*	x_M	y_M	z_M
Incisor point	IP	0	0	0
Left molar point	LMP	-35.2	26.37	12.26
Right molar point	RMP	-35.2	-26.37	12.26
Left condylar point	LCP	-79.75	41.1	38.77
Right condylar point	RCP	-79.75	-41.1	38.77

3.4.3 Chewing trajectory

To calculate the displacement change, velocity, acceleration, and angular movement of each actuator while chewing, a chewing trajectory has to be implemented at the incisor point. To fully describe a masticatory movement on a mandible, three reference points with their x, y, and z coordinates versus time or one reference point with its x, y, and z coordinates versus time and the angular movement about the x, y, and z axis of the mandible have to be implemented.

For the following simulation, measured data from the record of the masticatory sequence of a subject, provided by Institut National de la Recherche Agronmique (INRA), Clermont-Ferrand, France, were used (see chapter 2.2.1). The only available data were the time-history of y and z coordinates of the incisor point.

To have a nearly complete description of the masticatory sequence, an anteroposterior movement and the angular movement of the mandible about all three axes had to be defined. From Figure 2-2, a sagittal movement in the angle of about 35° can be estimated. However, Buschang *et al.* (2000) showed that the sagittal movement was in an angle between 0° to 15°. For the following simulation, a sagittal angle of 15° as middle value was chosen to represent the anteroposterior movement and calculated according to Figure 3-7, where α represents the sagittal angle, a the inferior-superior movement, and b the anteroposterior movement in every time step.

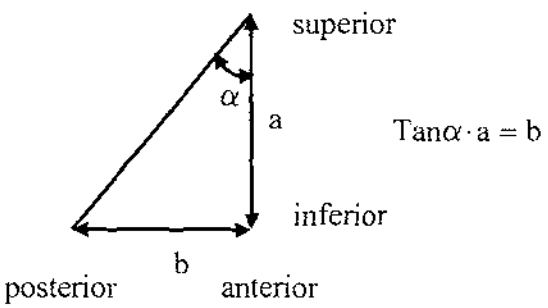

Figure 3-7. Diagram for calculating anteroposterior movements in sagittal plane.

To define the mandibular angular movement during chewing, some simplifications needed to be applied to the model. It was expected that the mandibular angular movement about the x axis would be around 0° and it was, therefore, set to zero in the simulation. To copy mandibular angular movement about the y and z axis, the middle point of the two reference points LCP and RCP at $[x\ y\ z]^T = [-79.75\ 0\ 38.77]^T$ in the mandible system $OXYZ_M$ were guided laterally through the origin of the skull system

($OXYZ_S$) in the sagittal plane and the angular movement about the y and z axis was set free. With these specifications it was possible to perform masticatory movements mimicking human chewing and, therefore, to specify the requirements to build a chewing robot.

3.4.4 Results

Screenshots of the simulation results with trace paths of the reference points shows Figure 3-8 in horizontal, frontal, and sagittal plane and a recorded movie in frontal view can be found in appendix B on the enclosed DVD.

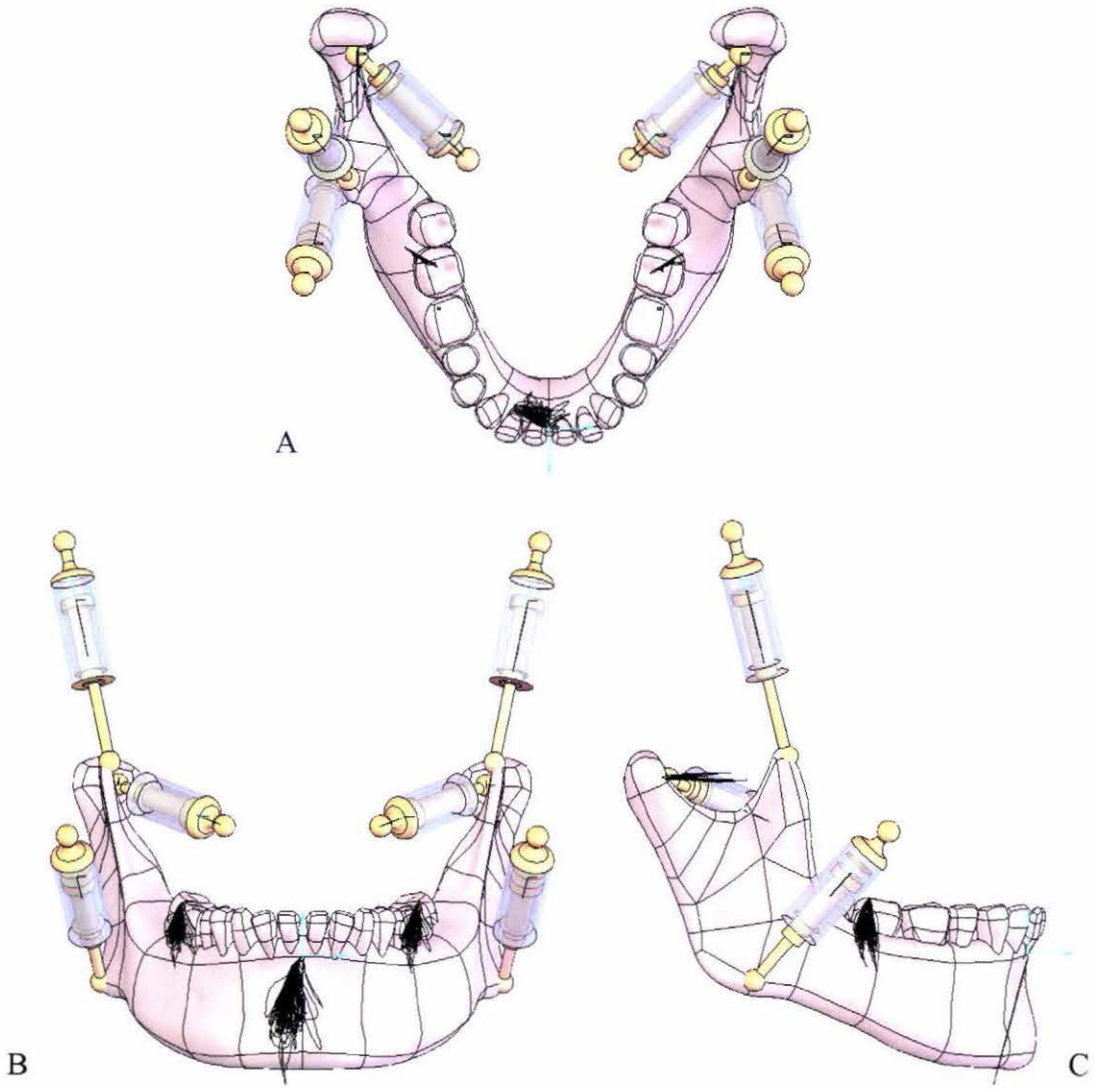

Figure 3-8. SolidWorks model with IP, LMP, RMP, LCP and RCP trajectories: (A) horizontal view, (B) frontal view, and (C) sagittal view.

It can be seen that the performance of the incisor point is within the Posselt envelope

(Posselt 1957). It is the approximated jaw movement described by Klineberg (2005), and is similar to a human masticatory movement (Anderson *et al.* 2002). The condylar movements match the clinical and biomechanical findings (Nakajima *et al.* 2001; Scapino 1997). These simulation results verified that the chosen chewing trajectory is suitable to determine actuator properties.

The time-functions for displacement, velocity, and acceleration for each of the six actuators that must be followed to reproduce the given chewing pattern, were obtained. As an example, the time-functions for the right temporalis actuator are given in Figure 3-9.

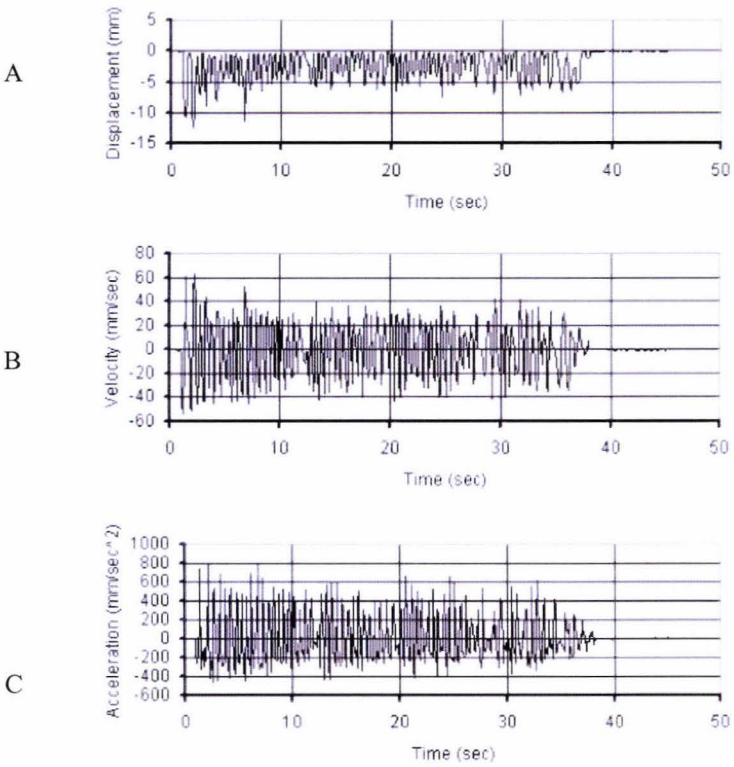

Figure 3-9. Right temporalis actuation required for the specified chewing pattern: (A) displacement, (B) velocity, and (C) acceleration.

It can be seen that in the first chewing cycles the biggest values for displacement, velocity and acceleration occur. The high velocity and acceleration values appear while the mouth is opening rather than closing. Additional to the time-functions, the angular movements about x, y, and z axis, which result out of the actuator attachment points and the masticatory movement, were recorded. Table 3-8 shows the maximum values of each time-function for all six actuators and their maximum angular movement.

Table 3-8. Determined actuator properties and their maximum angular movement in frontal and sagittal planes (maximum values).

	Actuator properties			Angular movement	
	Displacement (*mm*)	Velocity (*mm/s*)	Acceleration (mm/s^2)	Frontal angle (°)	Sagittal angle (°)
Masseter					
Left	7	40	500	2	4
Right	7	40	600	5	6
Temporalis					
Left	17	75	1000	4	12
Right	14	65	1000	4	8
Lt. Pterygoid					
Left	8	40	400	14	17
Right	8	40	450	10	15

Furthermore, the maximum angular movements for the mandible in sagittal and horizontal planes were 24° and 6°, respectively. These factors were used to define the spatial requirements for the mandible.

3.5 Actuator forces

To fully describe human chewing behaviour, the actuators have to produce enough force to apply the right amount of chewing force between the teeth. The chewing force between maxilla and mandible molars results in the interaction of all six applied muscle forces and the food properties. The maximum chewing force can be applied at two different stages: at the first breaking of the food between the molars or during the grinding process. The required muscular forces are not only dependent on the mandibular opening angle, but also on the chewing side.

The calculation of actuator forces is complicated due to the number of muscle groups and has to be done in three-dimensional space. Osborn and Baragar (1992) simplified the three-dimensional jaw model into a two-dimensional model in the sagittal plane. They studied the directions of the joint forces used to maintain the human jaw in three-dimensional static equilibrium.

A similar approach was used to calculate the actuator forces. Figure 3-10 shows the mathematical model in the sagittal and frontal view with applied muscle force directions and occlusal force position and direction.

It was assumed that the mandible was balanced at point A so that a hinged movement about an axis through this point in y direction could be applied. In this case, the lateral pterygoid actuator absorbed the arising reaction forces, which occurred

through the masseter and temporalis actuators and the occlusal force. It should be noted that the rotations about the x and z axis were set to zero.

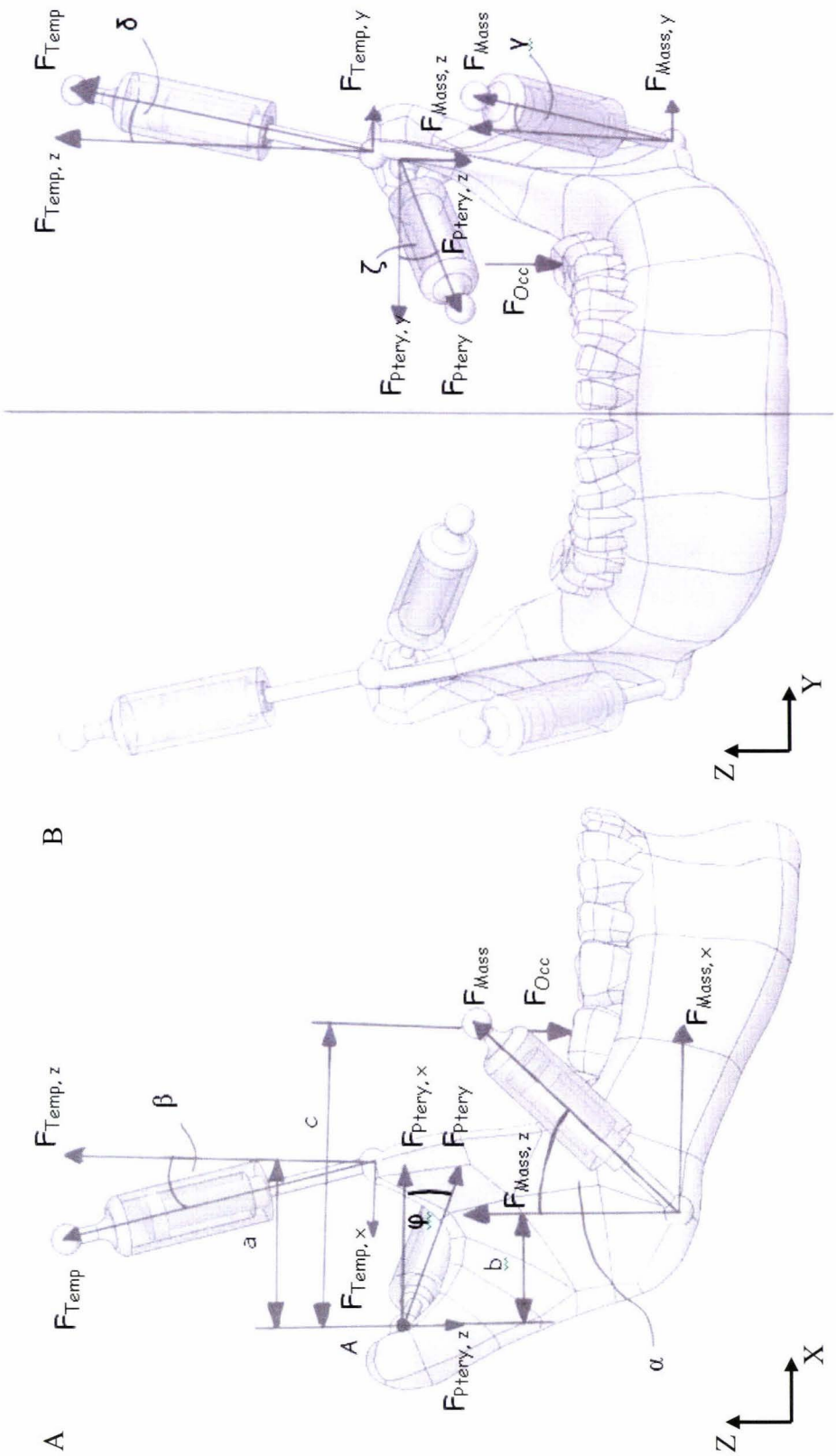

Figure 3-10. Two-dimensional model of the jaw with applied muscle and occlusal forces: (A) sagittal view and (B) frontal view.

If the mandible with its applied forces is balanced about the hinge axis through point A, the following equilibrium equation can be formulated:

$$\left(-F_{Temp,z}\cdot a\right)+\left(-F_{Mass,z}\cdot b\right)+\left(F_{Occ}\cdot c\right)=0\,, \tag{3.1}$$

where $F_{Temp,z}$ is the force [N] of the temporalis muscle group actuator in z direction, $F_{Mass,z}$ is the force [N] of the masseter muscle group actuator in z direction, F_{Occ} the occlusal force [N], and a, b and c are the normal distances [m] to the hinge axis. This equation is indetermined through the two unknown factors $F_{Temp,z}$ and $F_{Mass,z}$. By using the Pythagorean Theorem, $F_{Temp,z}$ and $F_{Mass,z}$ can be transformed into equations (3.2) and (3.3):

$$F_{Temp,z}=F_{Temp}\cdot\cos\beta\cdot\cos\delta\,, \tag{3.2}$$

and

$$F_{Mass,z}=F_{Mass}\cdot\cos\alpha\cdot\cos\gamma\,, \tag{3.3}$$

respectively, where α and β are the angles in the sagittal plane, and δ and γ the angles in the frontal plane. To obtain F_{Mass} and F_{Temp}, one solution could be to establish a relationship between them both. Van Eijden *et al.* (1997) published the PCS for various masticatory muscle groups (see chapter 3.3), where the PCS indicates, as a factor, the muscle force. In chapter 2.2.2 it was stated that the medial pterygoid, even though not used in the mathematical model, plays a major role in the masticatory process. The medial pterygoid muscle group supports the masseter muscle group in protruding the mandible. Since the masseter and medial pterygoid muscle groups have the biggest normal distance to the hinge axis, they can produce the highest force between the teeth. According to van Eijden *et al.* (1997), the masseter and pterygoid muscle groups can produce a combined maximum force $F_{Mass+M.Pterv}$ = 489.3 N. With a maximum temporalis muscle group force F_{Temp} = 309.3 N, the relational factor f_r [-] between both forces can be described with equation (3.4) as 0.81:

$$f_r=\frac{F_{Temp}}{F_{Mass}}\,. \tag{3.4}$$

Substituting equations (3.2) to (3.4) into equation (3.1), gives equation (3.5):

$$\left(-\left(\frac{0.81\cdot\cos\beta\cdot\cos\delta}{\cos\alpha\cdot\cos\gamma}\right)\cdot F_{Mass,z}\cdot a\right)+\left(-F_{Mass,z}\cdot b\right)+\left(F_{Occ}\cdot c\right)=0\,. \tag{3.5}$$

This equation can now be converted into equation (3.6) by rearrangement:

$$F_{Mass,z}=\frac{\left(F_{Occ}\cdot c\right)}{\left(\left(\frac{0.81\cdot\cos\beta\cdot\cos\delta}{\cos\alpha\cdot\cos\gamma}\cdot a\right)+b\right)}\,. \tag{3.6}$$

With a = 0.0265 m, b = 0.0189 m, c = 0.047 m, α = 42.02 °, β = 13.61 °, δ = 11.28 °, γ = 9.95 °, and F_{Occ} = 260 N, equation (3.6) gives $F_{Mass,z}$ = 260.78 N and by using equation (3.3), F_{Mass} = 356.38 N. Application of equations (3.4) and (3.2), gives F_{Temp} = 288.67 N and $F_{temp,z}$ = 275.15 N, respectively.

Furthermore, the reaction forces, which occur at the hinge axis, have to be produced by the lateral pterygoid. To obtain these forces, the horizontal equilibriums in x and y directions can be developed with equations (3.7) and (3.8):

$$F_{Ptery,x} + F_{Mass,x} - F_{Temp,x} = 0\,, \tag{3.7}$$

and

$$-F_{Ptery,y} + F_{Mass,x} + F_{Temp,x} = 0\,, \tag{3.8}$$

With equations (3.7) ,(3.9), and(3.10),

$$F_{Mass,x} = F_{Mass,z} \cdot \sin\alpha\,, \tag{3.9}$$

$$F_{Temp,x} = F_{Temp,z} \cdot \sin\beta\,, \tag{3.10}$$

gives $F_{Ptery,x}$ = 109.81 N. With equations (3.8), (3.11), and (3.12),

$$F_{Mass,y} = F_{Mass,z} \cdot \sin\gamma\,, \tag{3.11}$$

$$F_{Temp,y} = F_{Temp,z} \cdot \sin\delta\,, \tag{3.12}$$

gives $F_{Ptery,y}$ = 98.88 N. By using the Pythagorean Theorem, the actuator force F_{Ptery} for the lateral pterygoid muscle group can be calculated with equation (3.13):

$$F_{Ptery} = \sqrt{\left(F_{Ptery,y} \cdot \cos\xi\right)^2 + \left(F_{Ptery,x}\right)^2}\,. \tag{3.13}$$

With ζ = 17.53 °, gives F_{Ptery} = 144.74 N.

Since all these values were calculated for the actuators on the left and right side of the mandible, F_{Mass}, F_{Temp} and F_{Ptery} have to be divided by two, so that the required actuator forces are $F_{Mass,a}$ = 178.19 N, $F_{Temp,a}$ = 144.34 N and $F_{Ptery,a}$ = 72.37 N.

Due to the fact that this method of calculation approximated the values, a required force of F = 200 N for all actuators was chosen. It should be noted that safety factors have to be considered in the calculations to obtain the needed actuator torque (see chapter 4). This ensures that higher performances are achievable from the actuator.

3.6 System design requirements

Maintenance and control of the chewing robot should be designed as simply as possible. Therefore, an entire uniform actuation system by means of its transmission and energy system is suggested. To ensure that this uniform actuation system can perform in the required way, the maximum values of linear velocity, linear acceleration, angular movement, linear force and system accuracy out of all actuation systems were chosen. Only the muscle lengths in the closed mouth position and the maximum displacement changes were considered individually. Table 3-9 lists the required actuator properties.

Table 3-9. Required actuator properties.

	Minimum required values
Length (*mm*)	
Masseter	45.6
Lateral Pterygoid	32.6
Temporalis	52.2
Displacement (*mm*)	
Masseter	10
Lateral Pterygoid	10
Temporalis	20
Linear velocity (*mm/s*)	75
Linear acceleration (mm/s^2)	1000
Linear force (*N*)	200
Angular movement (°)	20
Displacement accuracy (*mm*)	0.1

Additional to these actuator properties, the angular movements of the mandible were obtained. Table 3-10 lists these system properties.

Table 3-10. Maximum angular movements of the mandible in sagittal and horizontal plane.

Name	Values (°)
Sagittal angle	24
Horizontal angle	6

3.7 Closure

In this chapter, a kinematically focused mathematical model for reproducing human chewing behaviours has been introduced. Six double acting actuators replaced the masseter, temporalis and lateral pterygoid main muscle groups. With their connection to the skull and the mandible via spherical joints, mandibular movement with six DOF became possible. The implementation of one chewing trajectory at the incisor point of the mandible has made the determination of kinematical actuator and system properties possible. Furthermore, the actuator forces for an estimated chewing force have been calculated.

The obtained actuator properties allowed the development of a physical actuation system.

4 LINEAR ACTUATION SYSTEM FOR CHEWING ROBOT

4.1 Introduction

This chapter outlines the development of one linear actuator, which will represent one muscle group in a physical chewing robot according to the previously introduced mathematical model. The linear actuator used a ball spindle to convert rotary movement, implemented by a geared brushless DC-motor, into linear movement following the shortening and expanding of main muscle groups. An optical encoder attached to the motor shaft allowed position and velocity control of the actuator according to the needs of human chewing behaviour. The actuator design was carried out in consideration of the specified actuator properties in Table 3-9.

4.2 Actuator design

An appropriate actuation system can be found in different ways. Firstly, off-the-shelf solutions can be reviewed and their specifications compared with the required actuator properties. If there is no actuation system that satisfies the set requirements, self-specified design solutions can be carried out in a second step.

4.2.1 Principles

Mechatronic actuators normally have an energy input and a mechanical output, (e.g., displacement, velocity or force), and use different kinds of auxiliary energies from electrical, pneumatic or hydraulic supplies.

The most important kinds of auxiliary energy are electricity, hydraulics, and pneumatics. Depending on these energies, the following actuator principles can be

distinguished:

- electromechanical actuators;
- fluidic actuators;
- unconventional actuators.

After examining other actuator types, the principle of an electromechanical actuator with a rotary motor seemed to be the most suitable for the given task.

Electromechanical actuators

In most cases, electrical energy already exists and is easy accessible. Because of its unproblematic generation in combination with transmission capability, it provides high flexibility. The signal conversion and the actuator drive can be operated with the same kind of energy which gives a big advantage over other kinds of energy. The electrical auxiliary energy is usually given preference, except in case of very high actuating forces, high temperatures or for safety reasons.

Electromechanical actuators can primarily be divided into translatory (electromagnets, linear motors) and rotary (electrical motors) transformers.

Voice coil actuators belong to the group of electromagnets and are electrical-magnetic-mechanical converters. They are direct drive, limited motion devices that utilise a permanent magnet field and coil winding (conductor) to produce a force that is proportional to the current applied to the coil. The standard voice coil actuator, consisting of a coil assembly and a permanent magnet assembly, must be supported and aligned to allow relative movement. Due to the physics of the coil-magnet system, the overall dimensions of such an actuator are too big for the given requirements.

The operation mode of a linear motor enables such a system to be used in a vertical axis. Due to its non-contact operation, if the motor is shut down, any load that has been held vertically would be allowed to fall down.

Electrical motors are usually used in conjunction with a gear mechanism in order to generate a different rotary or linear motion. Many linear actuators on the market are using this principle in combination with a spindle system.

Fluidic actuators

The oil and air flow of hydraulic and pneumatic circuits, respectively, have to be provided by an additional auxiliary energy supply. The advantages are high position forces and robust and compact actuator drives with a very high power-weight ratio for

hydraulic systems, robust design and a reliable and safe operation for pneumatic systems. Disadvantages are that both systems have limited positioning accuracy and, because of the complex system structure, also have some expensive servo-components, e.g., valves.

Unconventional actuators

The commonality of the unconventional actuators is the fact that they use certain physical phenomena, e.g., piezoelectric actuators, thermo-bimetal actuators, magnetostrictive actuators, memory metal actuators, and electrochemical actuators. However, all of these actuators can just provide small displacement changes and, therefore, are not suitable to satisfy the given requirements.

4.2.2 Actuator concept

Extensive research to find an electromechanical off-the-shelf actuator was carried out. Actuators, small in their dimensions, fast in their speed, and strong in their torque, were hard to find on the market. The specifications of various off-the-shelf products were compared with the required actuator properties listed in Table 3-9. For example, the 21000 Series Size 8 linear actuators from Haydon Switch & Instrument, Inc., Waterbury, USA. This actuator is small in size, but can not produce enough torque and speed. The same issue occurred with the Series 7220 from ACD & D Limited. Other actuators, such as the M-05 series from Nook Industries Inc., Cleveland, USA, or the S12 series from Power Drives Inc., Pittsburgh, USA, can produce enough torque, but are too slow and too big in their dimensions.

No actuator met the set requirements. Therefore, various design concepts for a linear actuator were carried out. Two actuator concepts seemed realisable. First, it seemed possible to design an actuator, where the gearbox and the motor are mounted sideways to the ball screw unit. This concept is widely used for linear actuators and, therefore, became the first design. The second concept chosen was an actuator based on a slider-crank mechanism. This mechanism does not provide movement as the muscle line of action, but has the advantage that it is a simple design. The following list gives an overview of the main ideas considered:

Double ball screw system. This concept involves a double ball screw system with two bi-directional threads (Figure 4-1).

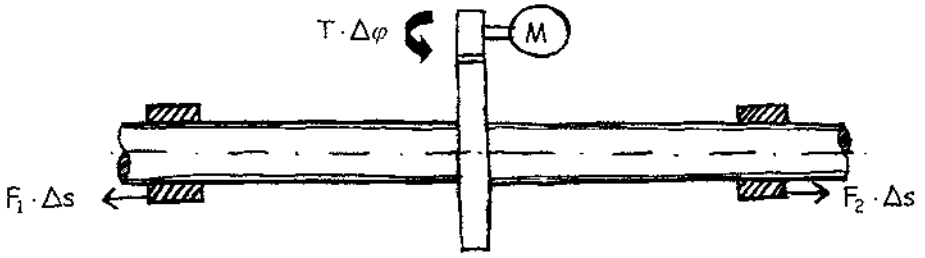

Figure 4-1. Double ball screw system.

If the spindle is turning in one direction, then both ball nuts will move either away from or to the gear. This design comes with various problems. The gearbox and the motor have to be fixed to the spindle so that the actuator is able to orientate in the needed position. To fix the actuator to the mandible and skull, two spherical joints could be mounted on both ball nuts. However, the outer diameter of the spherical joint could cause problems due to spatial requirements.

Reverse linear motion by using two racks and one pinion. This solution involves two racks and a pinion (Figure 4-2).

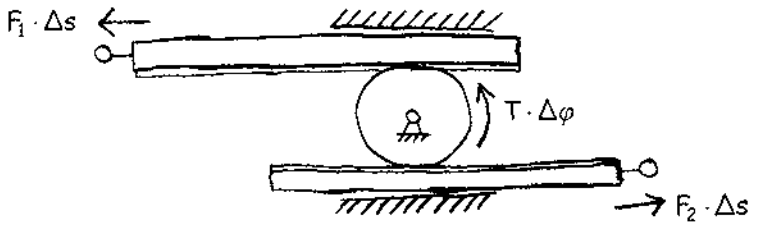

Figure 4-2. Reverse linear motion using two racks and one pinion.

While the pinion is turning in one direction both racks are either moving away or together. One problem is to ensure that both racks are parallel to each other. Another issue is the angle between the line of action and the racks. This has to be considered when developing control algorithms of the actuator. The required torque can be achieved using a gearbox.

Ball screw, gearbox and motor in line. This concept represents the most commonly used actuator. Motor, gearbox and ball screw system are in line (Figure 4-3). However, due to this arrangement, the overall length of the actuator will be bigger than required. A spherical joint, mounted on the ball nut, and a universal joint, mounted to the motor end, could be used for mounting the actuator to the mandible and skull. The gearbox and motor could be positioned parallel to the spindle shaft. This

would shorten down the actuator size.

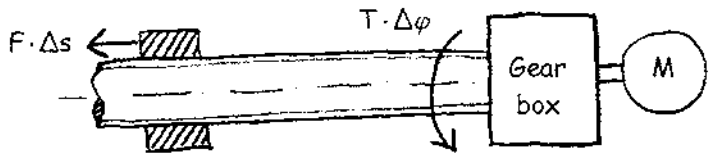

Figure 4-3. Concept with ball screw, gearbox and motor in line.

2-bar linkage mechanism. This concept involves a 2-bar linkage and a two pinion transmission system (Figure 4-4). Both bars are fixed to each other with a hinge joint. The motor and the smaller pinion are fixed on the middle of a bar, whereas the bigger pinion is connected to the second bar in the hinge. The big gear and the second bar move together. One drawback can be vibrations due to the motor weight.

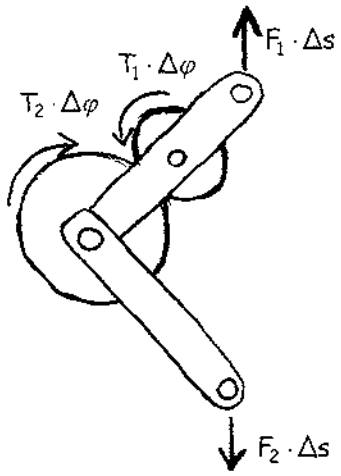

Figure 4-4. 2-bar linkage mechanism driven by two pinions.

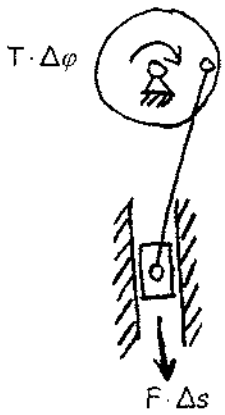

Figure 4-5. Slider-crank mechanism.

Slider-crank mechanism. This concept works like the piston in a car engine (Figure 4-5). The slider is fixed via a coupler to a crank. By turning the crank, the slider moves up and down along the guideway. For the robotic jaw, the slider would be fixed on the mandible. However, this is a simple solution, but does not work in the muscle line of action.

5-bar linkage mechanism. This solution is elaborate. The 5-bar linkage mechanism was originally developed for vertical dunking of a blender (Figure 4-6). For a certain rotation of the crank, the blender makes a vertical movement. However, this concept is hard to realise through the needed three-dimensional movements.

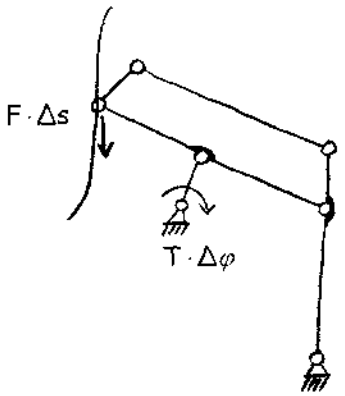

Figure 4-6. 5-bar linkage mechanism

4.3 Actuator control

The purpose of the chewing robot was to reproduce human chewing behaviour, which can be achieved by implementing actuator patterns by either following time-frame displacement changes or specific equations developed for a certain purpose. The basic structure for actuator controlling can be open-loop or closed-loop. With an open-loop-controlled actuator, position and velocity change is possible. However, this kind of actuator provides no feedback to control the mechanical output. Disturbances or properties like introduced forces, friction, backlash, or electromagnetic hysteresis can influence the mechanical output and because of the need of high precision, a feedback-controlled actuator is necessary. This feedback can be achieved by using a sensor in form of an encoder attached to the rear motor shaft. Figure 4-7 shows the basic system of an feedback-controlled electromechanical actuator, which is also called servo-system (Isermann 2003).

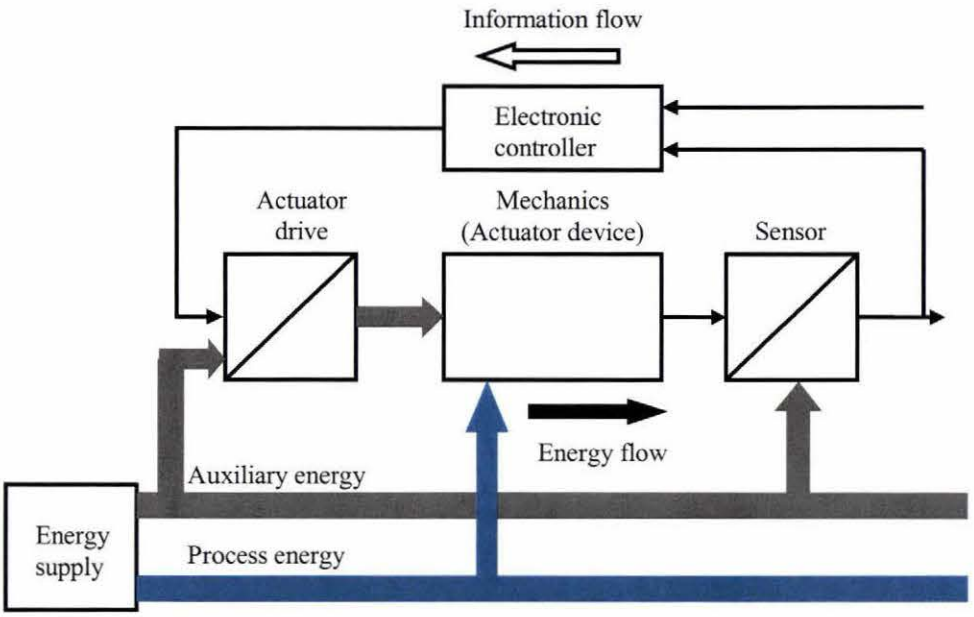

Figure 4-7. Electromechanical actuator as feedback controlled mechatronic system. Adapted from Isermann (2003).

The Galil motion control system allows the independent control of all six actuators by using one DMC-1860 series motion control card and two amplifiers AMP-19540 (Figure 4-8).

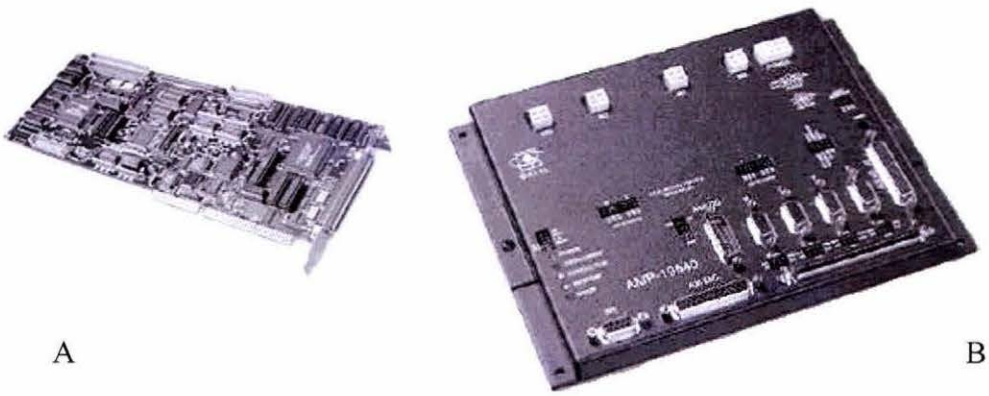

A B

Figure 4-8. (A) DMC-1860 series motion control card and (B) amplifier AMP-19540.

The control card provides motor control for standard servo motors, brushless servo motors and stepper motors. Therefore, one of these actuation systems had to be used. The amplifier can drive four servo motors with up to 500 Watt each.

4.4 Physical design

This section discusses the development of the physical design of a ball screw

unit linear actuator. The development process is distinguished into the following steps:

- Choosing a ball screw system,
- Gear ratio and motor selection, and
- Joint system design.

The SolidWorks model of the linear actuator, SolidWorks drawings and datasheets can be found in appendix C on the enclosed DVD. The printed drawings are enclosed in appendix F.

4.4.1 Ball screw system

An electrical motor generates rotary motion, which does not match the needed linear motion and will not satisfy the rotational velocity and torque requirements of the actuator device. These demands can be satisfied by using a ball screw system and a gear reduction, which enable the actuator to perform in the desired motion and conversion. To choose motor and gear ratio according to the specified performances of the actuator, the transmission system had to be defined first.

Rotary movement can be transformed into linear movement by using a ball screw system. The lead of the ball screw influences the required torque and motor speed. Various parameters, such as permissible rotational speed, permissible axial load, and static safety factor, need to be verified to ensure that the ball screw system is able to handle the required performance.

To satisfy the set requirements in chapter 3.6, the ball screw system needed to be as short as possible, precise, and have a stroke of at least 20 *mm*. The smallest ball screw (ball spindle) system found was the BNK 0401-3 system produced by THK Co., Ltd., Japan (Figure 4-9). The ball screw system consists of a spindle and a ball nut. The spindle has a 4 *mm* thread, a 1 *mm* lead, a 20 *mm* stroke, and a total length of 77 *mm*. The spindle is on one end fully supported with a mounting unit and on the other end free.

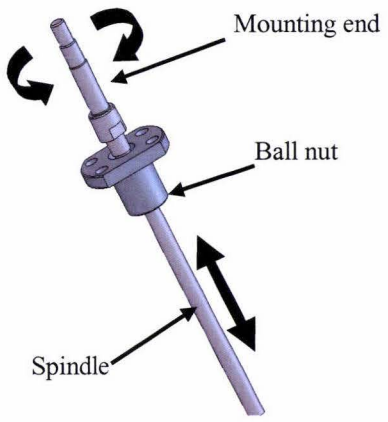

Figure 4-9. Ball screw system BNK 0401-3, THK Co., Ltd., Japan.

To verify that the right ball screw system was selected, the maximum rotational speed and the maximum axial load on the spindle shaft needed to be calculated. The

following calculations were carried out according to the standard ball screw system catalogue of THK Co., Ltd. (THK 2005).

The maximum rotational speed $n_{Spindle}$ [min^{-1}] of the spindle can be determined with equation (4.1):

$$n_{Spindle} = \frac{v_{Spindle} \cdot 60}{R}, \tag{4.1}$$

where $v_{Spindle}$ is the required linear velocity [m/s] and R the lead of the spindle [m] With, $v_{Spindle} = 0.075$ m/s (Table 3-9) and $R = 0.001$ m, gives $n_{Spindle} = 4500$ min^{-1}.

The maximum axial force F_{axial} [N] can be described as sum of the maximum constant force F [N] and the force due to acceleration F_{acc} [N],

$$F_{axial} = F + F_{acc}. \tag{4.2}$$

According to Newton's second law, F_{acc} is:

$$F_{acc} = m_F \cdot a, \tag{4.3}$$

where m_F represents the mass induced due to force [kg] and a the linear acceleration [m/s^2]. m_F can be described with equation (4.4):

$$m_F = \frac{F}{g}, \tag{4.4}$$

where g is the acceleration due to gravity [m/s^2]. With, $F = 200$ N (Table 3-9) and $g = 9.81$ m/s^2, gives $m_F = 20.39$ kg. With equation (4.3) and $a = 1$ m/s^2 (Table 3-9), gives F_{acc} =20.39 N. According to equation (4.2), F_{axial} = 220.39 N.

In the next step, the chosen ball screw system had to be verified in consideration of the permissible rotational speed and the permissible axial force.

Permissible rotational speed

The permissible rotational speed of the spindle should be determined based on the critical speed and a so-called DN value. At high speeds, the spindle causes resonance due to the characteristic frequency of the spindle shaft, which may make operation impossible. The shaft speed should be therefore set at a level below the resonant point (critical speed). The permissible rotational speed n_{cs} based on the critical speed [min^{-1}] can be calculated with equation (4.5):

$$n_{cs} = \frac{60 \cdot \lambda_1^2}{2 \cdot \pi \cdot l_u^2} \cdot \sqrt{\frac{E \cdot 10^3 \cdot I}{\gamma \cdot A}} \cdot f_{s1}, \tag{4.5}$$

where λ_1 is the mounting coefficient [-], l_u the unsupported spindle length [mm], E the Young's modulus [N/mm^2], I the geometrical moment of inertia [mm^4], γ the specific

density [kg/mm^2], A the screw-shaft cross sectional area [mm^2] and f_{s1} the safety factor [-]. The moment of inertia I can be calculated with equation (4.6):

$$I = \frac{\pi}{64} \cdot d_k^4, \tag{4.6}$$

where d_k is the screw shaft thread min diameter [mm]. With, $\lambda_1 = 1.875$, $l_u = 54\ mm$, $E = 2.06 \cdot 10^5\ N/mm^2$, $d_k = 3.4\ mm$, $\gamma = 7.85 \cdot 10^{-6}\ kg/mm^3$, $f_{s1} = 0.8$, all values according to the THK catalogue (THK 2005), equation (4.5) gives $n_{cs} = 40104.6\ min^{-1}$.

The permissible rotational speed n_{DN} based on the DN value [min^{-1}] can be calculated with equation (4.7):

$$n_{DN} = \frac{x_{DN}}{d_{BC} \cdot 60}, \tag{4.7}$$

where x_{DN} is the DN value [mm/s] and d_{BC} is the ball centre diameter [mm]. With, $x_{DN} = 70{,}000\ mm/s$ (THK 2005), $d_{BC} = 4.15$ mm, it gives $n_{DN} = 16867.47\ \text{min}^{-1}$.

Since, n_{cs} and n_{DN} are bigger than the requested value of $n_{Spindle}$, the chosen ball screw system suits the requirements.

Permissible axial force

Where an axial force is exerted on the ballscrew, the screw shaft should be determined in consideration of buckling force and the permissible tensile-compressive force that can exert yielding stress on the shaft. The ballscrew should not buckle under the maximum compressive force applied in its axial direction. The buckling force F_b [N] can be calculated with equation (4.8):

$$F_b = \frac{\lambda_2 \cdot \pi^2 \cdot E \cdot I}{(l_u)^2} \cdot f_{s2}, \tag{4.8}$$

where λ_2 is a mounting coefficient [-] and f_{s2} the safety factor [-]. With, $\lambda_2 = 0.25$, $f_s = 0.5$, all values according to the THK catalogue (THK 2005), gives a buckling force $F_b = 571.71\ N$. In this case, the maximum force F_{axial} is below the buckling force F_b.

The permissible tensile-compressive force F_{tc} [N] of the screw shaft can be calculated with equation (4.9):

$$F_{tc} = \delta \cdot \frac{\pi \cdot (d_k)^2}{4}, \tag{4.9}$$

where δ is the permissible tensile-compressive stress [N/mm^2]. With, $\delta = 147\ N/mm^2$,

equation (4.9) gives F_{tc} = 1334.64 *N*. However, the maximum force F_{axial} is below the permissible tensile-compressive force of F_{tc}. So the ball screw met the actuator force requirements.

Static safety factor

If the ball screw receives an excessive load or significant impact (e.g., crashing of food) localised permanent deformation develops between the raceway and balls. This deformation can hinder the movement of the ball screw. Therefore, the basic static load rating C_{0a} [*N*] was taken as the permissible axial load. C_{0a} is normally equal to the permissible static axial load of the ball screw. However, according to the operation conditions of the actuator, a static safety factor f_{s3} [-] was considered. Therefore, the permissible static axial load $F_{a,max}$ can be described with equation (4.10):

$$F_{a,.\max} = \frac{C_{0a}}{f_{s3}}. \tag{4.10}$$

With, C_{0a} = 420 *N* and f_{s3} = 2, according to THK (2005), equation (4.10) gives $F_{a,max}$ = 210 *N*. The permissible static axial load $F_{a,max}$ is bigger than the required static axial load F = 200 *N*.

These calculations verify that the chosen ball screw system was appropriate for the set requirements. With the assumption that the actuator was a prototype and some modification will be done in the future, the service life of the ball screw system was not calculated.

4.4.2 Motor, gear reduction, and encoder selections

Motor type selection

To find a suitable motor-gear reduction combination, the maximum required torque and speed of the motor need to be determined for various gear reductions to make comparisons possible. The equations used to make these calculations are presented in the following sections. A number of factors had to be considered before making the final choice of a brushless DC-Servomotor from Minimotor SA, Switzerland.

- Maximum motor torque

In order that the actuator will operate under different loadings induced while

chewing, the calculations for the motor torque were divided in torque under constant load T_c [Nm], torque under acceleration T_{acc} [Nm] and torque under deceleration T_{dec} [Nm]. All three determined values needed to be smaller than the maximum possible torque of the chosen motor.

The torque T_c under constant load [Nm] can be calculated with equation (4.11):

$$T_c = \frac{1}{i} \cdot T_{spindle}, \tag{4.11}$$

where $T_{Spindle}$ is the required torque on the spindle shaft before gear reduction [Nm] and i represents the reduction ratio [-] between , $n_{driving}$ [-], the rotation on the motor shaft, and n_{driven} [-], the rotation on the spindle shaft,

$$i = \frac{n_{driving}}{n_{driven}}. \tag{4.12}$$

$T_{Spindle}$ can be described with equation (4.13):

$$T_{Spindle} = \frac{F \cdot R}{2 \cdot \pi \cdot \mu} \cdot f_{s1}, \tag{4.13}$$

where μ is the spindle efficiency [-] and f_{s1} the safety factor [-]. With, F = 200 N, μ = 0.95 (95%), f_{s1} = 1.5, gives $T_{Spindle}$ = 0.05 Nm. The safety factor f_{s1} was included to ensure that the motor could handle unexpected torques and to consider the unknown efficiency factor of the gear drive.

The torque T_α throughout acceleration [Nm] can be described with the rotational form of Newton's second law:

$$T_\alpha = I_e \cdot \alpha, \tag{4.14}$$

where I_e is the entire mass moment of inertia [kgm^2] about the longitudinal axis through the mass centre and α the angular acceleration [s^{-2}]. I_e can be calculated with equation (4.15):

$$I = I_F \cdot \left(\frac{1}{i}\right)^2 \cdot 10^{-6} + I_{Spindle} \cdot \left(\frac{1}{i}\right)^2 \cdot 10^{-6} + I_{driven} \cdot \left(\frac{1}{i}\right)^2 + I_{driving}, \tag{4.15}$$

where I_F is the mass moment of inertia [$kgmm^2$] due to the axial force F_{axial}, $I_{Spindle}$ the mass moment of inertia of the spindle [$kgmm^2$], I_{driven} the entire mass moment of inertia [$kgmm^2$] of the driven parts and $I_{driving}$ the entire mass moment of inertia [$kgmm^2$] of the driving parts. The mass moments of inertia I_{driven} and $I_{driving}$, such as of gears, do not have a big impact on the calculations and were, therefore, not included. Using equation (4.4), the mass moment of inertia due to F_{axial} can be calculated with equation (4.16):

$$I_F = m_F \cdot \left(\frac{R}{2 \cdot \pi} \right)^2 \tag{4.16}$$

and was I_F = 0.52 $kgmm^2$. To calculate the mass moment of inertia of the spindle $I_{Spindle}$, the spindle shape was approximated with a cylinder shape. Therefore, $I_{Spindle}$ can be described with equation (4.17):

$$I_{Spindle} = \frac{m_c \cdot d_c^2}{8}. \tag{4.17}$$

where m_c is the cylinder mass [kg] and d_c the cylinder diameter [mm]. The cylinder mass m_c can be calculated with equation (4.18):

$$m_c = \frac{\pi \cdot d_c^2 \cdot l_c \cdot \gamma}{4}, \tag{4.18}$$

where l_c is the spindle length [mm]. With, d_c = 5 mm (approximated thickness), l_c = 77 mm (according to the spindle datasheet), it gives $I_{Spindle}$ = 0.04 $kgmm^2$.

The torque T_{acc} under acceleration is the sum of torque T_c under constant speed [Nm] and torque T_α trough acceleration [Nm],

$$T_{acc} = T_c + T_\alpha, \tag{4.19}$$

and the torque under deceleration T_{dec} is the difference of both,

$$T_{dec} = T_c - T_\alpha. \tag{4.20}$$

- Maximum speed

The maximum speed n_{max} of the motor [min^{-1}] is equal to the product of the gear reduction i [-] and the maximum speed $n_{Spindle}$ of the spindle [min^{-1}],

$$n_{\max} = i \cdot n_{Spindle}. \tag{4.21}$$

Thus, the factors T_c, T_{acc}, T_{dec}, and n_{max} are dependent on the gear reduction i. Therefore, the required torque values are listed for various gear reductions in Table 4-1. A high variety of motor types exist. The most commonly used motors, the DC-motors (Direct current motors), are either mechanically (brushed) or electronically (brushless) commutated (Isermann 2003). Both motor types have good response characteristics and small volumes and weights. However, mechanical commutation limits the maximum motor current during standstill as well as at high rotational velocities. Electronically commutated motors do not have these problems due to the absence of a mechanical commutator.

The comparison between the required properties in Table 4-1 and various

motor datasheets of brushed and brushless DC-motors showed that the brushless Minimotor DC-servomotor 2036 024 B with a torque of 4.9 *mNm* best suited the requirements.

Table 4-1. Calculation results for the linear actuator.

	Symbol	Unit	Solution									Chosen specification
			1	2	3	4	5	6	7	8	9	
Gear Reduction	i	-	100	75	50	25	20	15	10	5	1	**10.2**
Mass moment of inertia	J	kgm^2	6.E-11	1.E-10	2.E-10	9.E-10	1.E-09	2.E-09	6.E-09	2.E-08	6.E-07	5.E-09
Torque due to acceleration	T_A	Nm	6.E-08	1.E-07	2.E-07	9.E-07	1.E-06	2.E-06	6.E-06	2.E-05	6.E-04	5.E-06
Torque (constant speed)	T_c	mNm	0.5	0.7	1.0	2.0	2.5	3.3	5.0	10.0	50.0	4.9
Torque (acceleration)	T_{acc}	mNm	0.5	0.7	1.0	2.0	2.5	3.3	5.0	10.0	50.6	4.9
Torque (deceleration)	T_{dec}	mNm	0.5	0.7	1.0	2.0	2.5	3.3	5.0	10.0	49.4	4.9
Speed	n_{max}	min^{-1}	420000	315000	210000	105000	84000	63000	42000	33600	25200	16800

Gear reduction selection

The next step involved selection of the right transmission system with the gear reduction $i = 10$.

The motor could have been mounted in line, parallel or inclined to the ball screw system. The in line mounting would have increased the actuator length and was, therefore, not chosen.

For parallel and incline mounting, the most commonly used principles are gear drives and belt drives.

Gears drives can transmit rotary motion with spur gears (parallel shafts) and bevel gears (inclined shafts). The larger gear wheel is often called spur gear and the smaller the pinion. Gears can be distinguished between spur gears, gears with axial teeth, and helical gears, gears with helical teeth. To produce a large gear ratio, several stages of wheel pairs are required. Other possibilities are planetary gear drives and harmonic drives. These drives could be ordered with the needed gear ratio. However, the motor input shaft and the output shaft of the planetary gear drive are inline. To achieve parallel mounting, an additional transmission system would be necessary. Harmonic drives are widely used for high-precision motions with a gear ratio between 50 and 320. In addition, these drives require an additional transmission system to shift the motor and ball screw system from being in line. The additional transmission system would require a 1:1 gear ratio. However, to ensure that the motor shaft and the

spindle shaft are far enough apart, two wheels with big diameter would be needed. This would increase the overall dimensions of the actuator and maybe interfere with other parts.

Belt drives consist of a pair of wheels (pulleys) and a belt for the transmission of the motion and are usually used to overcome big distances. However, the gear ratio is limited to about three to maintain an adequate arc of contact (Isermann 2003). Therefore, at least three stages are necessary. Another disadvantage is the low nominal input speed with less than 6000 rotations per minute.

After considering all these facts, a custom made gearbox with spur gears was considered the most suitable solution. To achieve a reduction of $i = 10$, three gear stages are recommended to ensure that the overall dimensions of the gear system is not too big. The entire gear reduction i [-] can be described as the product of the three stage reductions i_x ($x = 1, 2, 3$) [-],

$$i = i_1 \cdot i_2 \cdot i_3, \tag{4.22}$$

and each stage reduction can be calculated with equation (4.23):

$$i_x = \frac{n_1}{n_2} = \frac{t_2}{t_1}, \tag{4.23}$$

where n_1 and t_1 are the speed and the teeth of the pinion gear, and n_2 and t_2 of the spur gear, respectively.

The company SDP/SI, USA, offers a good range of gears. When choosing the pinion and spur gear, it has to be ensured that the same module m_x (x = 1, 2, ..., 6) [-] is present. To fulfil the needed gear reduction, the following gears were chosen:

- A1B1MY04010 ($m_1 = 0.4$, $t_1 = 10$);
- A1B1MY04024 ($m_2 = 0.4$, $t_2 = 24$);
- 2x S10T05M020S0303 ($m_{3,5} = 0.5$, $t_{3,5} = 20$);
- S10T05M034S0303 ($m_4 = 0.5$, $t_4 = 34$);
- S10T05M050S0303 ($m_6 = 0.5$, $t_6 = 50$).

Figure 4-10 shows the positioned gears (1-6) in the gear drive, where No. 1 points to the gear on the motor shaft and No. 6 to the gear on the spindle shaft. Combining equation (4.22) and (4.23), gives the gear ratio as 10.2 using equation (4.24):

$$i = \frac{t_2}{t_1} \cdot \frac{t_4}{t_3} \cdot \frac{t_6}{t_5}. \tag{4.24}$$

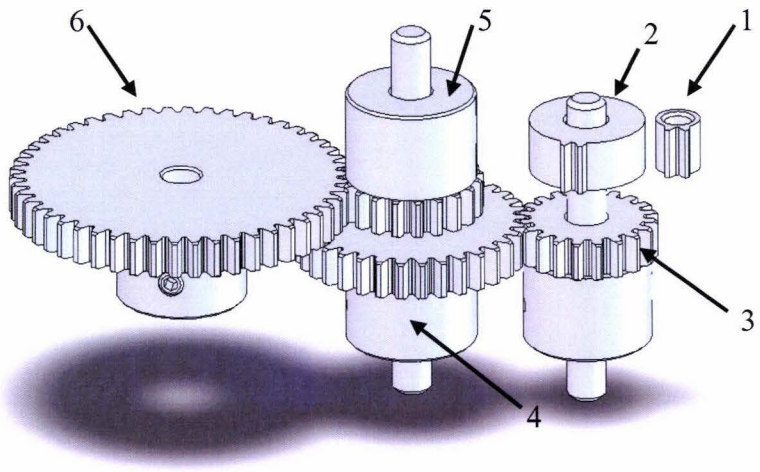

Figure 4-10. Gear reduction system for the linear actuator in SolidWorks.

Due to the fact that the new gear ratio is slightly different to the previously chosen one, the motor torques and speed have to be recalculated to verify that the motor can achieve the requirements with the new gear ratio. With equation (4.12) to (4.22), T_c, T_{acc}, and T_{dec} were around 4.9 mNm and n_{max} was 42840 min^{-1}. The comparison of these values with Figure 4-11 showed that the data points (n_{max}, T) were lying inside the recommended area for continuous operation.

Thus, the chosen motor suited the requirements.

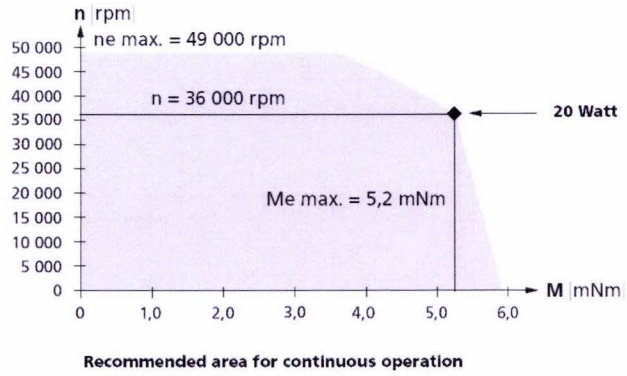

Figure 4-11. Motor performance diagram for brushless DC-Servomotor 2036 024 B from Minimotor SA, Switzerland.

Encoder selection

The required encoder resolution B [-] (counts per turn) can be described with equation (4.25):

$$B = \frac{R \cdot i}{f}, \tag{4.25}$$

where f is the minimum required feed accuracy [mm] of the entire system. With,

$f = 0.1\ mm$, it gives a required encoder resolution $B = 102$. The incremental shaft encoder HEDS 5540 A from Minimotor SA, Switzerland, has a resolution of $B = 500$. This shaft encoder in combination with the brushless DC-Servomotor 2036 024 B enabled the indication and control of both, shaft velocity and direction of rotation as well as for positioning.

4.4.3 Actuator assembly

The actuator was designed according to the calculations and the selected parts in this chapter. The design process included the following steps and will be explained in more detail:

- Choosing a spindle support unit,
- Designing a gearbox,
- Testing the gearbox for deformation, and
- Designing the joint systems.

Figure 4-12 shows the actuator assembly as a SolidWorks model and the manufactured actuator. Further pictures of the physical model are enclosed in appendix C on the enclosed DVD.

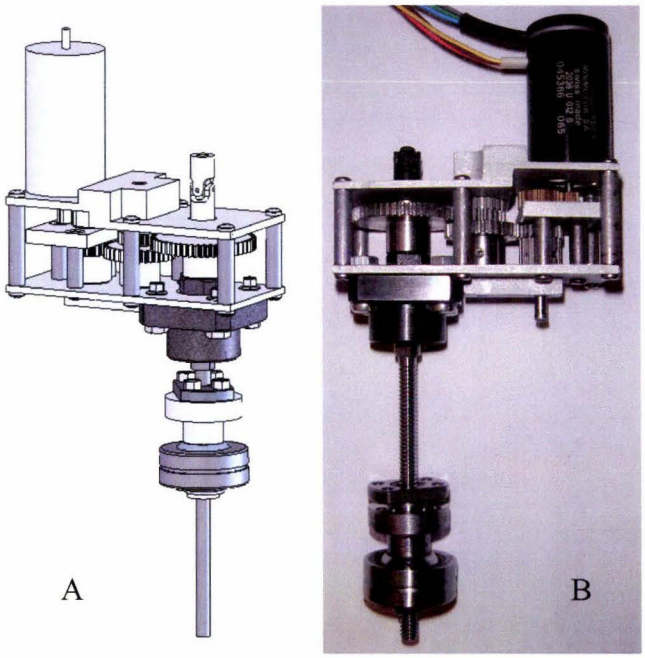

Figure 4-12. Actuator assembly: (A) model in SolidWorks, and (B) constructed actuator.

Spindle support unit

THK Co. offers a large range of support units for the previously chosen ball

screw system BNK0401-3. The support unit FK 4 was chosen because of its size. The unit used two single row angular contact bearings, which were mounted face to face, so that the load lines converged towards the bearing axis (SKF 2003). This bearing orientation allowed the accommodation of the axial loads acting in both directions.

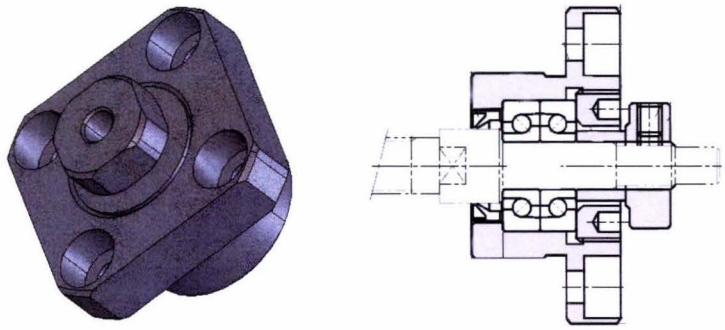

Figure 4-13. Support unit FK4: (A) isometric perspective, and (B) cut in the sagittal plane.

Gearbox design

The gearbox comprised an upper, middle and lower plate made out of stainless steel (Figure 4-14). The lower plate was joined to the upper and middle plates via six and three pins, respectively. Both ends of these pins were drilled and reamed to smaller diameter than the body diameter.

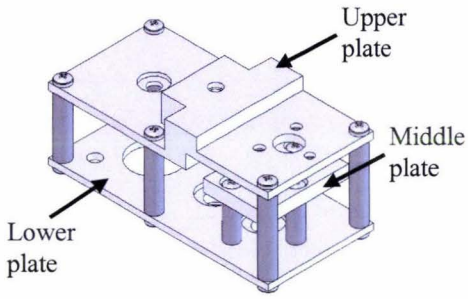

Figure 4-14. Gearbox assembly in SolidWorks.

The pin ends were put into reamed holes in the plates to work not just as parts to join the plates, but also as dowels to assure that everything was lined up correctly. Inside these pins there were drilled and taped holes to screw them on the plates, as seen in Figure 4-15.

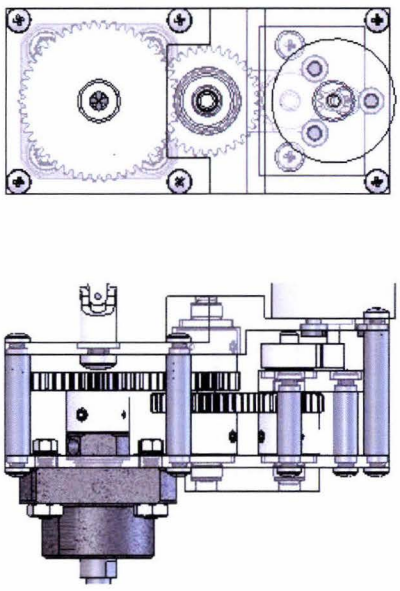

Figure 4-15. Designed gearbox in SolidWorks in (A) horizontal and (B) frontal view.

To ensure that the gear shafts were parallel and could turn with less friction, two sintered bearings were used for the both middle shafts. To fix these bearings, mounting holes were included in the plates. These bearings were mounted slightly higher than the plates and therefore allowed a smooth running of the gears in a vertical position. Otherwise the gears would have scratched on the plate surface causing high friction. To ensure that the motor was mounted in the right position, a reamed hole was inserted into the upper plate to locate the motor with its flange. For further support, it was fixed with three screws. The ball screw support unit was mounted with four screws.

Gearbox testing

To ensure that the designed gear box was strong enough to resist deformations due to applied forces while chewing, a FEM analysis was applied. The gearbox, as seen in Figure 4-14, was solid meshed with 18,917 elements in the size of 2.2 *mm*. The model was restrained on the mounting position for the ball screw support unit on the lower plate (four screw holes). A static force of 300 *N*, located on the universal joint mounting hole in the upper plate, was applied normal to it. Because an actuator applies dynamic forces in various frequencies to the gearbox when chewing, a static force, 1.5 times higher than the theoretical maximum applied force, was needed to consider the deformation due to dynamic influence. The displacement plot, including the maximum displacement [*mm*], with a scale factor $x = 1$ is shown in Figure 4-16.

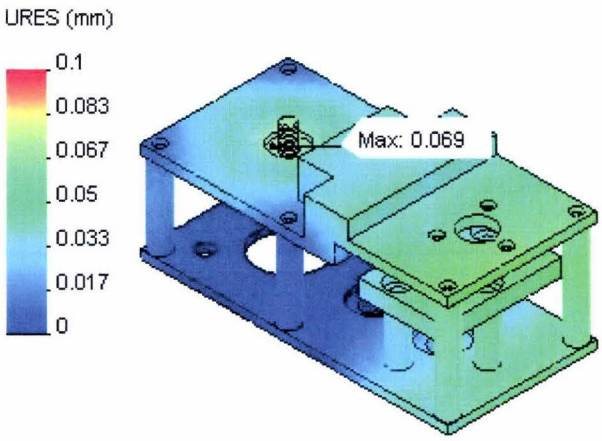

Figure 4-16. Material displacement of the gearbox due to 300 N static force.

It can be seen that the maximum displacement is $d = 0.069\ mm$ and therefore smaller than the required displacement accuracy of 0.1 mm, demonstrating that the gearbox is designed properly.

Joint systems

Two joints were required to fix and guide the actuator. The first joint was a standard steel universal joint from RS New Zealand with the item number 689-215 (RS 2005), see Figure 4-12. This joint allowed two DOF and was fixed with an M3x6 screw. The second joint was a spherical joint with three DOF. The bearing was fixed on a mounting unit, which was fixed on the ball nut. The mounting position of the mounting unit could be either before with spherical bearing PB12 or after the ball nut with spherical bearing PB8 (Figure 4-17).

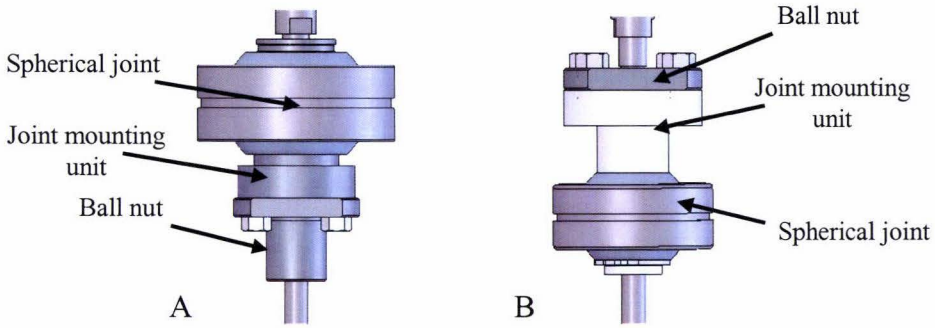

Figure 4-17. Different mountings for the spherical joints: Mounting (A) before the ball nut with bearing PB12, and (B) after the ball nut with bearing PB8.

Both bearings were purchased from THK Co., Japan. In both positions, an external retaining ring fixed the spherical bearing onto the mounting unit. The placement of the mounting unit before the ball nut reduces the distance between the

two joints, but expanded the spherical joint outer diameter due to the size of the spindle flange. The other placement produced the opposite effect. The first mounting position enabled an actuator length of 53 mm, the specified length for the temporalis muscle, whereas the second mounting position produced 73 *mm*.

4.4.4 Design related problems

The design of the linear actuator had the following drawbacks:

- *Backlash between gears.* Backlash causes inaccuracy and should be considered in the control of the actuator. A turning test showed that the inaccuracy was about 2°. Therefore, a second encoder, mounted on the spindle shaft, could improve the control.
- *Open spindle end.* Due to a mistake, the ball nut could be wounded past the spindle end and destroy the ball screw system by loosing the little balls inside. To prevent this, a metal ring with rubber should be mounted with a screw on the spindle end. The rubber would absorb the reaction force due to ball nut and metal ring contact and ensure that the balls would not wedge.
- *Mounting problems due to the outer diameter of the spherical bearing.* The actuator orientations make mounting with the big outer diameters of the spherical joint difficult. The actuator orientation should be re-evaluated in an attempt to solve this problem.
- *Actuator size.* It was possible to achieve the specified actuator length for the temporalis muscle, but the length specifications for the masseter and lateral pterygoid could not be achieved.

4.5 Chewing robot with linear actuation systems

In section 4.4 a physical model of a linear actuator was introduced. This actuator represented the temporalis muscle group, which was successful in terms of the defined actuator length in the closed mouth position, stroke, kinematic properties (velocity and acceleration), and actuator force. However, there were several problems related to building a chewing robot assembly. These problems include;

- the unachievable actuator length for the masseter and lateral pterygoid muscle group,

- difficulties in the actuator attachment to the mandible, and
- the actuator spindle and mandible collision.

This section introduces a model with longer actuators for the masseter and lateral pterygoid muscle groups. An approach to solve the problem with the actuator attachment is also outlined.

Assembly with extended actuator length

Due to the physically feasible actuators being longer than initially specified, a simplified assembly model with extended actuator lengths was built. To make comparisons between the original and the changed model possible, the actuator lengths for the two muscle groups were changed to the length of the temporalis muscle group. Due to the spatial position of the two actuators to the mandible and the actuator dimensions, it was necessary to turn them about 180° to the muscle line of action in the closed mouth position. Figure 4-18 shows the simplified robot assembly with the changed orientation and length for the masseter and temporalis actuator.

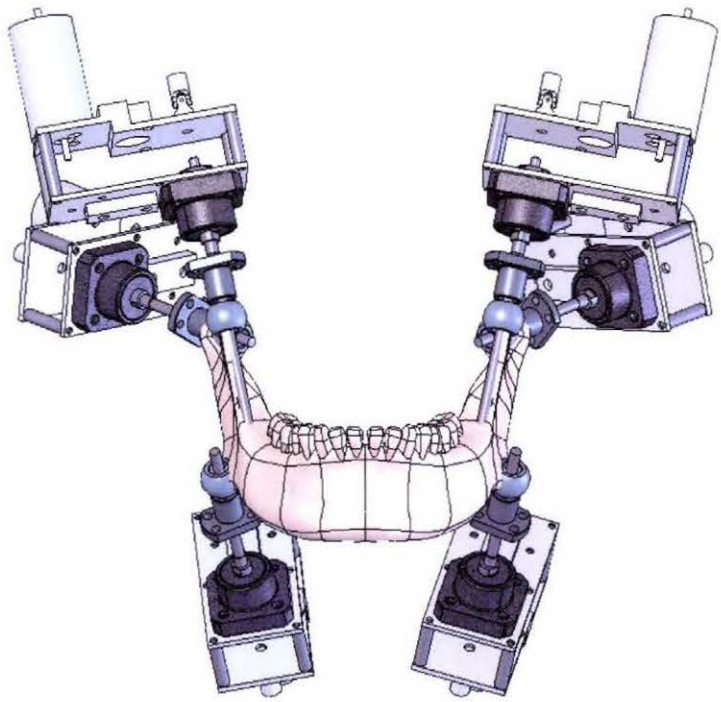

Figure 4-18. Simplified robot assembly with changed masseter and lateral pterygoid actuators.

Table 4-2 lists the new origin coordinates and actuator lengths. The mathematical model, as shown in Figure 3-5, was updated with the new actuator properties and

simulated according to section 3.4.

Table 4-2. New origin coordinates and actuator lengths in the closed mouth position for the masseter and lateral pterygoid muscle groups.

	Origin			Total actuator length (*mm*)
	x	y	z	
Masseter				
right side	-16.94	-35.68	-85.90	52.2
left side	-16.94	35.68	-85.90	52.2
Lateral Pterygoid				
right side	-36.83	-78.96	11.75	52.2
left side	-36.83	78.96	11.75	52.2

The position and orientation of the actuators for the temporalis muscle group was not changed and, therefore, no different values were determined. Table 4-3 lists the new maximum actuator properties and angular movement for the masseter and lateral pterygoid muscle groups.

Table 4-3. New determined actuator properties for masseter and lateral pterygoid muscle groups (maximum values).

	Actuator properties			Angular movement	
	Displacement (*mm*)	Velocity (*mm/s*)	Acceleration (mm/s^2)	Frontal angle (°)	Sagittal angle (°)
Masseter					
Left	4	30	1000	5	2
Right	5	30	1000	7	2
Lt. Pterygoid					
Left	16	130	3000	6	9
Right	19	130	3000	11	9

It can be seen that the values for the masseter muscle group actuators have changed only slightly, which was probably due to the fact that the masseter muscle group length stayed almost the same. The only significant change was the lower acceleration (see in comparison Table 3-8). The new masseter origins did not cause many differences to the previous model. For the pterygoid muscle group actuators, all properties were determined to be bigger. The actuator positions behind the mandible caused a bigger stroke. However, this stroke, the angular movement and the acceleration were still compatible with the actuator design in chapter 4.4. But the higher actuator velocities made changes in the actuator model necessary.

Spindle-mandible collision and actuator mounting

Very significant problems in the robot assembly were the spindle-mandible collisions, which restricted the mandibular movement. Due to the positions of the actuators close to each other and the long spindle ends, the spindle ends of each actuator collided with the mandible. Turning around the actuators, in terms of fixing the actuator with the universal joint on the mandible and with the spherical joint to the skull, solved the problem theoretically. A turning of either the lateral pterygoid or temporalis muscle group actuators was not possible, due to their close position to each other (Figure 4-19).

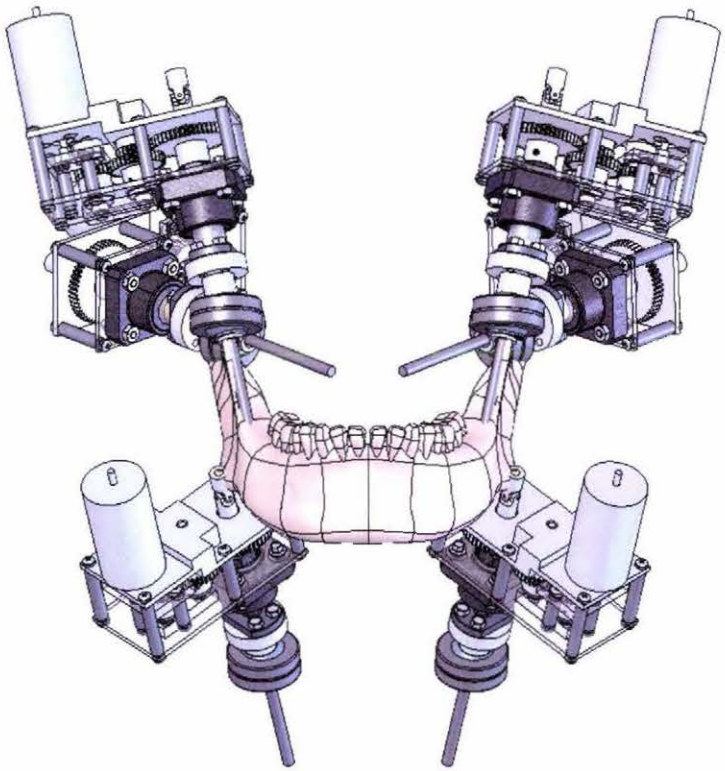

Figure 4-19. Simplified robot assembly with turned masseter muscle group actuators.

Another problem was the actuator mandible mountings. Due to the diameter of the spherical joints, fixing of the actuator to the mandible was hard to realise. Figure 4-20 shows a conceptual design of a mechanical jaw under consideration of the original actuator orientation. It can be seen that due to the diameters of the spherical joints and the position being so close to each other, a mechanical jaw would be hard to manufacture.

At this stage, it was hard to imagine that the problems through the spatial requirements could be solved with the current actuator design.

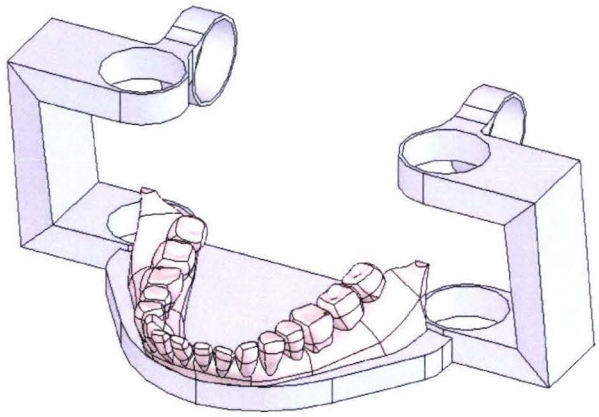

Figure 4-20. A design concept for the mechanical jaw under consideration of the original actuator orientations.

4.6 Closure

This chapter introduced an actuator design, which was required because no off-the-shelf product could suit the set requirements outlined in chapter 3. One physical actuator model for the temporalis muscle group was built successfully under consideration of the specified actuator properties. However, the actuator lengths for masseter and lateral pterygoid muscle groups were not achievable. Furthermore, the masseter and lateral pterygoid actuator origins had to be changed due to the dimensions of the actuators and their positions close to the mandible. To understand the influences of these changes, a new simulation with the updated actuator origins and lengths was carried out. The results showed that the lateral pterygoid actuator properties made a new design necessary. Furthermore, design related problems, such as mounting problems and mandible-spindle collision, showed that a different approach for the actuator design was absolutely necessary.

5 CRANK ACTUATION SYSTEM FOR CHEWING ROBOT

5.1 Introduction

The development of a kinematic model of an actuator system can be very useful in order to identify potential mechanism problems. This can be clearly seen in the development of the linear actuator system in the previous chapter.

This chapter outlines the development of such a model for an alternative crank mechanism and its implementation. The mathematical model and

5.2 Actuator design concept and its mathematical model

Following the design issues with the linear actuation mechanism, a second approach based on a slider-crank mechanism was considered. This involved an energy and transmission system with a crank and a coupler (Figure 5-1). The coupler was connected to the mandible and the crank via spherical joints to allow lateral, inferior-superior and anteroposterior movements of the mandible insertion point.

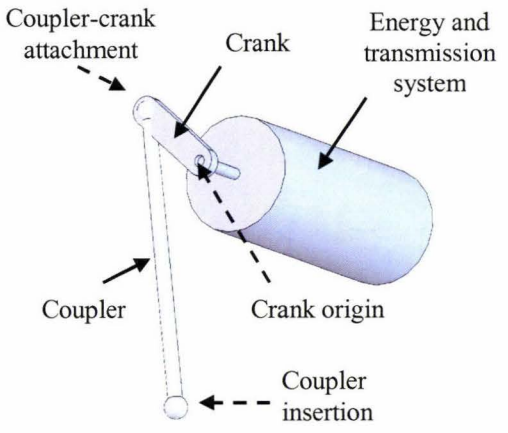

Figure 5-1. Single crank actuator in SolidWorks.

If the crank is rotated, then the mandible is moved due to actuation by the couplers.

Due to the crank rotation, the movement of the crank actuator differed from the

previous concept. If the mounting position of the crank were to be at the origin position of the linear actuator and the coupler were mounted at the insertion position on the mandible, the coupler and the muscle line of action would not coincide. This results in a different angle application of the force, which would influence the maximum chewing force of the robot.

To ensure that forces are applied coincidental to the muscle line of action, at least in the most likely mandibular position, the crank mounting position was shifted from the linear actuator origin position.

To establish the new crank mounting position, the dead centre position, which is a crank singularity, had to be considered. The dead centre position occurs if a crank and a coupler are 180° as extended ($A_0A_eB_e$) or folded ($A_0A_fB_f$) forms (Figure 5-2) (Söylemez 2002).

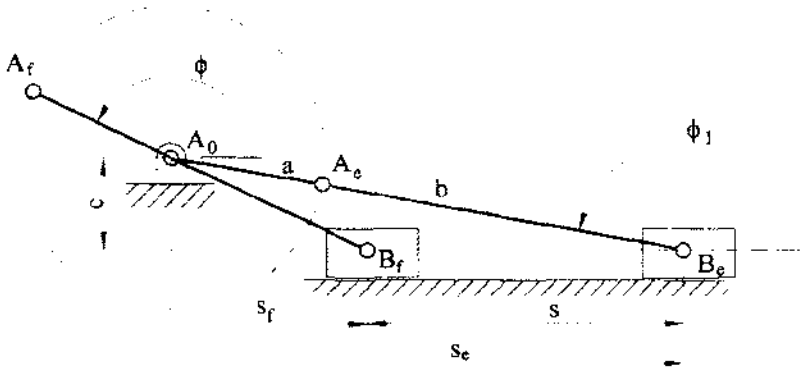

Figure 5-2. Death centre position of Slider-crank mechanism (Söylemez 2002).

The stroke $s = B_eB_f$ represents the total displacement of the slide while the crank rotates about an angle ϕ between the dead centres ($\phi < 180°$). This means that the maximum displacement of the mandible attachment point has to be reached between these dead centre positions.

To determine the optimal crank position, a graphical solution by hand was chosen. The graphical solution is explained for the temporalis actuator as an example as follows.

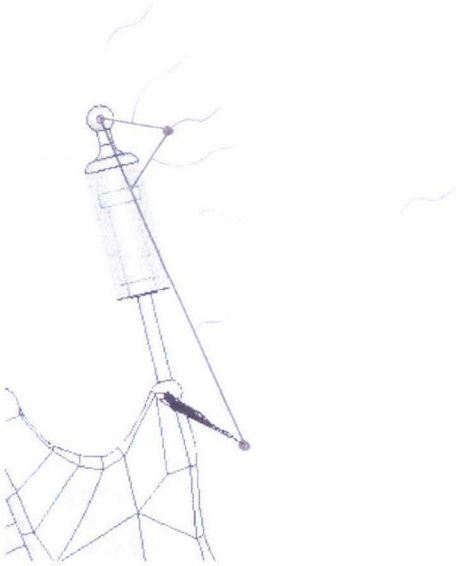

Figure 5-3. An example to graphically determine a new crank position.

COSMOS/Motion allows tracing the pathway of the temporalis insertion point after running simulations with the linear actuation system. This pathway represents the maximum movement of the temporalis insertion point for the chosen simulation and can be estimated as being linear as the maximum displacement in Figure 5-2. This model with the actuator length in the closed mouth position can be seen in Figure 5-3 for the actuator representing the right temporalis muscle group.

In this solution, the coupler of the crank actuation system was represented by the same length as the length of the linear actuator in its closed mouth position. The following steps were carried out to determine the new mounting positions for the cranks of each actuator:

- Circle 1 was drawn with the radius of the actuator length with its centre at the maximum displacement of the insertion point. With this circle, the maximum displacement *P* of the crank-coupler attachment point was defined.
- Circle 2 was drawn at the origin of the linear actuator with a radius *R* more than half of the maximum displacement between the edge of circle 1 and the origin of the linear actuator. The bigger the radius chosen, the bigger the crank was and the smaller was the needed rotation to reach all positions.
- Line *M* was drawn between the origin of the linear actuator and point *P*.
- At the intersection between line *M* and circle 1, a circle 3 with the same radius *R* as circle 2 was drawn. The intersection between circle 2 and 3 defined the mounting position *CP* for the crank.
- At the end, it was checked that no dead centre positions occurred.
- The crank length and the angle α between the crank R and the linear actuator were indicators for the new crank position in SolidWorks.

The required angles between the crank and the coupler were determined for all four chewing trajectories (see section 2.2.1). Therefore, the x, y, and z coordinates of

each chewing trajectories were implemented in the mathematical model with the linear actuators. Table 5-1 lists these angles.

Table 5-1. Maximum angles between crank and couplers in the closed mouth position.

	Angle (°)
Masseter	37
Temporalis	41
Lateral Pterygoid	78

Figure 5-4 shows the kinematic model of the chewing robot with the crank actuation system. The movement of the cranks were restricted so they could only rotate around their motor shafts. Due to the fact that angular changes of the masseter and temporalis actuators occurred not only in the sagittal plane but also in the frontal plane, the cranks were mounted in the same frontal angle as the couplers were in the closed mouth position. This ensured that only minimum angular movement between the crank and the coupler in this plane occurred. The actuators for the pterygoid muscle group were mounted horizontally, due to the angular position of the couplers and the spatial requirements set through the structure of the mandible.

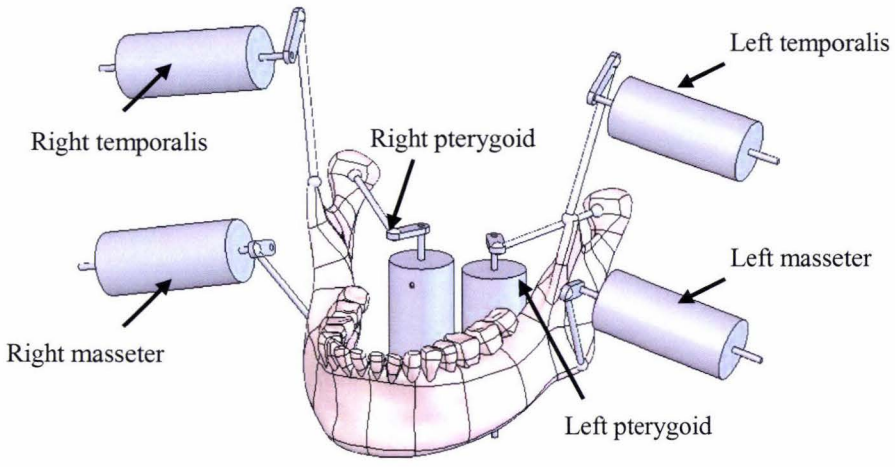

Figure 5-4. Kinematical model of the chewing robot with crank actuation system.

The mounting positions of the crank actuation systems were described with the x, y, and z coordinates of the crank origin, the coupler-crank attachment, and the coupler insertion for the closed-mouth position, as defined in Figure 5-1. The coordinates are listed in Table 5-2. The SolidWorks model can be found in appendix D on the enclosed DVD.

Table 5-2. Attachment coordinates for the chewing robot with crank actuations[6].

	Coupler insertion			Coupler and crank attachment			Crank origin		
	x	y	z	x	y	z	x	y	z
Masseter									
right side	18	-44.7	-47.7	48.2	-52.5	-14.7	38.7	-52.1	-16.4
left side	18	44.7	-47.7	48.2	52.5	-14.7	38.7	52.1	-16.4
Temporalis									
right side	25.6	-43	2	13.3	-53.2	51.8	25.6	-51.5	43.3
left side	25.6	43	2	13.3	53.2	51.8	25.6	51.5	43.3
Lt. Pterygoid									
right side	-0.9	-41.1	-3.1	21.5	-17.5	-12.4	13	-12.3	-12.4
left side	-0.9	41.1	-3.1	21.5	17.5	-12.4	13	12.3	-12.4

5.3 Kinematic simulations

To verify the mechanism using the mathematical model with crank actuators, all four chewing trajectories, as introduced in section 2.2.1, were performed. However, for determining the required actuator properties, only the results from chewing trajectory one were used. The same initial state for the mandible and reference points, as outlined in chapter 3.4.1 to 3.4.2, was used for all simulations. Screenshots of the model with trace paths of the reference points in frontal, sagittal, and horizontal plane and recorded movies for all four chewing trajectories can be found in appendix D on the enclosed DVD.

The simulations verified that all crank positions and lengths were correctly positioned because no dead centre positions were ever reached. The results for all six actuators are presented in Table 5-3.

Table 5-3. Crank actuator properties determined with trajectory one.

	Angular displacement (°)	Angular velocity (s^{-1})	Angular acceleration (s^{-2})	Angular movement for coupler Frontal angle (°)
Masseter				
Left	+48; -1	+7; -5	+200; -100	4
Right	+1; -51	+5; -6	+100; -150	3
Temporalis				
Left	0; -75	+8; -6	+200; -150	6
Right	0; -70	+5; -5	+100; -100	5
Lt. Pterygoid				
Left	0; -50	+5; -5	+100;-100	3
Right	+5; -42	+6; -4	+150; -100	3

[6] Attachment coordinates are presented in the skull coordinate system ($OXYZ_S$) and given in *mm*.

Plots of the left temporalis actuator are shown as an example in Figure 5-5. The results include the maximum angular displacement changes, velocity and acceleration of the crank.

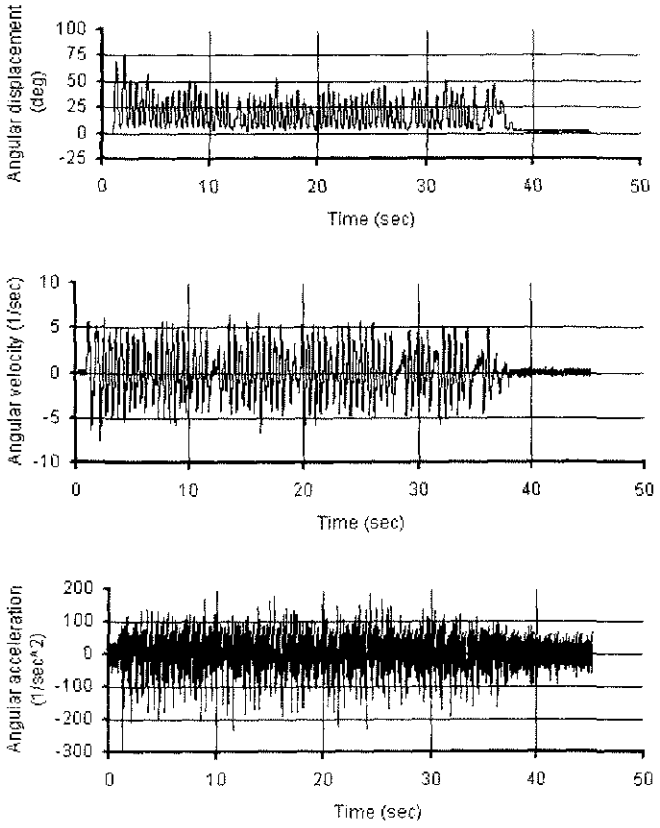

Figure 5-5. Left temporalis actuation for the crank actuator: (A) angular displacement, (B) angular velocity, and (C) angular acceleration.

As already stated in chapter 3.6, a suitable uniform actuator systems should replace all muscle groups to make maintenance and control of the chewing robot as simple as possible. Table 5-4 lists the minimum required properties for the uniform actuator system.

Table 5-4. Determined actuator requirements.

	Minimum required values
Coupler length (*mm*)	
Masseter	45.6
Lateral Pterygoid	32.6
Temporalis	52.2
Crank length (*mm*)	
Masseter	10
Lateral Pterygoid	10
Temporalis	15
Angular velocity (s^{-1})	8
Angular acceleration (s^{-2})	200
Linear force (*N*)	200
Angular movement (°)	10
Displacement accuracy (°)	0.1

5.4 Actuator control

As for the previous chosen linear actuation system, it had to be ensured that a closed-loop actuation system existed and that this system was compatible into the Galil motion system. It was proposed to attach an encoder to the rear shaft of the motor to make position and velocity control possible. The step accuracy of the rotational movement of the system had to be around 0.1 degrees.

5.5 Physical design

The selected actuator concept was outlined in section 5.2 and the design related parameters were listed in Table 5-4. The physical design was carried out for the left masseter actuator to ensure that the design for the shortest actuator was possible. The design process was divided into two parts:

- Motor, gear ratio, and encoder selection, and
- Crank and coupler design.

The component datasheets and the SolidWorks drawings can be found in appendix E on the enclosed DVD.

5.5.1 Motor, gear reduction, and encoder selections

Motor and gear ratio selection

To choose a suitable motor and gear ratio, the required torque on the mounting shaft of the crank and its speed were calculated.

- Maximum torque

The motor torque needed to be calculated as explained in chapter 4.4.2, under constant load T_c [Nm], under acceleration T_{acc} [Nm], and under deceleration T_{dec} [Nm]. Using equations (4.11) and (4.12), the constant torque T_c can be calculated with equation (6.1):

$$T_c = \frac{1}{i \cdot \mu} \cdot T_{cs} \cdot f_{s2}, \tag{5.1}$$

where T_{cs} is the needed torque on the crank shaft before gear reduction [Nm], μ is the gearbox efficiency [-] and f_{s2} a safety factor [-]. Figure 5-6 shows the trigonometrical coherences of the crank actuator for the temporalis muscle group in the closed mouth position that were used to determine T_{cs}.

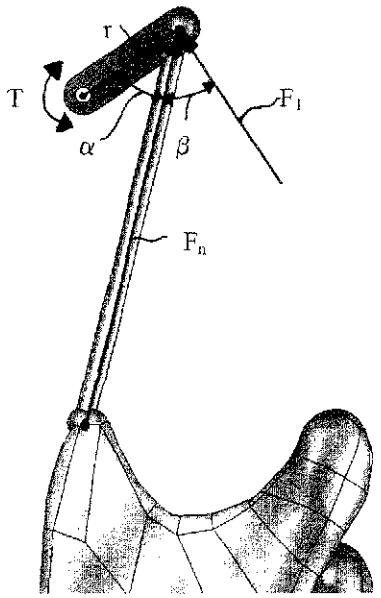

Figure 5-6. Trigonometrical coherences of the crank actuator for the temporalis muscle group.

The constant torque T_{cs} [Nm] is equal to the normal force F_n [N] applied to the crank times the radius r [m] from the force to the vector crank turning point. Since the coupler force in this position is applied in an angle α [°] smaller than 90 degrees, it gives:

$$T_{cs} = F_n \cdot r \cdot \sin\alpha\,, \tag{5.2}$$

With F_n = 200 *N*, the crank radii in Table 5-4, and the crank-coupler angles in Table 5-1, gives a T_{cs} for masseter, temporalis and lateral pterygoid of 1.204 *Nm*, 1.982 *Nm*, and 1.956 *Nm*, respectively. The torque T_a through acceleration [*Nm*] can be calculated using equation (4.14), where the entire moment of inertia *I* consists of the moment of inertia of the motor I_M [kgm^2], of the load, I_L [kgm^2], and of the gearbox, I_{GB} [kgm^2]:

$$I = I_M \cdot \left(\frac{1}{i}\right)^2 + I_L \cdot \left(\frac{1}{i}\right)^2 + I_{GB}\,. \tag{5.3}$$

The values for I_M and I_{GB} can be found in motor and gearbox datasheets. The moment of inertia I_L can be calculated with equation (6.4) and (6.5):

$$I_L = m_L \cdot r^2\,. \tag{5.4}$$

and

$$m_L = \frac{F_n \cdot \sin\alpha}{g}\,. \tag{5.5}$$

For the masseter, temporalis and lateral pterygoid actuator, the moment of inertias I_L are 0.0012 kgm^2, 0.003 kgm^2, and 0.0019 kgm^2, respectively. The torque T_{acc} and T_{dec} can thus be calculated with equations (4.19) and (4.20).

Since the value for T_{cs} for the temporalis and lateral pterygoid were almost the same and the moment of inertia I_L was the largest for the temporalis actuator, all further calculations were carried out for the temporalis actuator.

- Maximum speed

The maximum speed *n* [min^{-1}] can be determined with equation (6.6):

$$n = \frac{60 \cdot \omega}{2\pi}\,, \tag{5.6}$$

where ω is the angular velocity [s^{-1}]. With ω = 8 s^{-1}, gives *n* = 76.4 min^{-1}. This value symbolises the minimum required speed.

Table 5-5 lists T_c, T_{acc}, T_{dec} for several gear ratios. Due to the fact that no specific gearbox and motor for this comparison were chosen, a safety factor f_{s2} = 2 was used in the calculations to indirectly consider the moments of inertia for the motor and the gearbox and the gearbox efficiency.

After comparing the determined values with motor systems from various companies, a combination system with gearbox, motor and encoder of Maxon motor, Switzerland, was selected as the most appropriate system. The brushed DC-motor RE 30 provided a torque of 86.2 *mNm*, so that according to Table 5-5 a gear ratio *i* of

around 75 was needed. Maxon motor offered the planetary gearhead series GP 32 C with a recommended input speed of 8000 RPM. A close gear ratio offered was $i = 66$.

Table 5-5. Calculation results for the crank actuator.

	Symbol	Unit	Solution 1	2	3	4	5	6	7	8	9	Chosen specifications
Gear Reduction	i	-	100	75	50	25	20	15	10	5	1	**66**
Mass moment of inertia	J	kgm^2	1.E-06	1.E-06	2.E-06	6.E-06	8.E-06	1.E-05	3.E-05	1.E-04	3.E-03	1.E-06
Torque due to acceleration	T_α	Nm	2.E-04	2.E-04	4.E-04	1.E-03	2.E-03	3.E-03	6.E-03	2.E-02	6.E-01	3.E-04
Torque (constant speed)	T_c	mNm	57.1	76.2	114.3	228.6	285.7	381.0	571.4	1142.9	5714.3	**86.6**
Torque (acceleration)	T_{acc}	mNm	57.3	76.4	114.7	229.7	287.4	383.8	577.6	1167.3	6321.1	**86.9**
Torque (deceleration)	T_{dec}	mNm	57.1	76.2	114.3	228.6	285.7	381.0	571.4	1142.9	5714.3	**86.6**
Speed	n_{max}	min^{-1}	80.0	106.7	160.0	320.0	400.0	533.3	800.0	1600.0	8000.0	**121.2**

Due to the new gear ratio, the motor torques and speed had to be recalculated to verify that the motor suited the set requirements. Using a gearbox efficiency of 70%, a moment of inertia for the motor of $I_M = 3.22 \cdot 10^{-6}\ kgm^2$ and a moment of inertia for the gearbox of $I_{GB} = 0.7 \cdot 10^{-6}\ kgm^2$ (datasheets in appendix...), gives for T_c, T_{acc}, *and* T_{dec} around 86.6 *mNm*. Due to the recommended gearbox input speed of 8000 RPM, the maximum output speed n_{max} is 121.21 min^{-1}. The comparison of the torque values with the motor performance diagram in Figure 5-7 showed that the values were lying slightly outside the area for continuous operation. However, this is no problem since these performances were short term operations. Therefore, it was confirmed that the chosen motor combination met the requirements for the chewing robot.

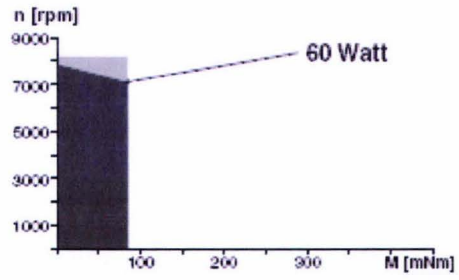

Figure 5-7. Motor performance diagram for brushed DC-motor RE 30 from Maxon Motor, Switzerland (Colors: black, recommended operating range; grey, continuous operation; white, short term operation).

Encoder selection

The Maxon motor company recommended using a digital MR encoder for the previous chosen DC-motor. The chosen encoder with the item number 228452 had 500 counts per turn. A whole circle of 360 degrees divided by 500 produces an accuracy of 0.72 degrees as motor output. To receive the accuracy after the gearbox, the determined value had to be divided by the gear ratio i = 66 and gave an output accuracy of 0.011 degrees, which was sufficient. Therefore, it can be said that this shaft encoder in combination with the brushed DC-motor RE 30 enabled the measurement and control of both, shaft velocity and direction of rotation as well as for positioning.

5.5.2 Crank and coupler design

Crank design

The crank was manufactured out of mild steel and was fixed with two sink screws to ensure that no shift between the crank and its supporting shaft occurred. A drawing of this crank can be seen in Figure 5-8.

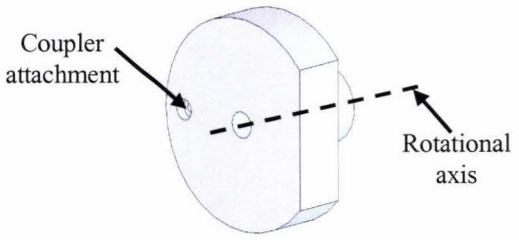

Figure 5-8. Crank model in SolidWorks.

Coupler design

The coupler consisted of two rod ends and a shaft. Shaft and rod ends were connected via threads at the shaft ends and screw groves in the rod ends (Figure 5-9).

Figure 5-9. A physical coupler, which includes one thread shaft and two rod ends.

All items were purchased from a model shop without additional information. Since the material and, therefore, the strength of the rod ends were unknown, a strain test needed to be done. Unfortunately, just seven coupler assemblies were made available. This meant that just one coupler test could be made. Due to the fact that only one test can give an estimation of the real strength value, a safety factor for the further calculations

was considered.

The coupler was assembled and fixed with two custom made mounting units in a static testing machine (JJ Instruments T30K). With such a machine, tensile tests of various shaft samples and recordings of the accordant stress-strain diagram are possible. One video and several pictures can be found in appendix E on the enclosed DVD.

In this test, the machine applied a force until the coupler broke and recorded the stress-strain diagram. The experimental set up and the plotted stress-strain diagram can be seen in Figure 5-10.

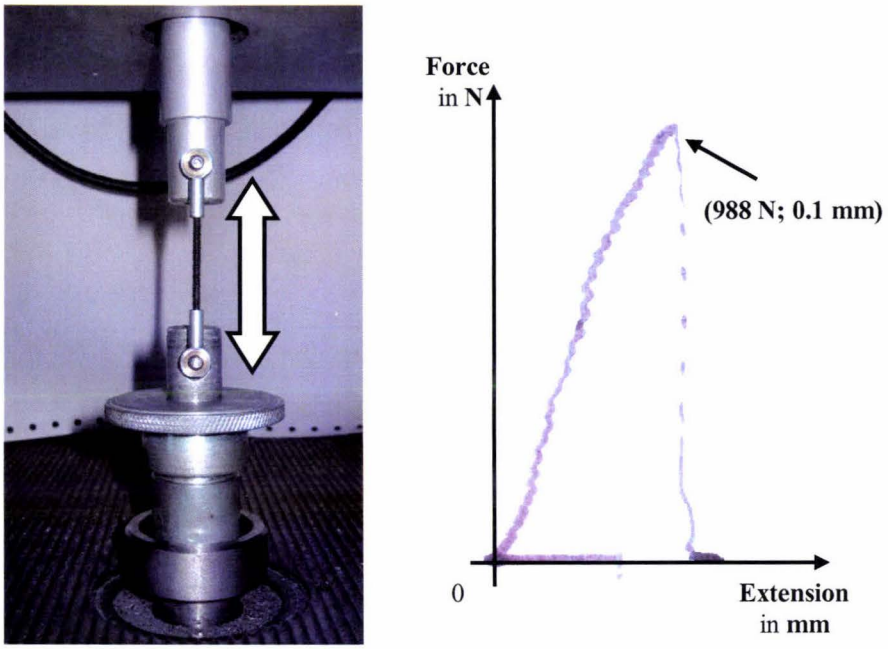

Figure 5-10. Experimental setup and the determined stress-strain diagram for the coupler testing in a static testing machine (JJ Instruments T30K).

The rising in the stress-strain diagram represents that with growing forces the coupler extends until its break point is reached. The coupler resisted a pulling force of 988 *N* and experienced a maximum extension of 0.9 *mm* until one ball of a rod end popped out. The coupler length after the experiment showed a lengthening of 0.1 *mm*. Such a high force resistance and small displacement change ensured that the coupler design was suitable for the given task.

Crank-coupler connection

The crank and the coupler were connected in such a way that the coupler was able to rotate around its connection shaft and could move freely in the frontal angle direction. The rod end was held in place with a bushing and a cap screw. The bushing worked not just as a part to keep distance between crank and rod end, it also supported the screw shaft in such a way that no buckling of the screw shaft occurred. The bushing was embedded in the crank to give more stability. The screw hat and the bushing were bevelled on the coupler connection site to allow a movement angle of about 25° in the frontal view.

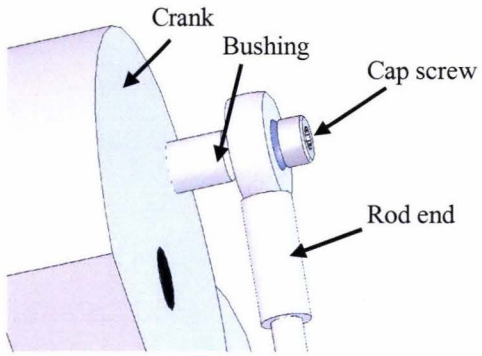

Figure 5-11. Crank-coupler connection as showed in SolidWorks.

5.6 Closure

In this chapter, a second actuation model for the chewing robot was introduced. Instead of a linear actuation system, a crank actuation system, consisting of crank, coupler and energy and transmission system, replaced the masseter, temporalis and lateral pterygoid muscle groups.

First, a kinematic model for reproducing human chewing behaviours was introduced. The crank lengths and origin positions were determined using a graphical solution method and the coupler lengths were chosen in accordance with the lengths of the muscle line of action in the closed mouth position. With the implementation of chewing trajectories at the incisor point, the mathematical model could be verified and actuator and system properties were obtained. This enabled the development of a physical actuation system based on the crank mechanism.

Secondly, the physical design of the crank actuation system was outlined. In particular, calculations for motor and gear reduction selection were presented. Furthermore, the crank and coupler designs, as well as the connection between both were introduced. To validate the strength of the coupler, a static strain test was conduced. No design related problems occurred, so that the design of the entire chewing robot as a next step could begin.

6 DESIGN AND ANALYSIS OF CHEWING ROBOT USING CRANK ACTUATION

6.1 Introduction

In the previous chapter an alternative actuation mechanism was designed. This new system then required combination into a total system, to facilitate food chewing. All six actuators required positioning and attachment to ground and the mandible in such a way that free movement of the mandible without collision of the components could occur. The entire assembly of the chewing robot is outlined in detail in this chapter, where drawings, pictures, and component datasheets can be found in appendix E on the enclosed DVD. Appendix G contains the printed drawings of the chewing robot. The framework to support the upper and lower jaw structures required considerable thought to ensure correct actuator positioning and adequate mechanical strength.

6.2 Design

6.2.1 Framework design

The entire framework of the robot consisted of four parts: bottom plate, left, middle and right mounting units (Figure 6-1). The overall dimensions of the bottom plate were chosen in such a way that it was large enough to accommodate all parts of the entire chewing robot mechanism. Due to its overall dimensions, aluminium was chosen as material to give the whole system a good stability and to minimise the weight. To make assembly of the mechanism easier, a cutaway was placed underneath

the mandible was placed. The three mounting units were each aligned with two dowels and fixed with four cap screws to the bottom plate. This prevented the three units from moving. The left and right mounting units supported the left and the right masseter and temporalis actuators respectively.

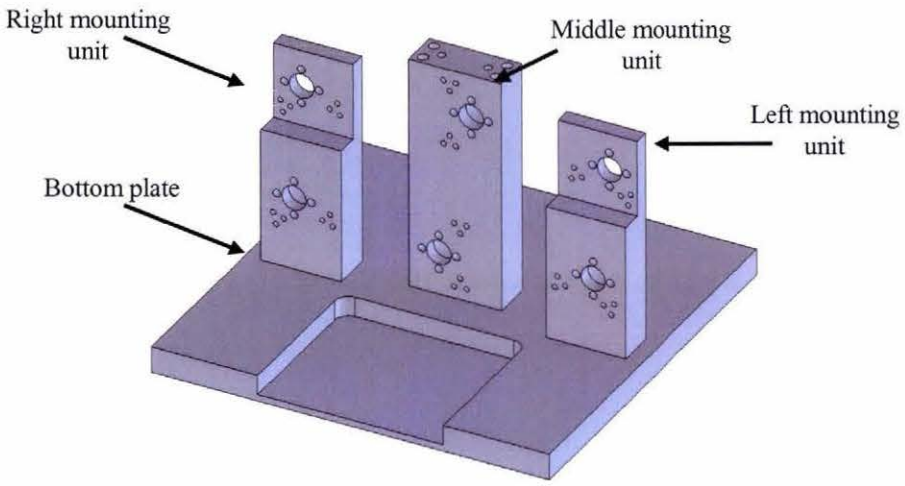

Figure 6-1. Framework of the chewing robot with bottom plate and three mounting units.

The middle mounting unit supported the left and right lateral pterygoid actuators and also the upper jaw. For this reason, the thickness of this unit was increased, compared with the other two units, to provide enough strength. The motor units (gearbox, motor, and encoder) were mounted to the three mounting units with four M3 x 6 cap screws which were embedded in the mounting units to prevent buckling of the screws or movement of the motor unit. By using bevel gearboxes with a gear ratio of 1:1 in front of each motor unit, it was possible to orientate all six motor units in the same direction (Figure 6-2). This provided a more compact looking model.

The bevel gearboxes had steel gears and shafts and ran in ball and sintered bearings. The housing moldings were 30 % glass filled nylon to provide better strength in comparison to normal nylon housings. The motor gearbox with a 66:1 gear ratio had a maximum permissible axial load on the output shaft of 140 N (see datasheet). This was below the force needed while chewing. Therefore, the bevel gearbox in front of the motor unit had also a supporting function and would absorb all axial loads which might occur. The output shafts of the motor units and the input shafts of the bevel gearboxes were connected to each other with shaft couplers. Gearboxes and shaft couplers were purchased from MFA/ Comodrills, United Kingdom. Each bevel gearbox was fixed with nine M2 screws to the bevel gearbox mounting unit.

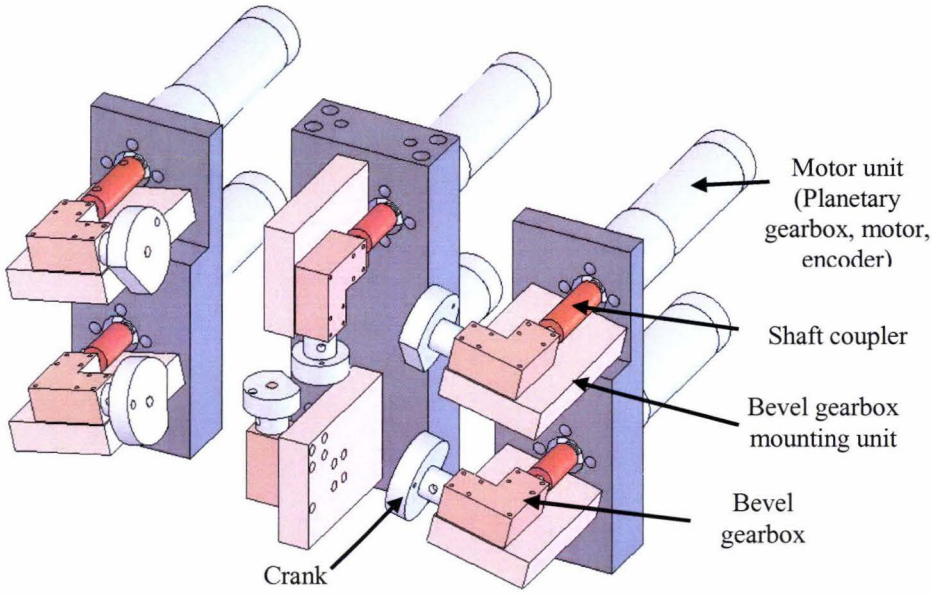

Figure 6-2. Left, right and middle mounting units with assembled motor units and bevel gearboxes.

6.2.2 Lower and upper jaw

Real denture morphology was necessary to make comparisons to the human system possible. Important points on the jaw (i.e., reference points, attachment points and denture morphology) needed to be represented similar to an average human jaw. Therefore, a basic study model from Trimut Corporation, Kyoto, Japan, was used to provide realistic morphology with the important 2:1 tooth relationship between mandible and maxilla, and reliable contact points (Figure 6-3) (Trimunt 2001).

Figure 6-3. Basic study model with replacement teeth (Trimunt 2001).

The teeth were made out of melamine, a type of plastic, and were considered strong enough for the first chewing tests. For more advanced testing, two layered composite teeth with natural hardness were also available from the company.

The structure of the lower mechanical jaw consisted of three aluminium parts: base, left and right ramus (Figure 6-4). Each ramus was fixed to the base with four M4

cap screws and two 4 mm dowels. The dowels ensured a very good lining between the parts. The connections between mandible and couplers were also undertaken with bushings and cap screws as already shown in Figure 5-11.

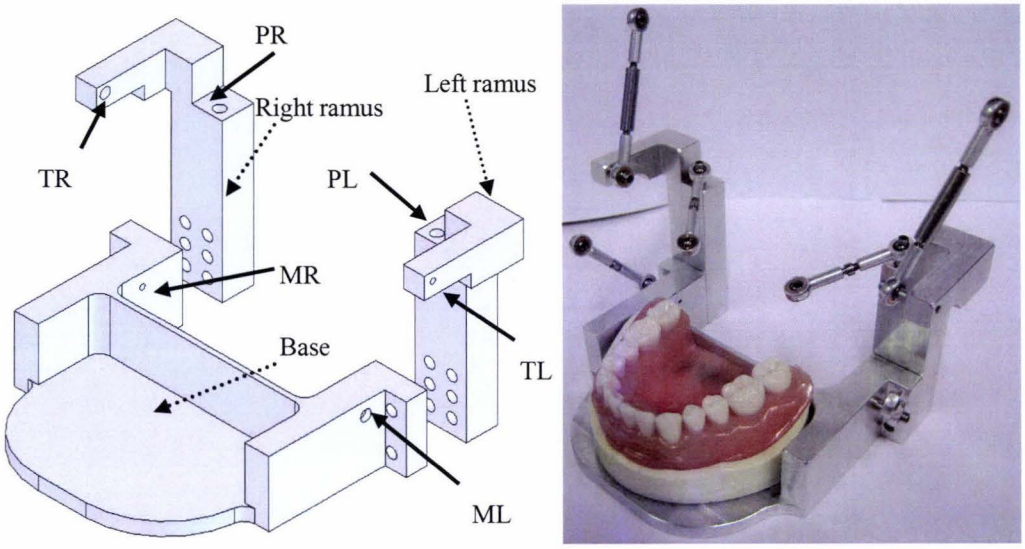

Figure 6-4. Assembly of the lower mechanical jaw in SolidWorks and as physical model. ML: left masseter, MR: right masseter, TL: left temporalis, TR: right temporalis, PL: left lateral pterygoid, PR: right lateral pterygoid.

The lower part of the study model was fixed with screws on the base. Spatial requirements between the lower jaw and the bevel gearbox mounting unit of the right lateral pterygoid actuator made a cut out on the base unit necessary (Figure 5-6).

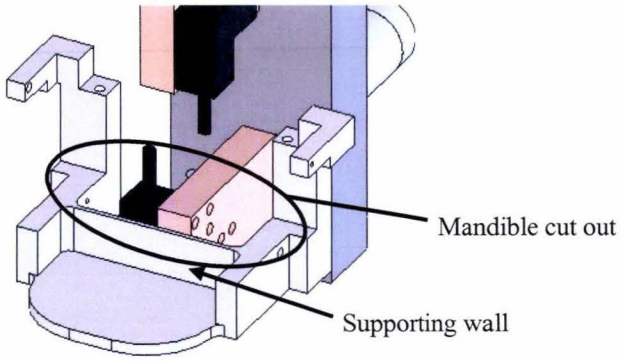

Figure 6-5. Lower mechanical jaw with bevel gearbox mounting units for the lateral pterygoid muscle group.

The basic study model of the upper and lower jaw were shortened in depths of about 10 mm to keep the same relationship between the actuator attachment points on the mandible and the denture position due to the position of the bevel gearbox mounting units for the lateral pterygoid. To stabilise the back molar teeth of both the upper and lower jaw, walls with 2 mm thickness were implemented in the mandible base unit and upper jaw mounting unit, where the upper jaw is mounted. The upper jaw was fixed

with one cap screw on the top and two countersink screws from behind. The upper jaw mounting unit was then connected to the middle mounting unit via a connecting unit (Figure 6-6). All units were lined up each with two dowels and fixed with four cap screws.

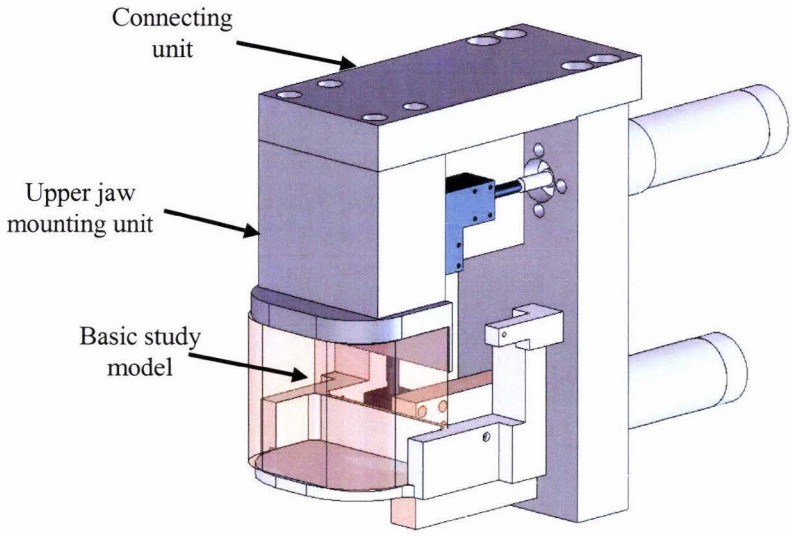

Figure 6-6. The mounting system of the upper jaw.

6.3 Simulation

6.3.1 Simulation model

The chewing robot with its new design was simulated to ensure that the mechanical jaw did not interfere with any other parts. The simplified mathematical model of the entire chewing robot can be seen in Figure 6-7 and found in appendix E on the enclosed DVD.

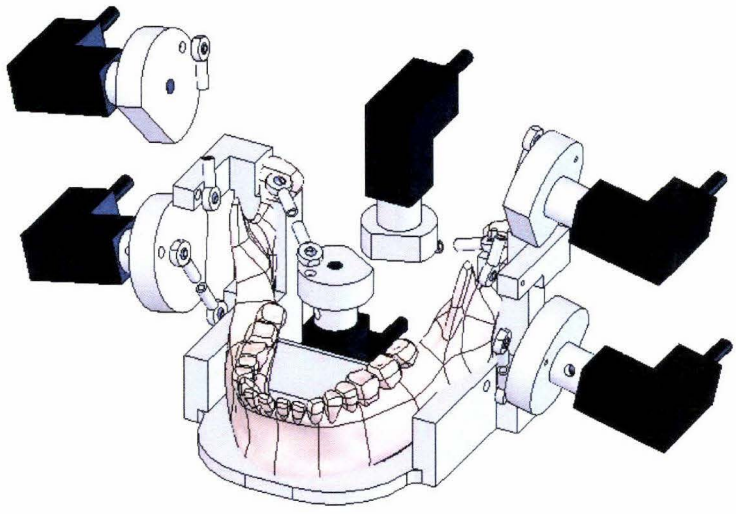

Figure 6-7. Simplified model of the entire chewing robot to verify the mandible design.

The simulations were conducted with all four chewing trajectories which were introduced in chapter 2.2.1. For all four chewing trajectories, the time history of the x, y, and z coordinates of the incisor movement were implemented. Pictures and recorded movies can be found in appendix E on the enclosed DVD.

6.3.2 Results

Two problems occurred while running the simulations. First of all, the mandible collided with the upper jaw model on its temporalis coupler attachment points. The distance between the left and the right points did not allow a free movement around the upper jaw. Therefore, the temporalis actuators were shifted 10 mm to the outer side. Through these changes, another problem occurred in the subsequent simulations. The part of the mandible where the coupler for the temporalis muscle group was attached, collided with the coupler-crank attachment point of the masseter actuator, as can be seen in Figure 6-8. The movie of the collision can be found in appendix E on the enclosed DVD.

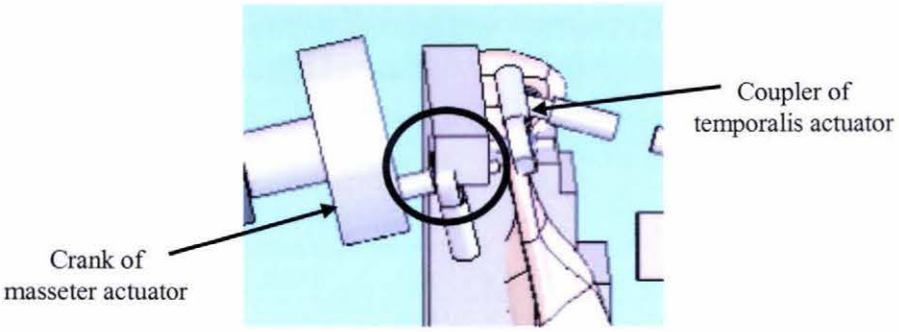

Figure 6-8. Collision between mandible and crank of the masseter muscle group.

To prevent these interferences, the masseter actuators were shifted 10 *mm* to the outer side as well. Furthermore, the coupler lengths were shortened down to 32 *mm*. The shortening of the crank made it necessary to extend the crank radii from 10 *mm* to 15 *mm*. These changes enabled the mandible to reach every position without any collision. Table 6-1 lists the new attachment coordinates for the crank actuation systems as used in the mathematical model (Figure 5-4). The shifting to the outer side did not influence the required actuator properties. Only the angular movements of the couplers in the frontal plane were influenced due to the new actuator positions. The changes of the angular movement were negligible small. The comparison between the actuator properties before and after the coupler shortening and the crank extension of the masseter actuators showed that no appreciable differences could be named.

Table 6-1. Attachment coordinates for the chewing robot with the changed crank actuations.

	Coupler insertion			Coupler and crank attachment			Crank origin		
	x	y	z	x	y	z	x	y	z
Masseter									
right side	18	-54.7	-47.7	32.1	-61.5	-18.6	18.9	-59.9	-25.6
left side	18	54.7	-47.7	32.1	61.5	-18.6	18.9	59.9	-25.6
Temporalis									
right side	25.6	-53	2	13.3	-63.5	51.7	25.6	-61.5	43.3
left side	25.6	53	2	13.3	63.5	51.7	25.6	61.5	43.3
Lt. Pterygoid									
right side	-0.9	-41.1	-3.1	21.5	-17.5	-12.4	13	-12.3	-12.4
left side	-0.9	41.1	-3.1	21.5	17.5	-12.4	13	12.3	-12.4

Figure 6-9 shows the entire chewing robot with simplified denture in SolidWorks and as a physical model. Thus, the chewing robot was successfully built. Various clenching and grinding movements can bee seen in Figure 6-10.

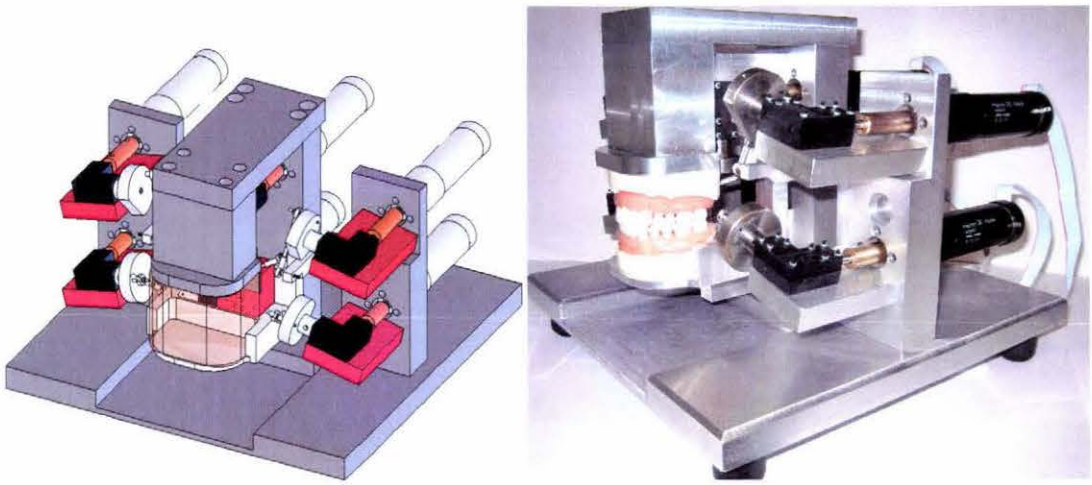

Figure 6-9. Entire chewing robot (A) with crank actuators and simplified denture model in SolidWorks and (B) as physical model.

Figure 6-10. The physical model in various clenching and grinding movements.

6.4 Testing and analysis

6.4.1 Testing

The physical chewing robot was tested for its mechanical functionality. Testing showed that the bevel gearboxes introduced play while the crank turned. Movies of the recorded crank plays can be found in appendix E on the enclosed DVD. It was

assumed that the bevel gearboxes had not been manufactured well enough. This could be improved with manufacturing new metal housings and using two angular contact bearings.

The second issue was the alignment of the upper and lower jaw. Due to its irregular shape, the mechanics had problems to centre the upper and lower jaw. This alignment resulted in slightly different frontal angles of the couplers between the left and right side, and the lower jaw was shifted to the left side. This issue could be removed with repositioning the basic denture models. However, to conduct first mandibular movement tests, the design was carried out well enough. At a later stage, when the force appliance of the actuation system in relation to the chewing of food is the major point of interest, these issues would have to be removed as much as possible.

6.4.2 Analysis

The movement area or the angular movement of the mandible could not be analysed extensively, since no equations were available. However, it was possible with the chewing robot to reproduce all four trajectories in terms of their movement area and related their angular movement to the mandible.

Due to the physical design of the mandible and the crank actuators, the maximum angular movements about the x, y, and z-axis were determined by hand with angles of about 6, 33, and 10 degrees, respectively, to either side, beginning from the starting position. It is recommended that the needed angular movement and movement area of the mandible is verified with simulations as was done in the previously introduced mathematical model.

6.4.3 Mandible positioning

From the beginning, controlling tests of the physical robot without the upper jaw are recommended to prevent any damage on the robot. To set up the mandible to the correct starting positions, all cranks were designed with a reference plane on the diameter of the crank (Figure 6-11).

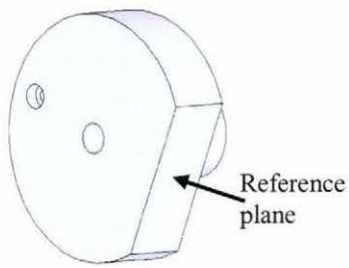

Figure 6-11. Reference plane on the crank.

This reference plane can be orientated normal to the bottom plate using a square. After

this the motors can now orientate the cranks relative to their starting position. The angular changes of the cranks can be found in Table 6-2.

Table 6-2. Required rotational movements of the cranks to find starting position of the mandible.

	Angle (°)
Masseter	35.7
Temporalis	28.6
Lateral pterygoid	20.1

6.5 Closure

In this chapter, the entire design of the chewing robot with its crank actuators was presented, and especially, the framework, and the upper and lower jaw design were introduced. Various simulations were used to verify the physical model, whereby position and dimensional changes for the masseter and temporalis actuator were necessary to prevent any collisions between parts on the robot. The chewing robot was tested on its mechanical functions and the movement area and the angular movement of the mandible were determined by hand showing that the robot could do the required performances.

7 CONCLUSION AND RECOMMENDATION

7.1 Conclusion

After almost one year of research on designing a chewing robot to reproduce human chewing behaviours, the following conclusions were made. To realise a physical chewing robot, two designs for actuation systems were carried out. Both design concepts were based on biological fundamentals, such as jaw structure and the muscles of mastication. Through the use of the biological structure, the entire design became highly complicated due to spatial requirements and the chewing force. With the first design, with linear actuation systems replacing the line of actions of the three main muscle groups, a design of the chewing robot based on the biological structure was not possible. The required actuator lengths, as well as the mounting positions could not be met by using linear actuators. Theoretically, the actuators could perform the required tasks by using a normal platform mechanism where the actuator positions and lengths would not be an issue. However, under such circumstances, off-the-shelf actuators would probably have been chosen.

The second design, based on a slider-crank mechanism, focused on the muscular line of action only in the most likely position, where forces are applied during occlusion. However, also with this model, it was not possible to build a physical model without making modifications to the biological structure.

The robot, which has been built, enables reproduction of chewing trajectories and application of estimated chewing forces. Except for the changes related to the muscle attachment points and the muscle length, the entire design of the chewing robot has been a success. The changes on the physical model required do not prevent comparisons between the human system and the physical chewing robot possible. If

the actuator attachment points and the actuator length could have been chosen, a more sophisticated and compact chewing robot could have been designed.

7.2 Recommendation

The designed chewing robot is far from being perfect; therefore, still a number of issues have to be improved or changed.

One of the biggest issues, which is related to the accuracy of the entire system, is the play of the cranks. With manufacturing custom-made housings and the use of proper gears and angular contact bearings, the crank play could be minimised a lot.

Furthermore, to make proper chewing tests possible, the upper and lower jaws have to be realigned.

The biggest concern in this project was the unknown actuator forces. Due to the use of no proper calculations and the fact that the needed actuator forces could only be estimated, more research in this field definitely needs to be undertaken.

It shall also be mentioned that food retention systems and food manipulation requirements have to be added before real chewing could commence. These mechanisms would create more spacious constrains. Therefore, a more conventional platform design could make it easier to deal with these spatial requirements even through the biological basis would be lost.

REFERENCES

Anderson, D. J. (1956). "Measurements of stress in mastication." *Journal of Dental Research*, 41, 175-189.

Anderson, K., Throckmorton, G. S., Buschang, P. H., and Hayasaki, H. (2002). "The effects of bolus hardness on masticatory kinematics." *Journal of Oral Rehabilitation*, 29, 689-696.

Bourne, M. C. (2002). "Relationship between rheology and food texture." in Engineering and Food for the 21st Century, J. Welti-Chanes, G. V. Barbosa-Canovas, and J. M. Aguilera, eds., CRC Press LLC.

Buschang, P. H., Hayasaki, H., and Throckmorton, G. S. (2000). "Quantification of human chewing-cycle kinematics." *Archives of Oral Biology*, 45, 461-474.

Cooke, R. (1982). "Dental prosthetic demonstrator." Roll Back the Years, C&S Publication, Wellington, 209-212.

Daumas, B., Xu, W. L., and Bronlund, J. (2005). "Jaw mechanism modelling and simulation." *Mechanism and Machine Theory*, 40(7), 821-833.

Douglass, G. D., and DeVreugd, R. T. (1997). "The dynamics of occlusal relationships." in Science and Practice of Occlusion, C. McNeill, ed., Quintessence Publishing Co, Inc, Berlin, 69-78.

Flores, E., and Fels, S. (2005). "Design of a 6 DOF antropomorphic robotic jaw." *Journal of the Acoustical Society of America*, 117(4), 2547.

Foster, K. (2005). "Personal communication." Institute of Food, Nutrition and Human Health, Massey University, Auckland, New Zealand.

Foster, K., Woda, A., and Peyron, M.-A. (2005). "Effect of texture of plastic and elastic model foods on the parameters of mastication." *Journal of Neurophysiology*, accepted for publication.

Gibbs, C. H., Mahan, P. E., Lundeen, H. C., Brehnan, K., Walsh, F. K., Sinkewiz, S. L., and Ginsberg, S. B. (1981). "Occlusal forces during chewing - Influences of biting strength and food consistency." *Journal of Prosthentic Dentistry*, 46, 561-567.

Gray, H. (1918). *Anatomy of the human body*, Lea & Febiger, Philadelphia.

Hannam, A. G. (1997). "Jaw muscle structure and function." Science and Practice of Occlusion, C. McNeill, ed., Quintessence Publishing Co, Inc, Berlin, 41-49.

Hannam, A. G., Langenbach, G. E. J., and Peck, C. C. (1997). "Computer simulations of jaw biomechanics." Science and Practice of Occlusion, C. McNeill, ed., Quintessence Publishing Co, Inc, Berlin, 187-194.

Hayashi, T., Kato, S., Nakajima, S., Yamada, Y., and Kobayashi, H. "Physiological control scheme of jaw simulator JSN/ 2A for improving reproducibility of open-close movement." *Proc. 1st Joint BMES/EMBS Conf. Serving Humanity, Advancing Technology*, Atlanta, GA, 564.

Hayashi, T., Kato, S., Yamada, S., Nakajima, S., Yamada, Y., and Kobayashi, H. "A physiological control of chewing-like jaw movement for robotized jaw simulator JSN/ 2A." *Proc. 22nd Annu. EMBS Int. Conf.*, Chicago, 730-731.

Heath, M. R., and Prinz, J. F. (1999). "Oral processing of foods and the sensory evaluation of texture." Food Texture: Measurement and Perception, A. J. Rosenthal, ed., Aspen Publishers, Inc., Gaithersburg, 19.

Helkimo, E., and Ingervall, B. (1978). "Bite force and functional state of the masticatory system in young men." *Swed Dent J*, 2, 167-175.

Ichim, I. (2005). "Personal communication." School of Dentistry, University of Otago, Dunedin, New Zealand.

Ichim, I., Swain, M. V., and Kieser, J. A. (2005). "Mandibular stiffness in humans: Numerical predictions." *Journal of Biomechanics*, in press.

Isermann, R. (2003). *Mechatronic systems: Fundamentals*, Springer-Verlag London Limited, London.

Klineberg, I. (2005). "Interarch relationships of teeth." in Occlusion and Clinical Practice: An Evidence-Based Approach, I. Klineberg and R. Jagger, eds., Elsevier Limited, Edinburgh, 3-12.

Koolstra, J. H. (2002). "Dynamics of the human masticatory system." *Crit Rev Oral Biol Med*, 13(4), 366-376.

Koolstra, J. H., and van Eijden, T. M. G. J. (1995). "Biomechanical analysis of jaw-closing movements." *Journal of Dental Research*, 74(9), 1564-1570.

Koolstra, J. H., and van Eijden, T. M. G. J. (1996). "Influence of the dynamical properties of the human masticatory muscles on jaw closing movements." *European Journal of Morphology*, 34(1), 11-18.

Koolstra, J. H., and van Eijden, T. M. G. J. (1997). "The jaw open-close movements predicted by biomechanical modelling." *Journal of Biomechanics*, 30(9), 943-950.

Koolstra, J. H., and van Eijden, T. M. G. J. (2001). "A method to predict muscle control in the kinematically and mechanically indeterminate human masticatory system." *Journal of Biomechanics*, 34(9), 1179-1188.

Lin, B. (2005). "Chew on this." UBC Reports, Vancouver, BC, Canada, 1-8.

Martin, W. E. (1999). "Geriatric nutrition." in Oral Health in the Elderly, R. Chernoff, ed., Jones and Barlett Publishers, Sudbury, Canada, 152.

MedicineNet. (2005). "Definition of anatomic orientation terms." www.medterms.com/script/main/art.asp?articlekey=9210.

Nakajima, J., Hidesshima, M., Takahashi, M., Tanginuchi, H., and Ohyama, T. (2001). "Masticatory mandibular movements for different food texture related to onomatopoetic words." *J. Med. Dental Sci.*, 48(4), 121-129.

Ogawa, T., Ogawa, M., and Koyano, K. (2001). "Different responses of masticatory movements after alternation of occlusal guidance related to individual movement pattern." *Journal of Oral Rehabilitation*, 28, 830-841.

Osborn, J. W., and Baragar, F. A. (1985). "Predicted pattern of human muscle activity during clenching derived from a computer assisted model: symmetric vertical bite forces." *J. Biomechanics*, 18(8), 599-612.

Osborn, J. W., and Baragar, F. A. (1992). "Predicted and observed shapes of human mandibular condyles." *J. Biomechanics*, 25(9), 967-974.

Palmer, B. (2005). "Basics of occlusion." www.brianpalmerdds.com.

Pap, J.-S., Xu, W. L., and Bronlund, J. (2005). "A robotic human masticatory system: Kinematic simulations." *International Journal of Intelligent Systems Technologies and Applications*, 1(1/2), 3-17.

Peyron, M. A., Lassauzay, C., and Woda, A. (2002). "Effects of increased hardness on jaw movement and muscle activity during chewing of visco-elastic model foods." *Exp. Brain Research*, 142, 41-51.

Peyron, M. A., Mioche, L., Renon, P., and Abouelkaram, S. (1996). "Masticatory jaw movement recordings: A new method to investigate food texture." *Food Quality and Preference*, 7(3/4), 229-237.

Posselt, U. (1957). "Movement areas of the mandible." *J. Prosthodontic Dentistry*, 7(3), 375-385.

Röhrle, O. (2005). "Personal communication." Institute of Bioengineering, University of Auckland, Auckland, New Zealand.

Röhrle, O., Anderson, I. A., and Pullan, A. J. "From jaw tracking towards dynamic computer models of human mastication." *IFBME Proceedings to 12th*

International Conference on Biomedical Engineering, Singapore.

RS. (2005). *The catalogue*, RS New Zealand.

Scapino, R. P. (1997). "Morphology and mechanism of the jaw joint." Science and Practice of Occlusion, C. McNeill, ed., Quintessence Publishing Co, Inc, Berlin, 23-40.

Sharkey, P., Boyle, D. K., POrchardson, R., and McGowan, D. A. (1984). "Jaw opening forces in human subjects." *British Dental Journal*, 156, 89-92.

Shigley, E., and Uicker, J. J. (1980). *Theory of machines and mechanisms*, New York.

SKF. (2003). *SKF - General catalogue.*

Söylemez, E. (2002). "Classical transmission-angle problem for slider-crank mechanismus." *Mechanism and Machine Theory*, 37, 419-425.

Takanobu, H., Takanishi, A., and Kato, I. "Design of a mastication robot mechanism using a human skull model." *Proceedings of the 1993 IEEE/RSJ International Conference on Intelligent Robots and Systems*, Yokohama, Japan, 203-208.

Takanobu, H., Yajima, T., Nakazawa, N., Takanishi, A., Ohtsuki, K., and Ohnishi, M. "Quantification of masticatory efficiency with a mastication robot." *Proceeding of the IEEE International Conference on Robotics and Automation*, Leuven, Belgium, 1635-1640.

Takanobu, H., Yajima, T., and Takanishi, A. "Development of a mastication robot using nonlinear viscoelastic mechanism." *Proceedings of the IEEE/RSJ International Conference on Intelligent Robots and Systems*, Pittsburgh, PA, 1527-1532.

THK. (2005). "Linear motion guide." www.thk.com.

Trimunt. (2001). *Catalog*, Trimunt Corp., Kyoto.

van Eijden, T. M. G. J. (2005). "Personal communication." Department of Functional Anatomy, Academic Centre for Dentistry, Amsterdam, The Netherlands.

van Eijden, T. M. G. J., Koolstra, J. H., and Brugman, P. (1995). "Architecture of the human pterygoid muscles." *Journal of Dental Research*, 74, 1489-1495.

van Eijden, T. M. G. J., Koolstra, J. H., and Brugman, P. (1996). "Three-dimensional structure of the human temporalis muscle." *Anatomical Record*, 248, 565-572.

van Eijden, T. M. G. J., Korfage, J. A. M., and Brugman, P. (1997). "Architecture of the human jaw-closing and jaw-opening muscles." *Anatomical Record*, 248, 464-474.

van Essen, N. L., Anderson, I. A., Hunter, P. J., Carman, J., Clarke, R. D., and Pullan, A. J. (2005). "Anatomically based modelling of the human skull and jaw." *Cells, Tissues and Organs*, 180, 44-53.

Wood, G. D., and Williams, J. E. (1981). "Gnathodynamometers: Measuring opening and closing forces." *Dental Update*, 8, 239-250.

Xu, W. L., Bronlund, J., and Kieser, J. (2005). "Choosing new ways to chew." *IEEE Robotics & Automation Magazine*, 12(2), 90-98.

Zahntechnik Braunwarth. (2005). "Aufgabe und Aufbau der Zaehne." www.braunwarth.de, Stuttgart, (in German).

APPENDICES

APPENDIX A

This section shows the diagrams of three incisor trajectories. These trajectories have been recorded while chewing foods at the Bioengineering Institute at the University of Auckland, Auckland, New Zealand. This includes the translatory and rotary movement.

- Chewing trajectory two

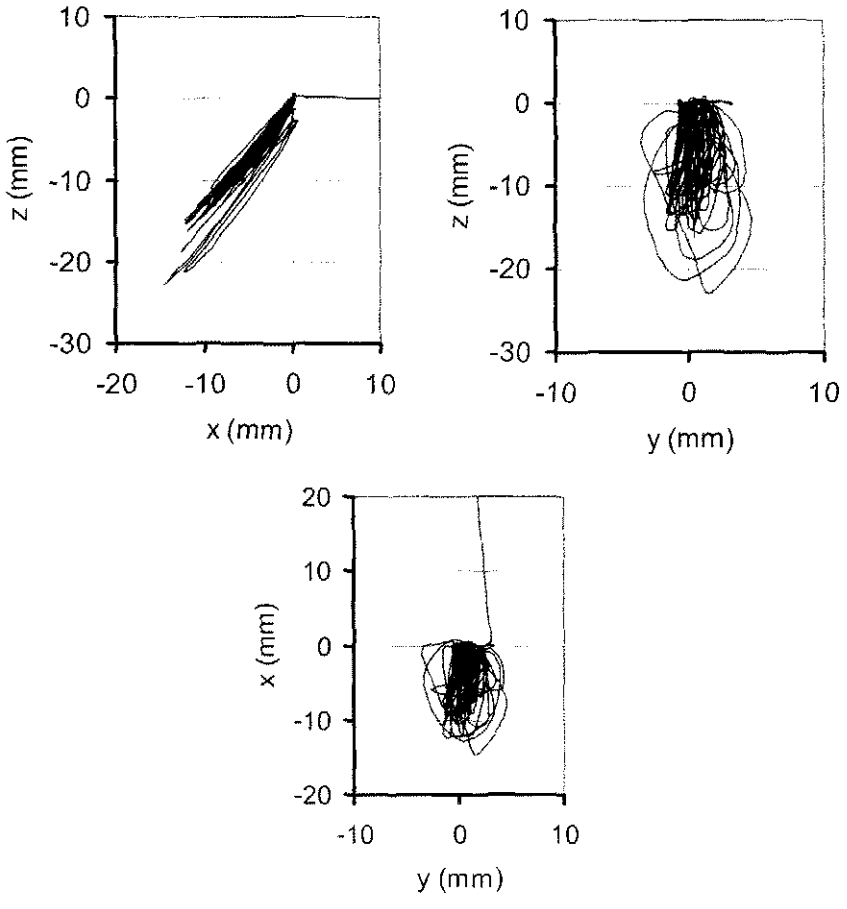

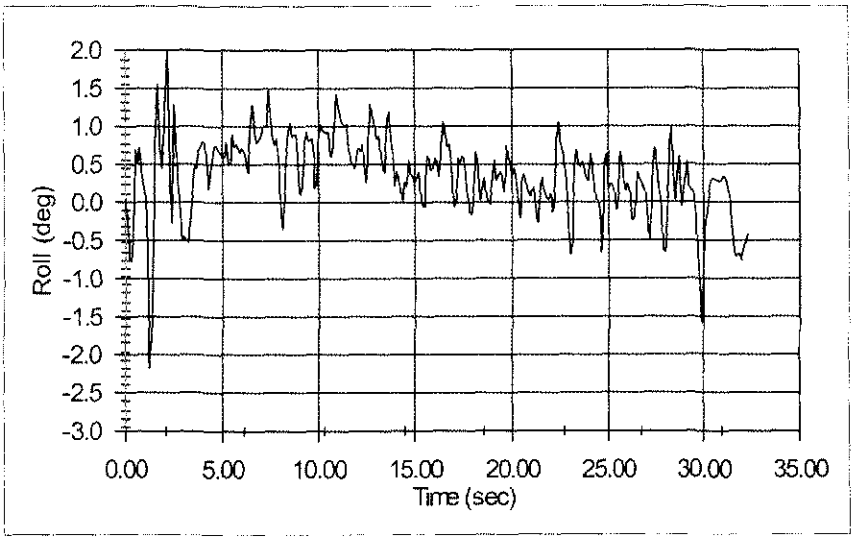
Roll (deg)
2.0
1.5
1.0
0.5
0.0
-0.5
-1.0
-1.5
-2.0
-2.5
-3.0
0.00
5.00
10.00
15.00
20.00
25.00
30.00
35.00
Time (sec)

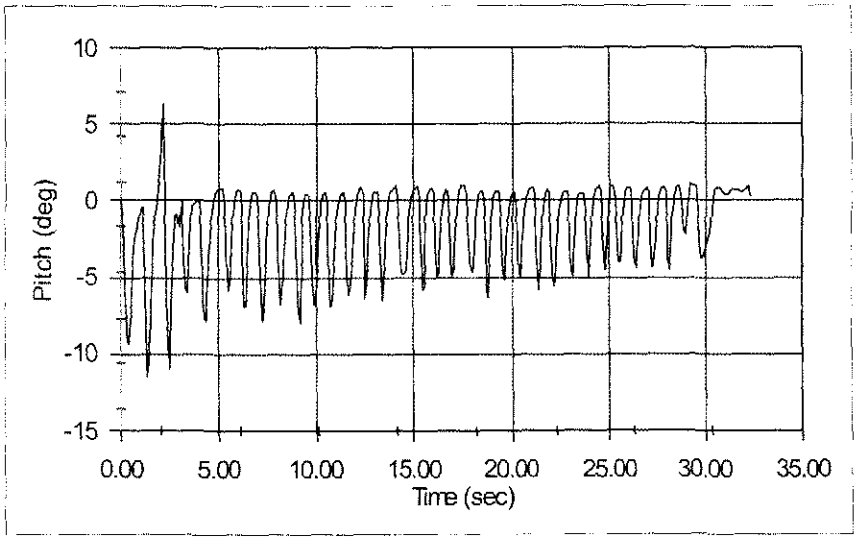
Pitch (deg)
10
5
0
-5
-10
-15
0.00
5.00
10.00
15.00
20.00
25.00
30.00
35.00
Time (sec)

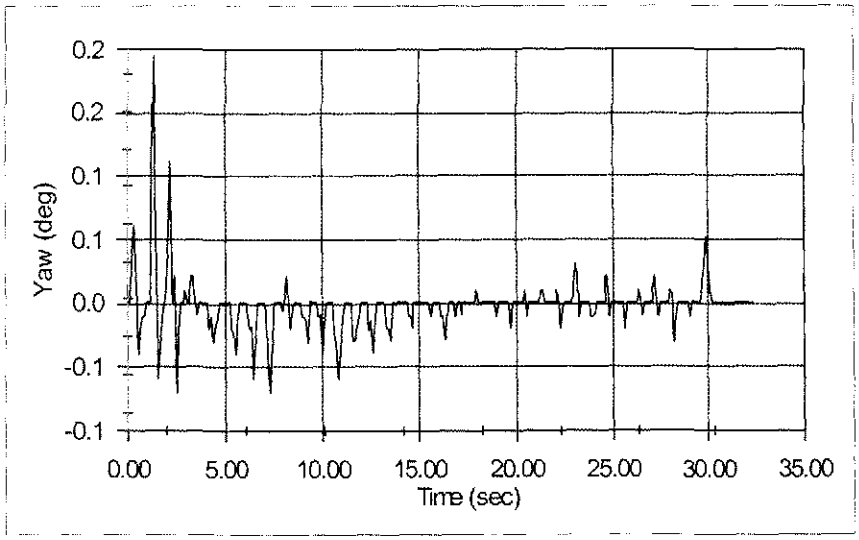
Yaw (deg)
0.2
0.2
0.1
0.1
0.0
-0.1
-0.1
0.00
5.00
10.00
15.00
20.00
25.00
30.00
35.00
Time (sec)

- Chewing trajectory three

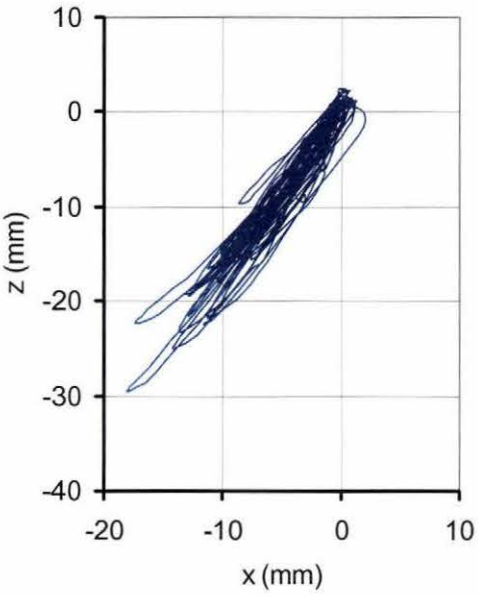

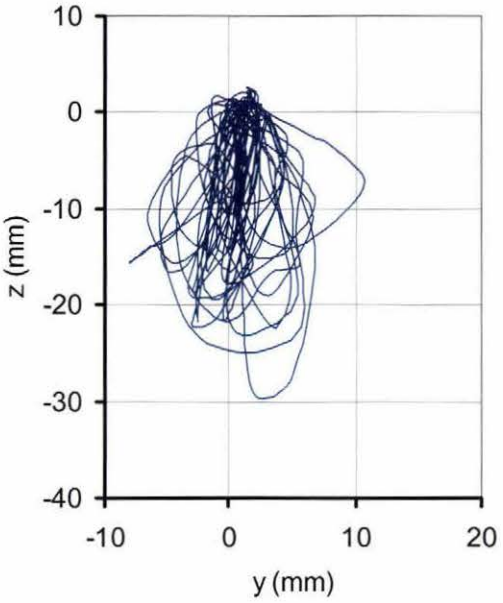

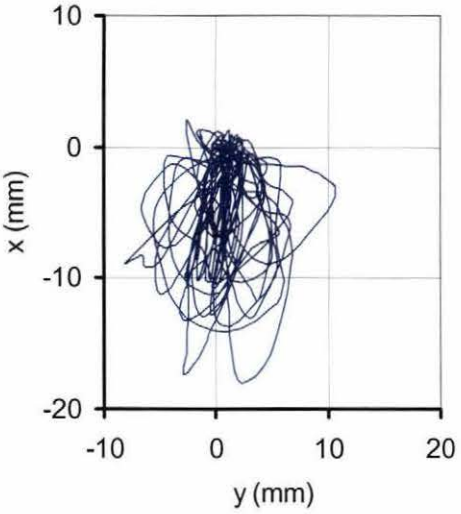

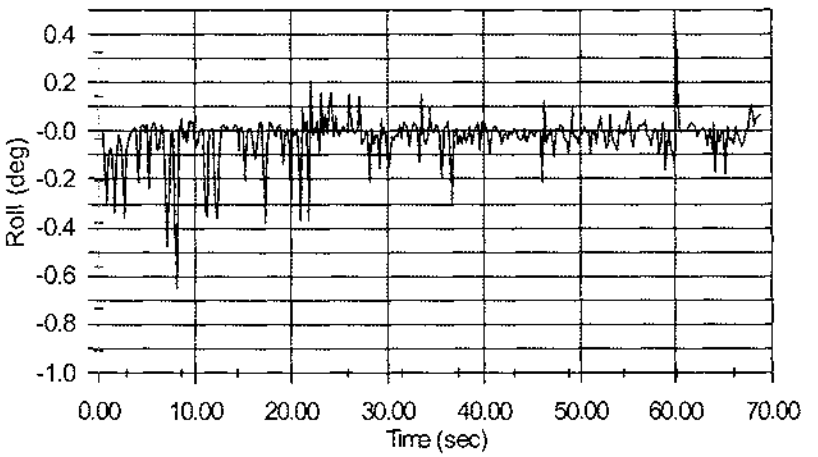
Roll (deg)
0.4
0.2
-0.0
-0.2
-0.4
-0.6
-0.8
-1.0
0.00
10.00
20.00
30.00
40.00
50.00
60.00
70.00
Time (sec)

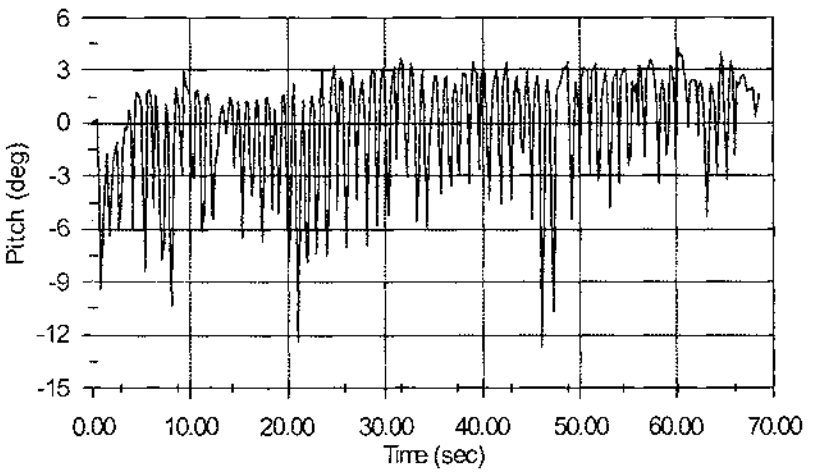
Pitch (deg)
6
3
0
-3
-6
-9
-12
-15
0.00
10.00
20.00
30.00
40.00
50.00
60.00
70.00
Time (sec)

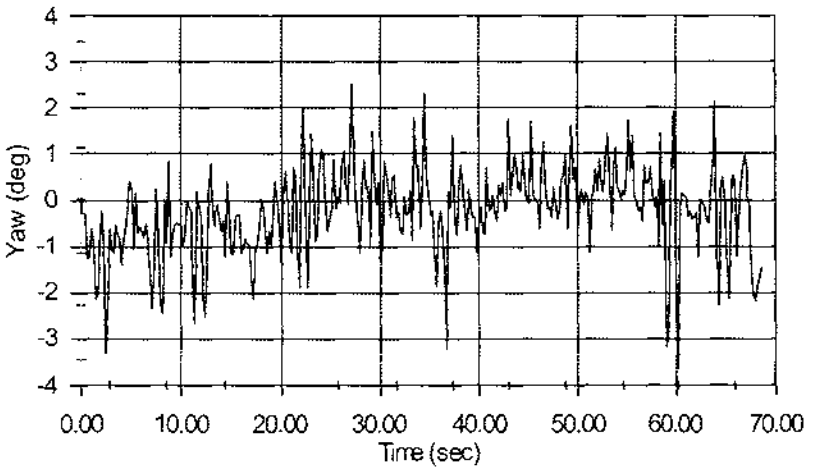
Yaw (deg)
4
3
2
1
0
-1
-2
-3
-4
0.00
10.00
20.00
30.00
40.00
50.00
60.00
70.00
Time (sec)

- Chewing trajectory four

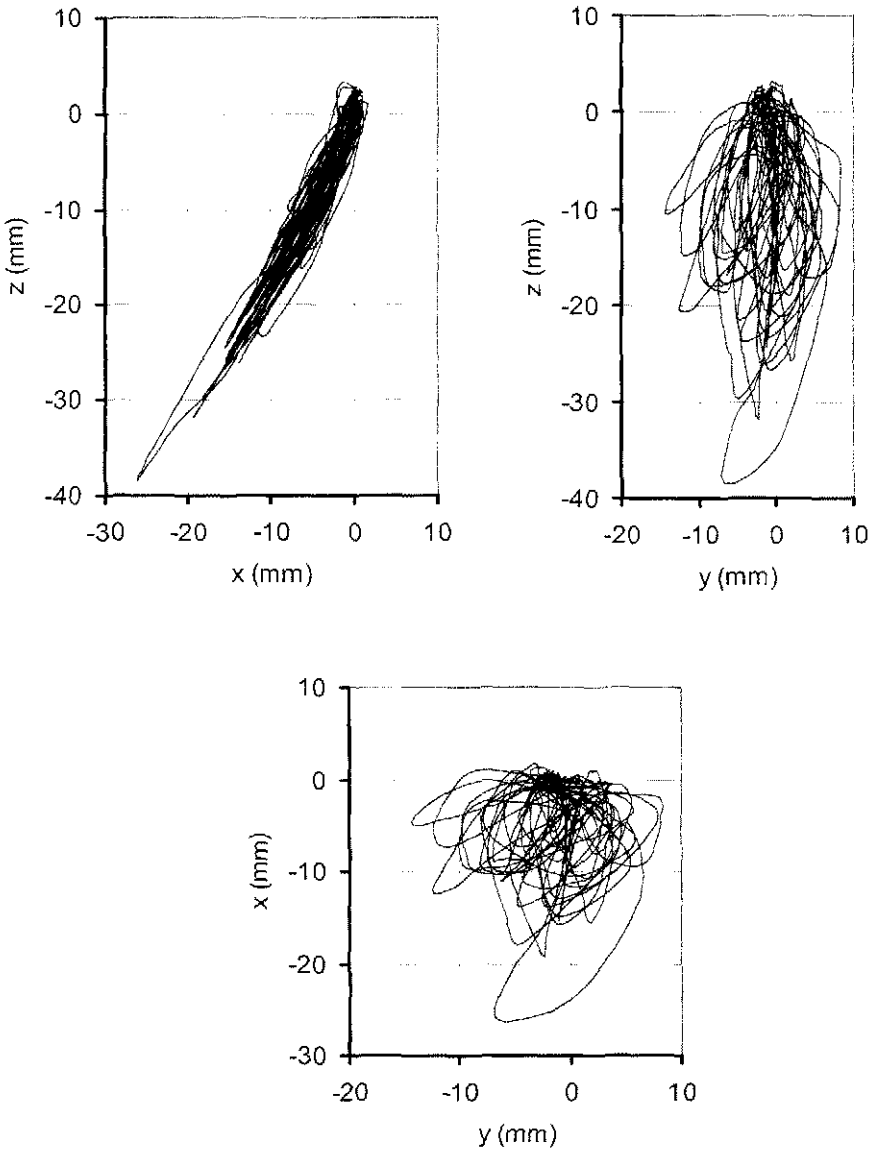

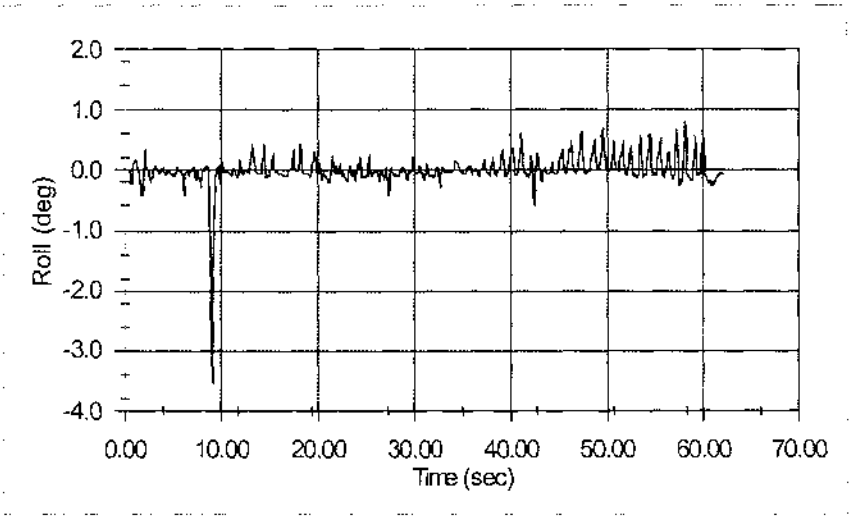
2.0
1.0
0.0
-1.0
-2.0
-3.0
-4.0
Roll (deg)
0.00
10.00
20.00
30.00
40.00
50.00
60.00
70.00
Time (sec)

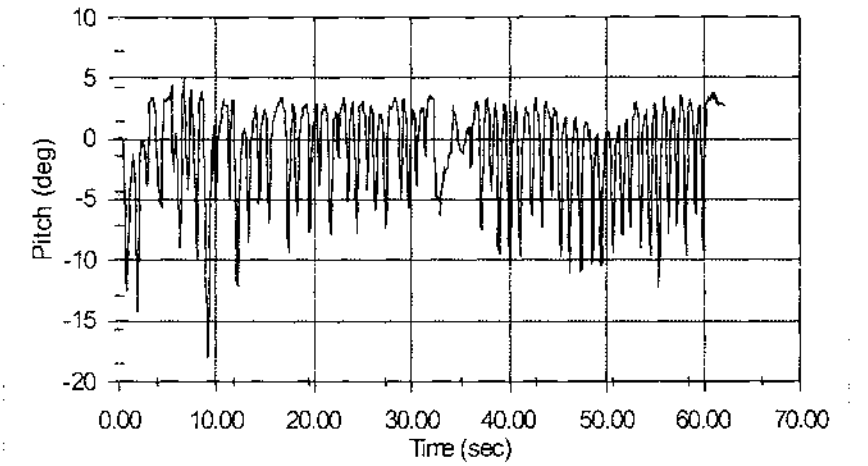
10
5
0
-5
-10
-15
-20
Pitch (deg)
0.00
10.00
20.00
30.00
40.00
50.00
60.00
70.00
Time (sec)

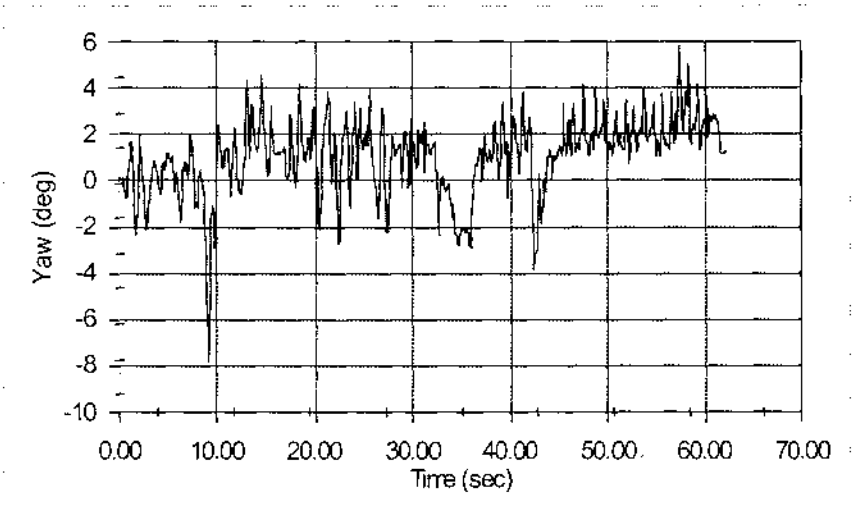
6
4
2
0
-2
-4
-6
-8
-10
Yaw (deg)
0.00
10.00
20.00
30.00
40.00
50.00
60.00
70.00
Time (sec)

APPENDICES B - G

Appendices B to E can be found on the enclosed DVD and appendices F and G are enclosed as separate folders. *Appendix B* contains the mathematical model of the chewing robot with linear actuation systems and is divided as follow:

- the mathematical model as SolidWorks files, and
- a recorded video of chewing trajectory one.

Appendix C contains the SolidWorks model of the linear actuator and the component datasheets. It is divided into:

- the SolidWorks model and drawings,
- component datasheets, and
- pictures of the built actuator.

Appendix D contains the mathematical model of the chewing robot with crank actuation systems. It covers:

- the mathematical model as SolidWorks files,
- pictures of the mathematical model with all four trajectories,
- recorded videos for all four chewing trajectories, and
- the actuator results.

Appendix E deals with the chewing robot with crank actuation systems. This covers:

- the SolidWorks model and drawings,
- the model used for simulations,
- a video and pictures of the coupler testing,
- recorded videos with the crank plays,
- recorded videos for all four trajectories,
- component datasheets, and
- pictures of the physical chewing robot.

The folder of *appendix F* contains: bill of materials, an assembly overview, and all drawings of the linear actuator.

The folder of *appendix G* contains: bill of materials, an assembly overview, and all drawings of the chewing robot with crank actuation systems.

Thesis DVD